Mineralogical Analysis of Primary and Secondary Source Sediments to Linnévatnet, Spitsbergen, Svalbard

An Honors Thesis

Presented to

The Faculty of the Department of Geology

Bates College

In partial fulfillment of the requirements for the
Degree of Bachelor of Science

by

Lauren Marie Perreault

Lewiston, Maine

March 14, 2006

Note to Reader:

The valley and many of the geomorphic features in the valley are named after the Swedish taxonomist, Carl von Linné. In this study, I refer to these features by their Norwegian names, which combine Linné with the Norwegian nouns. Thus, Linnévatnet signifies “Lake Linné ”. In Norwegian, “dalen” means valley, “elva” means river, and “breen” means glacier, yielding the names Linnédalen, Linnéelva and Linnébreen.

Abstract

Linnévatnet, Spitsbergen, Svalbard is a high Arctic lake containing a sediment record that extends through most of the Holocene. Laminated lake sediments such as those found in Linnévatnet can serve as high resolution proxies for long term climate change. This study utilizes detailed mineralogical analysis to identify changes in the source of sediments to Linnévatnet during the late Holocene. These climatically sensitive sediment sources include a major proglacial river; alluvial fans, solifluction lobes and the meltwater stream from a small cirque are secondary sources. Distinct bedrock lithologies (phyllite, sandstone, carbonate and dolerite) in the valley strike north-south parallel to the lake, making provenance work possible.

Pebble counts, conducted in the field at each sediment source, reveal a strong correlation between cobble and boulder lithology and underlying bedrock source. Laboratory identification of the gravel fraction of surficial sediment samples indicates increased break down of phyllite and carbonate in comparison to the sandstone. Grain size analysis of source sediments implicates differences in the mechanism of sediment transport and deposition at different sources.

Unique mineral compositions were identified for each sediment source studied using paired x-ray diffractometer (XRD) and quantitative analysis of the sand, silt and clay-sized fractions. West shore solifluction sources are recognized by the abundance and presence of sheet silicates (muscovite, chlorite, kaolinite) in all size fractions. The cirque outwash stream is distinguished by higher amounts of chlorite in all size fractions and the abundance of albite in the silt fraction. East shore sources are characterized by higher amounts of carbonate minerals and the presence of accessory minerals (rutile, pyroxene). Linnéelva sediments contain relatively less carbonate, albite and chlorite/kaolinite than the west and east shore sources.

Continuous grain size analysis of four surface cores from different locations in the lake show variations in grain size through time, indicating changes in sediment transport. Paired XRD and quantitative analysis of the silt and clay fractions from core subsamples indicate changes in mineralogical composition down core at all locations but are limited in scope. Higher amounts of silt, paired with an increase in chlorite/kaolinite and a distinct stratigraphy, indicate increased glacier activity in the core proximal to the cirque. Higher amounts of sand, decoupled from silt trends and paired with the presence of local mineralogy (orthopyroxene, calcite) in the two deep basin cores indicate increased east slope activity. Differences in grain size distribution of the two deep basin cores implicate solifluction lobes as a contributor to sedimentation in the north end of the deep basin.

Acknowledgements

More people deserve thanks for helping to start and finish this project than I will be able to name on this page at this late hour, but I trust you will all understand and accept my gratitude at large. Sincerest thanks to Dr. Mike Retelle, advisor extraordinaire, for his invaluable guidance, experience and expertise on this project, in Svalbard and in my undergraduate geology career in general. And for the melkesjokolade. Brilliant! This project would not have been possible without funding from the National Science Foundation (Svalbard REU Program 2005) and the Bates Student Research Fund.

A resounding thank you to the Bates College Geology Department (John, Dyk, Gene, Phaedra and Marita), and a particular thank you to Associate Professor Beverly Johnson, for the knowledge and inspiration you've imparted, and most of all, for saving me from the grips of the Chemistry Department by showing me the way to geology. My gratitude to my fellow REUers, Bob, and our fearless leaders, Steve and Al (from afar). 8,523 pebbles have never been so fun.

To Professor Allen, I offer many, many thanks. This project would not have been possible without your generosity with time and equipment, guidance, and patience when I created equipment problems you'd never seen before. Thanks to the Colby College Geology Department, which is clearly not superior to the Bates Geology Department, but was nonetheless a welcoming and generous second home and most importantly, did not drop their x-ray diffractometer.

My sincerest gratitude to all the geology majors – past and present – who have made this department so much fun. No one else will ever quite understand why rocks and mud are cool enough to justify braving waist deep snow, rising tides and raging polar bears, or why walkie talkies and original song composition are imperative to field work. Particular thanks to Kristin and Brooks, for invaluable help, advice and moral support during the long haul, and more importantly, for being exceptionally fun comrades far beyond the walls of Carnegie.

Thank you to my dearest friends and roommates, without whom I would not have had food to sustain myself these last few weeks, or a multitude of good memories completely irrelevant to this thesis.

Most of all, my deepest thanks, appreciation and love to my family.

Table of Contents

Table of Contents (cont.)

Table of Figures

Table of Tables

Table of Tables (cont.)

Chapter 1. Introduction

1.1 Purpose

The purpose of this study is to identify the unique mineralogical composition of sediments entering Linnévatnet, a high Arctic lake in Svalbard, from sources other than the primary inflow from a glacier fed river. These climatically sensitive alternative sources include alluvial fans, solifluction lobes and the meltwater stream from a small cirque. The sources are distinct not only in transport mechanism but also in source rock, causing them to be well suited to provenance work. The mineralogical "fingerprints" are used to identify changes in sediment source to the lake over time, potentially providing more information about climate change in the last several centuries. Fieldwork for this study was conducted as a part of the 2005 Svalbard REU (Research Experience for Undergraduates) Program. The overall goal of that project is to conduct a comprehensive modern processes study of the high arctic glacier, valley and lake system that comprises Linnédalen in order to calibrate and better interpret the long term climate record contained within the lake sediments. This study provides a better understanding of sedimentation in the lake basin, which in turn enables better interpretation of the long-term climate record.

1.2 Justification: Global and Arctic Climate Change

The debate on global warming has brought current climate change into the scientific and political spotlight. Globally, average temperature since the industrial revolution has risen approximately 0.6˚C, while the concentration of carbon dioxide in the atmosphere has increased by 35% (Arctic Climate Change Assement [ACIA], 2004). The International Panel on Climate Change (IPCC) reports with certainty that there exists

a natural greenhouse effect and that human activities – namely the burning of fossil fuels – are amplifying this effect. Moreover, the IPCC suggests that global temperature will rise an additional 1.4-5.8˚C in this century if greenhouse gases continue to be added to the atmosphere at their present rate (1990).

Studies of climate change in the Arctic are of particular importance given the sensitivity of this region to even small changes in climate (ACIA 2004, IPCC 1990). This sensitivity is the result of several mechanisms. First, snow and ice have a much greater value of reflectivity (albedo) than water or soil. As snow and ice cover decrease due to rising temperatures, the amount of soil and water exposed increases, resulting in more radiation absorbed and subsequently greater warming. This is known as a positive feedback loop; that is, an effect of warming that in turn amplifies warming. Second, unlike tropical regions, the majority of the energy absorbed at high latitudes goes into warming rather than evaporation. Furthermore, heat absorbed by the ocean is transferred back to the atmosphere more easily as sea ice thins and/or disappears (ACIA, 2004). Finally, the Arctic itself plays a significant role in determining the climate of the rest of the globe because of its driving influence on global atmospheric and oceanic circulation patterns. Not only may the rapid and dramatic response of the Arctic to climate change serve as a portent of things to come for the rest of the globe, but this response in itself has the potential to cause significant shifts in climate that would have global effects.

A variety of changes in the Arctic consistent with the predicted effects of global warming have been documented (Serreze et al., 1999). Temperatures in the Arctic are rising at nearly twice the rate of global temperatures. Winter temperatures in some parts of Alaska and Canada have risen 3-4˚C in the past 50 years (ACIA, 2004). Serreze et al.

report temperature increases during the winter and spring over North America and Eurasia as well as over the Arctic Ocean. An 8% increase in precipitation has been recorded across the Arctic during the last 100 years. At the same time, negative net snow cover has been observed in the Arctic since the 1980s. Small glaciers across the Arctic are demonstrating negative mass balances, sea ice is thinning and the Arctic is now considered a net CO_2 source instead of sink due to increased emissions of carbon by terrestrial ecosystems (Serreze et al., 1999). Despite these apparents signs of dramatic climate change, it should be noted that the warming observed is not greater than the range of interdecadal temperature changes observed during this century. Nonetheless, the combined effect of atmospheric circulation, insolation and volcanic aerosols on global temperature is insufficient to account for the observed warming, indicating that anthropogenic forcings are influencing current climate change (Serreze et al., 1999).

Thus, it is of vital importance to continue studying global and Arctic records of climate change in order to better understand the influence of anthropogenic and natural forcings on climate change. Projects such as this one provide valuable information about climate change in the past and can help to predict environmental responses to current climate change.

1.3 Site Description

Svalbard is a high Arctic archipelago located between 74 and 81˚N and 10 to 35˚E and comprises 62,000km^2 of total land area. Of this, 60% is covered by glaciers and inland ice (Steel and Worsley, 1983). Svalbard experiences a relatively mild climate compared to other land masses located at similar latitudes owing to the moderating

influence of the Western Spitsbergen Current, which is a branch of the North Atlantic Current. Western Spitsbergen in particular experiences warmer temperatures and more precipitation. The mean annual air temperature is -4.7˚C, as reported from Isfjord Radio, located 4km northeast of Linnédalen; the average air temperature is 4.7˚C in July and -11.5˚C in January. Precipitation is estimated to be 43.5cm annually but it should be noted that this is at best an approximation due to the inherent difficulty of measuring snowfall (Snyder et al., 2000).

1.3.1 Location and Lake Morphometry

Linnédalen is located at 78.3˚N 13.50˚E on western shore of Spitsbergen, which is the biggest island of the Svalbard archipelago (Figure 1.1). A small valley glacier, Linnébreen, sits at the southern end of the north-south trending valley (Figure 1.2). Previous work shows that Linnébreen has had a negative mass balance since at least the mid 20th century (Schiff, unpublished B.Sc. thesis, 2005). Nearly 8km separate Linnébreen from Linnévatnet. Connecting the two is a braided proglacial river, Linnéelva.

Linnévatnet is an elongate lake oriented roughly north-south, is 4.7km long and 1.3km wide, and lies 12m above sea level (Snyder et al., 2000; Svendsen et al., 1989). The lake developed in a glacially over deepened basin; it is well mixed - lacking thermal or chemical stratification - and experiences temperatures less than 4˚C all year (Boyum and Kjenso, 1978). Circulation in the lake is described as counter clockwise due to the influence of the Coriolis Effect on currents (Werner, 1988 in Svendsen 1989). Linnévatnet has three distinct basins – two smaller, shallower basins in the south end are

See Figure 1.1

See Figure 1.2

divided by a bedrock high that extends into a small elongate island (Figure 1.3). A deeper, bigger basin lies in the northern end of the lake. This main basin is 35m deep, the eastern basin is 16m deep and the western basin is 11m deep. The smaller basins are separated from the northern basin by a ~1m bathymetric high (Snyder et al., 2000). Linnéelva represents the major water and sediment inflow for the lake. A smaller meltwater stream derived from a cirque on the western valley wall enters the lake on the southwestern corner. Several smaller, intermittent streams also enter the lake from the eastern and western valley walls. The outlet to the lake is located in the northeastern corner and drains into Isfjorden, approximately 2km north of the Linnévatnet.

1.3.2 Sediments in Linnévatnet

Laminated lake sediments in a proglacial environment can serve as a valuable proxy for climate change. Such lakes receive a significant amount of sediment laden glacial meltwater. Coarse sediments are deposited primarily during the spring and summer while fine sediments settle out during the winter, forming distinct annual couplets. Annual and diurnal changes in temperature and precipitation affect glacial melt and therefore the amount of sediment delivered annually to proglacial lakes. Thus laminated lake sediments can be interpreted as a signal of climate change by examining changes in the thickness, grain size and mineral composition of layers. The sediment in Linnévatnet represents nearly 10,000 years of lacustrine deposition (Svendsen et al., 1989) and thus provides an invaluable record of climate change.

Svendsen, Mangerud and colleagues have done extensive research characterizing the sediments contained in Linnévatnet (1987, 1989, 1990, and 1997). Two distinct units

See Figure 1.3

of sediment exist above the acoustic basement: a lower, massive marine unit and an upper lacustrine unit showing subhorizontal layering of silt and clay. The acoustic basement represents bedrock covered by a thin layer of till. Radiocarbon dating of marine molluscs show that deglaciation in the valley must have occurred prior to 12,500yr B.P. and that the isolation of the lake from the fjord occurred around 9,600 ^{14}C yr B.P. (8,800 cal. yrs) (Svendsen et al., 1989; Mangerud and Svendsen, 1990). The maximum sediment thickness is approximately 12m and occurs at the Linnéelva delta; moving further from the delta front the sediment thickness decreases. Mean marine and lacustrine sediment thickness is estimated to be 4.3m and 1.9m respectively. From this, mean sedimentation rates are determined to be .2mm/yr for lacustrine sediments and 1.6mm/yr for marine sediments (Svendsen et al., 1989). Werner has asserted that heightened glacial activity in the second half of the Holocene resulted in higher sedimentation rates during this time but dating downcore is necessary to substantiate this claim (Svendsen et al., 1989).

1.4 Bedrock Geology

1.4.1 Tectonic Background

The basement rock of Svalbard dates from the Precambrian to the mid-Silurian and is known more generally as the Hecla Hoek Formation; its metamorphic origin is in the Caledonian Orogeny as a fold belt. About 400 million years ago, during the Devonian, Svalbard was located near the equator and large river systems deposited sediment – what is now the Old Red Sandstones – into basins caused by contractional tectonic movement. During the Carboniferous, as Svalbard moved north and rapid

subsidence occurred, the environment was humid and non-marine, characterized by alluvial fans prograding into swamps and flood basins. Deposition of carbonates, red alluvial sandstones and coals took place at this time. During the Permian, a marine transgression occurred as Svalbard continued to move north; this movement shifted the depositional environment to arid, resulting in the formation of shallow marine carbonates and sabkha evaporites. In the Mesozoic, what is now Greenland and Europe began to break apart and the Arctic and North Atlantic Oceans began to open, resulting in basalt and dolerite intrusions and the broad uplift of the Svalbard platform. During the Tertiary, the Spitsbergen fracture zone experienced local convergent movement due to tectonic transform faulting between Greenland and Svalbard. This movement resulted in the uplift of basement rock in western Svalbard and the formation of rift basins as the Norwegian-Greenland Sea opened. The uplift of Svalbard in the Tertiary, in addition to its polar position, initiated a period of colder climate and glaciation during the Quaternary (Steel and Worsley, 1984; Dallman, 1999 and Worsley and Aga, 1986 in field guide).

1.4.2 Bedrock of Linnédalen

The bedrock in Linnédalen spans from the Hecla Hoek to the Mesozoic volcanics. As the composition and location of the lithologies present in the valley is highly relevant to provenance work, more detailed descriptions of the bedrock are provided. Figure 1.4 is a geologic map of the valley. Five distinct lithologies are located within the Linnévatnet watershed: Precambrian phyllite, Carboniferous quartzitic sandstone, late Carboniferous - Permian dolomites and limestones, late Permian silicified shales and siltstones, and Mesozoic dolerites (Dallman et al., 1992).

See Figure 1.4

The topographic highs on the western side of the valley are dominated by the Precambrian areno-argillaceous phyllite, which is part of the Løvliebreen Formation of the St. Jonsfjorden sequence. It more commonly referred to as simply Heckla Hoek and has its metamorphic origins in the Caledonian orogeny. The phyllite is characterized by well developed cleavage and parageneses of sericite, chlorite and other opaque minerals. It is interbedded with quartzites and has a mainly siliceous matrix (Dallman et al., 1992).

The quartzitic sandstones of the central and lower western portions of the valley belong to the Billefjorden Group, and primarily to the Orustdalen Formation although a small band of the Vegard Formation is also present. These rocks date from the early Carboniferous and represent alluvial and fluvial (fan, braided stream and flood-plain) deposition into fault bounded basins. The coal-bearing Orustdalen Formation lies unconformably on the Heckla Hoek basement. Although minor amounts of rounded quartzite conglomerate and black carbon-rich shales are present, the most common lithology of the formation is a grey to white quartzitic sandstone. Plant fossils and fragments of tree trunk are abundant. In contrast, the Vegard formation is comprised of interbedded sandstones, siltstones and shales with a reddish color (Dallman et al., 1992).

The contact between the Gipsdalen and the Billefjorden Groups is an angular unconformity. Two formations of the Gipsdalen Group – the Nordenskiöldbreen and Gipshuken – dominate the eastern side of valley. The Nordenskiöldbreen Formation dates to the late Permian and represents part of a marine transgression sequence, where deposition occurred in a coastal or shallow marine setting. It is characterized by interbedded dolomites and limestones, dolomitic sandstones and grey shales. Marine fossils are common. The Gipshuken Formation represents a regression from shallow

marine to a more arid sabkha (evaporite) depositional environment. Common lithologies include dolomite, dolomitic breccia and limestone (Dallman et al., 1992).

The Kapp Starostin Formation of the Tempelfjorden Group outcrops high on the eastern side of Linnédalen. This lithology dates from the Late Permian and consists of silicified shales, siltstones and sandstones. The Tempelfjorden Group represents the transition from shallow marine to low-energy, oxygenated shelf deposition (Dallman et al., 1992).

Finally, tectonic extension between Greenland and Europe in the Mesozoic led to the intrusion of dolerite dykes and sills into Proterozoic, Carboniferous/Permian and Triassic strata in Svalbard. In Linnédalen, such an intrusion exists on the eastern side of the valley in the Nordenskiöldbreen Formation (Dallman et al., 1992).

1.5 Glacial Geology

Multiple glaciations have occurred on Svalbard during the Quaternary but the exact number remains unknown because subsequent glaciation often erodes evidence of previous glaciations. Mangerud et al. (1998) have found evidence in marine sediments for at least three major glaciations – each extending to the edge of the continental shelf of western Svalbard – during the Weichselian. The last of these glaciations represents the Last Glacial Maximum (LGM).

The extent and style of glaciation on Svalbard during the LGM has been hotly contested. Marine geology, combined with the raised shoreline record preserved on Svalbard, finally solved the puzzle left by the incomplete glacial terrestrial record. Exploration of the Barents Sea revealed only a few meters of uncompacted marine

sediment, underlain by highly compacted glacial till. Marine coring and seismic and acoustic soundings show huge fans of glacial sediment leading out of troughs at the edge of the continental shelf, indicating that glaciers must have extended at least this far (Mangerud et al., 1992, Mangerud et al., 1998, Siegert et al., 2002). Development of an oxygen isotope chronology of the marine sediments, combined with dating of glacial sediments, have constrained the timing of deposition of the uppermost layer to the LGM (Mangerud et al., 1992). Finally, patterns of raised shorelines – recording the history of isostatic rebound following the LGM – demonstrate increased unloading from west to east across Svalbard, pointing to the fact that the center of the ice sheet must have been east of Svalbard (Mangerud et al., 1992; Siegert et al., 2002). This evidence points to the existence of a large ice sheet, centered on the Barents Sea, which covered Svalbard and extended to the edge of the continental shelf. The mechanism of formation for this marine based ice sheet, as well as the southern and eastern extent of the ice sheet, are still under debate (Siegert et al. 2002). The timing of the onset of the LGM is difficult to discern, but Mangerud et al. suggest that it is unlikely to have begun earlier than 23,000yr B.P. and possibly began as late as 18,000yr B.P. (1992).

Deglaciation following the LGM is thought to have occurred in two steps. Forman et al. (1987) and Lehman and Forman (1992) report that initial ice breakup occurred prior to 13,000yr B.P. and that a second period of relatively stable sea level began around 10,700yr B.P. and ended by 9500yr B.P (Lehman and Forman 1992, Landvik et al., 1987). Marine limit in West Spitsbergen, reached between 13,000 – 12,000yr B.P., was 64m a.s.l. (Forman et al., 1987; Lehman and Forman, 1992; Landvik et al., 1987). An intermediate shoreline at 50m a.s.l. that corresponds to a second period

of stable sea level is recorded by Landvik et al. (1987). This second period of stability reflects renewed glacial loading during the Younger Dryas (Lehman and Forman, 1992; Landvik et al., 1987), although glaciers in western Svalbard did not readvance significantly during this time (Lehman and Forman, 1992; Mangerud et al., 1992). Complete deglaciation following the Younger Dryas occurred rapidly (Lehman and Forman, 1992; Landvik et al., 1987, Forman et al., 1987).

Several minor glacial advances occurred in Linnédalen during the Holocene. Svendsen and Mangerud interpret the lack of continuous lamination and low sedimentation rates in Linnévatnet as evidence of complete deglaciation of the valley from 10,000yr B.P. to 4400yr B.P. Local glacial maxima, as determined by periods of strong lamination and high coal content, occurred 2800-2900yr B.P., 2400-2500yr B.P, 1500-1600yr B.P. and during the Little Ice Age. Using lichenometry, Werner (1992) describes four periods of moraine stabilization in the Holocene: 1500, 1000 and 650yr B.P. and again within the last several centuries. Lichens are assumed to start growing on moraine material only after the moraines have stabilized (i.e. glaciers have stopped expanding) and are dated by size according to established growth curves (Werner, 1990). Werner (1992) asserts that Little Ice Age glacier advances (corresponding to the two most recent stabilization dates) represent the most extensive glaciation in the Holocene and have subsequently destroyed much evidence of earlier Neoglacial advances.

1.6 Hydrology and Geomorphology

1.6.1 Arctic Hydrology

Arctic watersheds are unique in both their structure and hydrologic regime. An understanding of what factors determine water flow is criticical to understanding controls on sedimentation in Arctic lakes. The dynamics of moisture, temperature and annual snowmelt are of particular importance for the sediment sources examined in this study.

Permafrost is the single most important factor determining the structure of Arctic watersheds, while spring snowmelt is the event which dominates the annual hydrology. The depth from ground surface of permafrost – permanently frozen soil – determines the thickness of the active layer. The active layer refers to soil above the permafrost which freezes during the winter and thaws during the summer. This layer is seldom greater than a meter deep in zones of continuous permafrost. Subsurface water storage and movement in Arctic watersheds is limited to the active layer due to the impermeability of the underlying permafrost. When the active layer becomes saturated, or is still frozen, overland movement of water downslope occurs (Kane et al., 1992).

Snowmelt generally begins and ends within a one to two week period, thus producing a large volume of runoff in a short period of time (Kane et al., 1992). Melt water begins to form within snow pack only once the temperature of the entire snow cover is uniform at 0˚C (Scherer et al., 1998). The redistribution and concentration of snow by wind during the winter has a large effect on the subsequent distribution of meltwater across a watershed. Snowmelt often represents the peak discharge period in Arctic watersheds (Kane et al., 1992). Beylich found that during this period of high flow

75-95% of the total annual sediment load was delivered to lakes at two sites in the Arctic in Swedish Lapland and Northern Siberia (2004).

Slush flows refer to the flow of water-saturated snow; they represent an intermediate process between fluvial flow and avalanches. Their flow regime is similar to that of mudflows (Gude and Scherer, 1998). Slush torrents refer specifically to high magnitude, low frequency slush flows. Slush flows are often initiated by extended periods of rainfall, or a particularly intense rainfall event (Hestnes, 1998). In addition, research by Scherer (1998) demonstrates that slush flows can be initiated within normal conditions of the high latitude snowmelt period; that is, within normal levels of energy input and precipitation. In such a scenario, slush flows may be released during snowmelt because of the increasing hydraulic gradient of the meltwater table within the snow pack itself (Gude and Scherer, 1998). Slush flows represent an important mechanism for sediment transport because they mobilize sandy and coarser material in the watershed (Beylich, 2004).

Climate change affects the mass and energy inputs into Arctic hydrological systems by changing precipitation amounts and increasing air and ground surface temperatures. The latter change may increase the thickness of the active layer and decrease the thickness of the permafrost, thus affecting the water storage capacity of the soil. Given no change in the amount of precipitation, an increase in temperature may cause the spring melt to occur earlier and be less intense due to increased water storage capacity in soils. Changes in precipitation amount will alter the water balance of watersheds, potentially causing changes in soil moisture and vegetation cover, among other effects (Kane et al., 1992).

1.6.2 Geomorphologic Features: Solifluction Lobes and Alluvial Fans

Linnédalen contains a variety of geomorphologic features. Two of these – solifluction lobes and alluvial fans – are examined by this study as sources of sediment into the lake. The northwestern shores of the lake are characterized by the extensive development of solifluction lobes which terminate at the lake edge. Five major alluvial fans appear to be the dominant mechanism of sediment and water transport on the eastern shore of the lake. Based on the lack of stream flow observed in the summer of 2005, it is thought that these fans are primarily active during spring melt and/or higher magnitude lower frequency events. Both processes – solifluction and fluvial transport – are sensitive to changes in climatic conditions.

Solifluction refers to the slow movement of soils downslope under the influence of gravity; gelifluction refers specifically to the slow movement of soils associated with freeze-thaw action of the ground (Ritter, 1978; Matsuoka, 2001). The term connotes specifically periglacial phenomena but downslope movement of soil can in fact occur anywhere (Ritter, 1978). Solifluction lobes (tongue-shaped masses of soil and debris) are the surface expression of overturn movement in the underlying soil. They generally form where hillslopes decrease in gradient, resulting in a reduction of soil velocity (Matsuoka, 2001). Lobes consist of unsorted debris, ranging in size from silt to boulders, and terminate with a scarp, which can be 1-6m in height (Ritter, 1978). In cold, non-glacial environments, the freezing and thawing of the ground surface facilitates downslope movement of soils, a process which is further aided by sparse vegetative cover. The freezing action heaves soil perpendicular to the ground surface, while subsequent thawing causes contraction; this contraction, combined with the influence of gravity, results in an

overall downslope displacement (Matsuoka, 2001). Solifluction is identified as an important component of slope denudation and a source for sediment in streams by Rapp and Åkerman (1993; in Mann et al., 2001).

Mann et al. (2001) investigated the effects of increased moisture due to climate change from 13,000-8,000yr B.P. on the north slope of Alaska. They inferred that increased temperatures caused deeper thawing to occur in the ground, while greater winter precipitation provided additional moisture. These changes caused the widespread solifluction that is indicated in the stratigraphy of the soil deposit. In addition, increased permafrost melting and hillslope erosion provided more sediment, while increases in summer rainfall caused higher discharge. These processes contributed to an increase in alluviation and incision during this time period (Mann et al., 2001).

Alluvial fans are common fluvial features, especially in semi-arid regions. Fans are deposited on plains or valley floors by streams generally issuing from narrow, steep, mountain valleys. They are relatively low, convex, topographic features which decrease in gradient with increasing distance from the valley mouth and consist of loose sediments (Jackson, 1997). The dominant mechanisms of deposition are sediment-gravity flows, often initiated in arid or semiarid regions by infrequent, heavy rainstorms. In addition to debris and mud flows, streamflow processes may also occur on all types of alluvial fans. Fans can be classified by aspect and dominant sedimentation mechanism; the three principal types (ordered by decreasing aspect) are debris-flow dominated fans, braided fluvial fans and low-sinuosity meandering fluvial fans (Boggs, 2001).

1.7 Provenance

Previous studies have utilized the distinctive lithologies of Linnédalen to indicate glacial activity in order to interpret climatic conditions. Linnébreen rests primarily on the coal-bearing quartzitic sandstones while the alluvial fans of the eastern side of the valley rest primarily on the carbonate rocks. Variations in the relative abundances of carbonate and organic carbon (coal) downcore have been interpreted to represent changes in source contribution. Periods of high coal content indicate times of increased glacial activity and periods of greater carbonate content indicate less upvalley (glacial) input (Svendsen and Mangerud, 1997).

Snyder et al. (2000) analyzed sediments from the southwestern basin of Linnévatnet and interpreted a distinct signal of cirque glacier activity. The cirque glacier rests primarily on phyllite; the meltwater stream from this cirque feeds into the southwestern basin of Linnévatnet. Sediment from this cirque consists of metamorphic lithic fragments, in contrast to sediments from Linnéelva which are primarily mono-mineralic and of higher coal content. The study inferred periods of cirque glaciation from times of increased lithic fragment deposition and decreased sedimentation from Linnéelva. Some uncertainty exists pertaining to whether periods of increased Linnéelva sediment indicate decreased cirque glacier activity or increased Linnéelva activity (and a subsequently diluted cirque glacier signal) (Snyder et al., 2000).

Thomas (unpublished B. Sc. thesis, 2005) also used the distinctive lithologies to study relative source contributions to the lake. The study established that unique geochemical "fingerprints" exist for the three lithologies investigated (phyllite, quartzitic sandstone, and the carbonates). However, major differences in geochemistry occur

between grain size fractions; failure to account for this prevented the study from definitively correlating source material to lake sediments.

While previous works have concentrated on sediments originating from Linnébreen and upvalley, this study focuses on the contribution of alternative sediment sources located proximal to the lake. The main objective is to relate the mineralogy of the source rock to the sediments found in the lake. To achieve this, the mineralogy of the source rock and of the sand, silt and clay sampled from the geomorphic features studied are analyzed to establish the unique mineral compositions characteristic of each source. These compositions are correlated to sediments retrieved from the lake bottom to indicate sediment source. Given the climatically sensitive nature of sediment delivery, changes in the relative contribution of sources are thought to have occurred over time. The ability to distinguish between sediment delivered from Linnéelva and from each alternative source allows for a better interpretation of the long term climate change record contained in the lake sediments.

Chapter 2. Methods

2.1 Field work

Between July 25 and August 12, 2005, field work was done in Linnédalen. During this time general site reconnaissance and observation took place and pebble counts were conducted in addition to the collection of rock and surficial sediment samples and sediment cores.

2.1.1 Site selection

Different geomorphic and fluvial features dominate sediment transport in different areas of the lakeshore. The shoreline of the northwestern quadrant of the lake is characterized primarily by solifluction sheets and lobes. Site selection, pebble counts and sample collection in this area aimed to achieve good spatial distribution rather than focus on individual lobes. Figure 2.1, an aerial photograph of Linnévatnet, shows the selected sites. The eastern shore of the lake is dominated by several large alluvial fans. Five fans of particular prominence were selected for further study: the northeastern most fan, the central fan, two "twin" fans located immediately adjacent to each other and the southernmost fan, located immediately below a prominent dolerite outcrop. In the southern end of the lake, fluvial feature dominate. Samples collection and pebble counts targeted the large outwash fan associated with the mouth Linnéelva to enable comparison to alternative source compositions. Finally, the outwash fan issuing from a small cirque located in the southwestern quadrant of the lake basin was studied.

Sites are underlain by different north-south trending lithologies. The western sites – the solifluction lobes and cirque fan – are underlain by phyllite and white sandstone. The eastern fans are primarily underlain by carbonates. Because Linnéelva has multiple

See Figure 2.1

tributaries on both sides of the valley, all three rock types are considered sources of sediment to the river. Site selection was thus based on differences in both transport mechanism and source rock, as well as overall spatial distribution around the lakeshore.

2.1.2 Rock and Surficial Sediment Sample Collection

Hand samples representative of each of the distinct lithologies present in the valley were collected from the lake shores. A minimum of three surficial sediment samples were collected from each alluvial and outwash fan. Samples were selected to represent the finer-grained matrix material that comprises each fan. Sediment was collected from at least two "fresh" cut stream channels and from at least one older (vegetated) surface on each fan. Samples from the eleven locations on the northwestern shores were collected for spatial distribution, with one sample taken for a given location. These samples represent the fine-grained matrix of the solifluction lobes. Figure 2.2 shows the locations of sample collection, pebble counts and sediment core recovery.

2.1.3 Pebble Counts

Pebble counts were conducted at each of the eastern fans, at the mouth of Linnéelva and the cirque outwash fan, and in conjunction with surficial sediment sample collection along the northwestern shores (Figure 2.2.). With the exception of transect A on the western shore, twenty five meters of tape measure were laid out on the ground for every transect. The rock underlying every meter and half meter mark on the tape measure was identified (n=51). Due to the unusual length of the lobe at transect A, a tape length of fifty meters was placed on the ground and the rock at every meter mark was

See Figure 2.2

identified (n=51). On each fan, between three and five pebble counts were conducted, depending on the size of the fan. Of these, two to three were conducted perpendicular to the lake shore and the remainder were conducted parallel to the lake shore. Both the perpendicular and parallel transects were selected to encompass a range of freshly cut and older surfaces. The Linnéelva and cirque fans are more active and thus all transects at these locations were conducted on fresh surfaces. The northwestern transects were all laid out perpendicular to the lake shore because each one traced the long-axis profile of a solifluction lobe.

2.1.4 Sediment Core Recovery

Eleven sediment cores were recovered by boat from Linnévatnet through the use of a Universal Surface Corer. Cores were collected from locations proximal and distal to the northeast fan, the east central fan, the dolerite fan, and the cirque outwash fan, as well as from a site proximal to the central western shore (Figure 2.2).

A plastic core tube (diameter 7.5cm) was attached to the Universal Surface Percussion Corer. Two separate ropes were attached to device; one was used to control the descent of the corer through the water and the second was used to control the hammer. By watching the screen of a fish finder, the surface corer was held poised just above the sediment surface and then rapidly dropped in. The second rope was utilized to pull the hammer mounted above the coring device up and down, providing the force to lightly hammer the core tube further down in the sediment. The entire apparatus was hauled up from the lake bottom until the open bottom of the core tube was held just below the water surface; there it was capped and then brought on board. The core tube

was removed from the coring device and excess water siphoned from the top of core, leaving a couple of centimeters of water to minimize disruption to the sediment-water interface.

Cores were brought to shore and let to sit and dewater in an unheated (~40ºF) storage shed for at least twenty four hours. The remaining water was carefully removed by siphon and pipette. Empty space in the core tube was packed with paper and foam packing material and the core caps firmly secured with duct tape. Cores were transported back to the United States in checked personal baggage. Upon arrival at Bates College, cores were stored upright in cold storage (45ºF) until analysis was conducted.

2.2 Laboratory Methods

Surficial and core sediments underwent grain size analysis. Core stratigraphy was logged visually and digitally recorded. Extensive x-ray diffraction (XRD) analysis to identify and quantify mineral content was conducted on select surficial sediment and rock samples and on sediment from cores 6, 8, 11 and 12.

2.2.1 Preparation of Surficial Sediment Samples for XRD Analysis

Seven sample locations were selected for extensive mineralogical analysis: two western shore locations, the northeast, east central, and twin alluvial fans, and the Linnéelva and cirque outwash fans. Two sediment samples from each focus site were combined into one sample in order to obtain enough fine sediment for three XRD slides (target wet sediment weight = 120g). For each of the alluvial fans, two samples taken from freshly cut streams channels were selected. Because all of the outwash fan samples

were fresh, two were arbitrarily selected to be combined. The northwestern shore samples were divided into two groups spatially – the western samples and the northwestern samples. Within each of these groups, two samples were arbitrarily selected to be combined. Samples were weighed to obtain wet sediment weights and then put in a Fisher Isotemp® 500 drying oven at 100ºC for at least twenty four hours, removed, and allowed to cool for several hours in the desiccator. Samples were then weighed again to obtain dry weights. Microsoft Excel was utilized to calculate the total percent water lost: $\frac{(wet\_weight - dry\_weight)}{wet\_weight} * 100$. The dry sediment was transferred to plastic deli cups and covered with about three centimeters of deionized water. Clumps of sediment were gently disaggregated using a rubber tipped fork. Samples were sonified using a Fisher Scientific Sonic Dismembrator 60 at approximately 15 Watts for one minute. The samples were covered and left in deionized water overnight. Disaggregation with the fork and sonic dismembrator was repeated the following day immediately prior to wet sieving.

Samples were carefully poured onto a 63µm sieve. Silt and clay sized particles were washed through the sieve using deionized water until the water moving through the sieve was relatively clear. The sand and gravel trapped on the sieve was washed into a separate beaker and the sieve backwashed to dislodge stuck particles. The sand and gravel fraction was then transferred back onto the sieve and washed again until the deionized water ran completely clear. The silt and clay fraction was covered and put aside. The sand and gravel fraction was transferred into a glass beaker and excess water decanted. The beaker was then transferred to the drying oven, set at 100ºC, to evaporate the remaining water. After drying, the combined sand and gravel fraction was weighed

and then separated by a 2mm sieve. Each size fraction was weighed and then put aside. Deionized water was used to rinse and backwash the sieve between every sample to avoid cross contamination.

The silt and clay fraction for each sample was evenly divided between four 1L plastic Nalgene® bottles and put in a Damon IEC CU-5000 Centrifuge for six minutes and thirty seconds at 1500rpm for separation (Newton, 1978). The effluent (water and clay sized particles) of each bottle was carefully decanted into a stainless steel filter funnel and filtered, one at a time, through a 47mm cellulose nitrate membrane with .45µm pore size. The wet filter was quickly and smoothly rolled across a standard petrographic microscope slide (27x46mm, 1.2mm thick) to transfer the oriented clay sized minerals from the filter to the slide. This procedure is outlined in US Geological Survey open-file report 82-71 (Pollastro, 1982). The filtering process was repeated twice more to yield three slides for every sample, all of which were air dried. The fourth bottle of sample was put aside. According to the standard XRD analysis technique outlined by Carroll (1970), one air-dried slide was run on the XRD. A second slide was put on a ceramic plate in the furnace at 300ºC for one hour. The ceramic plate is used to prevent the rapid cooling that can cause the glass slides to crack, an amendment outlined by Pollastro (1982). This slide was run on the XRD and then again put in the furnace at 550ºC for one hour. After cooling, it was run on the XRD. The third slide was put in a glass desiccator with a plate of ethylene glycol for approximately 48 hours and then promptly run on the XRD (Carroll 1970).

Nine rock hand samples were chosen for XRD analysis: red and white sandstones, green and grey phyllites, two limestones, dolomite, conglomerate and

dolerite. Hand samples were smashed with a rock hammer to obtain five to six pieces with a diameter of approximately one centimeter. These pieces were put in a ball mill (4cm in diameter, 6cm long) and into a Spex 8000 Mixer Mill for between five and seven minutes depending on the minerals present (samples with high amounts of phyllosilicates required more time). This sediment was then transferred to finer ball mill (1cm in diameter, 3cm long) in small batches (two to three batches to grind one third of the total sediment) and put into a Spex 5100 Mixer Mill for between two and five minutes. This clay sized sediment was firmly packed into a welled petrographic slide (.05mm deep) using a putty knife. The putty knife was then used to level the surface of the sediment to flush with the glass slide surface. The same ball mill procedure was used to grind the sand fraction of the surficial sediment samples into clay-sized particles. For the silt fraction of these samples, only the use of the finer ball mill was necessary. Welled slides for the sand and silt fractions were filled in the same way that the ground rock samples were prepared. Kimwipes and compressed air were used to clean the ball mills in between samples to avoid cross contamination.

2.2.2 Sediment Core Analysis

Sediment cores were kept upright in cold storage until January 2006. The lengthwise halves of the core tubes were marked using a permanent marker. A Dremmel® handsaw was used to score each core tube, utilizing the marker lines as guides. Next the cores tubes were cut entirely through by using the same tool. The core halves were slightly parted to allow a piece to fishing line to be drawn through the sediment, cutting the sediment cylinder neatly in half. A bead of deionized water was

squirted between the halves to ease the parting, and then the two halves were carefully pulled apart. One half was designated the archive half and left untouched; the second half was designated the working half. The surface of the working half was carefully scraped with a putty knife to remove excess sediment and to clearly reveal clean stratigraphy. The stratigraphy was immediately recorded and core color identified with the aid of a Munsell color chart. A digital camera was also used to document stratigraphy. Stratigraphic columns were later created using Adobe Illustrator CS2.

Subsampling for XRD analysis was based on structural and coloration differences observed in the cores. Core 6 was continuously laminated and lacked identifiable stratigraphic units; therefore samples were selected from 0, 3, 5, 7 and 9cm for spatial distribution. Core 8 had extremely variable stratigraphy. Samples at 1, 6, 10, 15 and 21cm were chosen to be representative of distinct units and for spatial distribution. In both cores 11 and 12, five distinct stratigraphic units were identified and subsamples were thus collected to be representative of these units. In core 11, samples at 3, 6, 10, 16 and 19cm were selected for XRD analysis. Samples at 5, 10, 15, 22, and 30.5cm in core 12 underwent XRD analysis. To ensure an adequate amount of clay for XRD analysis, a total of 4 cm^3 was collected at each of these depths using a 2cm^3 cutter (twice). Samples were transferred to a pre-weighed glass petri dish and weighed to obtain a wet sediment weight. Sediment was put in the drying oven overnight at 100ºC, removed and allowed to cool in a desiccator for several hours. Samples were then weighed again to obtain a dry sediment weight. The procedure used to prepare XRD slides for surficial sample sediments was also utilized for the preparation of the core sediment samples and is therefore described in detail above (section 2.2.1). Samples were disaggregated and wet

sieved to separate the sand fraction from the mud. Sand was dried, weighed and put aside. The mud fraction was centrifuged to separate silt from clay; clay particles were filtered to produce two oriented XRD slides. One slide was analyzed as an air dried sample while the second sample was heated at a temperature of 550ºC for one hour and then analyzed. Glycolated slides were not produced for core samples because previous surficial sediment analysis determined these samples to be unnecessary. The silt fraction was dried, weighed and ground into clay sized particles to produce welled XRD slides.

2.2.3 XRD Analysis

All samples were run on a Rigaku DMAX 11B 1342 x-ray diffractometer housed in the Colby College Geology Department. MDI Data Scan software parameters were set as follows for all samples except the powdered dolerite sample. Scanning started at 3.0º two-theta and ended 65.0º two-theta and proceeded at a rate of 3.0 degrees per minute. Scans were continuous, with a .02° step size and an initial theta value of 1.5°. The powdered dolerite sample was scanned at a rate of 1.0 degree per minute because poor resolution obtained at the standard rate in the initial analysis seriously impeded mineral identification.

Mineral identification and quantitative analysis were made using Jade 7.0 software and the ICSD Minerals database. The background pattern of sample diffractograms was removed and the peaks refined before using the search-match function. The search-match process compares the peaks in the sample diffractogram to a database of mineral diffractograms using an algorithm that incorporates peaks properties (e.g. intensity and centroid position). Search-match parameters are chosen to broaden or

limit the rigor the program uses to match known mineral peaks to the peaks obtained in the diffractograms. Search-match parameters were set as follows: the two-theta error window was .18°, two-theta matching and intensity matching were set at 6 (on a scale of 10, with 10 being the most rigorous). For all clay samples (air dried, glycolated and heated), the severe orientation search-match filter was utilized. Powdered rock, sand and silt samples were analyzed without the use of this filter. Mineral matching occurs at three different levels: identifying major, minor and trace peaks, based on their relative intensities. For each level, the program provides lists of potential mineral matches and the user selects the minerals present. Table 2.1 lists the major and diagnostic peaks of the minerals encountered in this study. Two-theta values were produced by reviewing diffractograms generated by this study.

Some difficulties and uncertainties occur in positively identifying minerals using XRD. The following discussion addresses some of the common problems encountered in and strategies used by this study, but it is by no means an inclusive discussion. Kaolinite is recognized by comparing diffractograms of air dried clay slides to diffractograms of clay slides heated to 550ºC. At that high temperature, the structure of kaolinite collapses and thus the mineral “disappears” from the diffractogram. Specifically, the absence in the heated sample of peaks at 12° and 25° two-theta indicates the presence of kaolinite. An example of this pattern can be seen in Figure 2.3. Where chlorite is present in silt and sand samples (which were not heated), kaolinite must also be assumed to be present because without heating the samples, it is impossible to distinguish the kaolinite diffraction pattern from the chlorite pattern. It is, however, possible to determine whether chlorite is absent because the peak at 6° two-theta is unique to chlorite; thus if this peak

Table 2.1 Selected Diagnostic Major and Minor XRD Peaks for Minerals Identified or Pertinent to Study in Linnédalen

Mineral	**Major Peaks (2θ)**		
quartz	26.5	20.8	50
albite	27.8	23.4	24
labradorite/andesine	23.7	28.2	25.5
muscovite	8.8	17.8	26.2
biotite	8.8	25.3	27.4
chlorite	6.3	12.4	25.1
kaolinite	12.4	20.5	25
calcite	29.5	35.1	36.1
dolomite	30.8	41.2	44.9
ankerite	30.6	41	44.7
clinoferrosilite	29.5	27.5	26.4
graphite	26.5	42.3	44.5
rutile	28	36	54
enstatite	30.3	27.5	20.2
kanoite	27.4	29.6	34.7
orthopyroxene	27.2	27.4	30
augite	29.7	30.6	34.8
ilmenite	32.5	40.2	48.7
lepidocrocite	14.1	27	47
hematite	35.7	33.1	40.9
magnetite	35.7	26.7	30.2

See Figure 2.3

does not show up on the diffractogram but peaks at 12° and 25° two-theta do, kaolinite is present but not chlorite. An example of this pattern is shown in Figure 2.4.

Similarly, where muscovite is present it must be assumed that biotite is present because the diffractograms of the two minerals can not be distinguished by the treatments used in this study. Muscovite is distinguished from illite by comparing the diffractograms of air dried samples to glycolated samples (refer back to Figure 2.3). An offset to the left (to a lower two-theta value) of the major muscovite peak at 12Å or a broadening of these peaks in the glycolated sample would indicate the presence of illite because the structure of this mineral undergoes expansion of the interlayer space after saturation by ethylene glycol.

Variables in sample composition and preparation can affect the search-match and identification process. The amount of sample material on the slide contributes to the intensity and resolution of the peak. Thus the minor amounts of clay present in some of the surficial sediment and core samples resulted in low intensity counts and hence limited resolution in those diffractograms. An example of this is seen in Figure 2.5. The poor resolution, combined with the severely oriented nature, means that the quantitative analysis of clay samples generally results in the highest errors. Heating samples to 550ºC also causes the peak intensity and resolution to diminish (see Figure 2.6), but because the primary function of these samples is to observe any peak disappearance, resolution is less important. Powdered sample materials with heterogeneous grain size can also diminish peak resolution. An uneven or unlevel distribution of sample on the slide can alter the

See Figure 2.4

See Figure 2.5

See Figure 2.6

two-theta angle measured and thus offset peaks from the ideal peak pattern in the mineral database. To minimize this source of error, consistent and good sample preparation is vital, especially during the filter to slide transfer of clays and when leveling powdered samples.

Clay minerals (chlorite, kaolinite, illite etc.) are particularly complex to analyze because they often do not conform to their idealized structures. Moreover, clays can contain more than one layer structure; in this condition they are called mixed layer clays. Clays, as well as other minerals, also vary in elemental content. These variations in composition and structure result in slight differences in the mineral's lattice spacing and thus in the diffraction patterns, an effect which is observed in the offset of peaks from their ideal centroids. In addition, the composition of clay minerals and sheet silicates may vary from sample to sample, resulting in offset between the "muscovite" peaks of two different samples. Figure 2.7 displays this offset.

Peak overlap presents another problem in mineral identification. Major peaks for many minerals occur in the same location, as has been discussed for sheet silicates already. Major peaks for carbonates (calcite, dolomite, and ankerite), pyroxenes (enstatite, kanoite) and plagioclase all occur in the 27°-35° two-theta region, making positive identification of minerals difficult at times. Figure 2.8 illustrates this problem in peak overlap and resolution. The best option for these minerals is to look for minor, diagnostic peaks outside of this range (for example, albite has several minor peaks around 24° two-theta).

See Figure 2.7

See Figure 2.8

Quantitative analysis is another feature of the Jade 7.0 software. After peak identification, well resolved and preferably unique peaks are selected and integrated for each mineral identified. The program compares this value to the RIR (reference intensity ratio) of the mineral, to calculate the quantity of the mineral present, a value that is given in weight percent, weight percent normalized, and volume percent (which takes into account mineral density). A percent error is automatically calculated based on counting statistics. Coefficients of variance (CEV) were calculated to help evaluate if the percent error associated with the quantity calculated was too high to consider the absolute quantity of the mineral significant. $CEV = \left(\frac{percent\_error\_sample}{mean\_\min eral\_quantity} \right) * 100$ The coefficient of variance evaluates the magnitude of the error relative to the sample quantity.

Considerable limitations exist on the use of XRD quantitative analysis. Poor peak resolution (low height to base ratio) adversely affects the calculation. Peak overlap, where the peaks for multiple minerals align to create one peak, also affects the calculation because multiple minerals are producing one peak. Minerals present in only very small amounts can not be quantified without high error and thus are generally left out of quantitative analysis. Furthermore, as in peak identification, many variants of minerals and clays exist and thus the RIR associated with a particular mineral peak may not represent the specific end member or polytype present, introducing uncertainty into the quantity provided. Finally, the chlorite and kaolinite fractions must be measured as one entity due to the difficulty inherent in resolving the two minerals.

2.2.4 Grain Size Analysis

For the purpose of this study, grain-size fractions are defined as follows: gravel >2mm, sand 2mm - 63µm, silt 63µm - 2µm, and clay <2µm. The process of sediment separation by grain size fraction was conducted during XRD sample preparation and is thus described in greater detail in section 2.2.1.

The sand and gravel fractions of surficial sediments samples were separated from the fines through the process of wet sieving. This coarse fraction was collected in a pre-weighed glass beaker, excess water decanted, and dried in the oven for at least 24 hours. The total dry weight was obtained and the sample sieved (mesh size 2mm) to separate the sand from the gravel. Each fraction was then weighed separately. Percent silt and clay was calculated together as percent fines:

$$\left(\frac{total\_sediment\_dry\_wgt - (wgt\_gravel + wgt\_sand)}{total\_sediment\_dry\_wgt}\right) * 100 = \%\, fines\,.$$

All four cores were sampled continuously using a $1cm^3$ cutter. Depths already sampled for XRD analysis were not resampled. Sediments were put into pre-weighed porcelain crucibles and wet sediment weights obtained. Samples were put in the drying oven for a minimum of 24 hours at 100ºC and reweighed to obtain a dry total sediment weight. Sediment was disaggregated, let to sit overnight, and disaggregated again before being wet sieved (mesh size 63µm) to separate the fines from the sand. The sand was rinsed into beakers and dried in the oven overnight. Due to the small amount of sand present in the core sediments, sand was transferred to weighing paper and weighed using a more sensitive analytical balance.

Fines were centrifuged as described in section 2.2.1. The suspended clay fraction was poured off the settled silt fraction and discarded if it was not being used for XRD

analysis. The silt fraction was rinsed out of the centrifuge bottles into pre-weighed glass beakers and dried in the oven at 100ºC for at least 24 hours. After the silt was dry, it was allowed to cool in a desiccator for at least one hour before a dry silt weight was obtained. For core sediment samples, sand and silt weights were obtained directly as described above. Percent clay was calculated by subtracting the weight of sand and silt from the total original dry weight:

$$\left(\frac{total\_sediment\_dry\_wgt - (wgt\_sand + wgt\_silt)}{total\_sediment\_dry\_wgt}\right) * 100 = \%clay\,.$$

Chapter 3. Results

Summary tables and figures based on XRD data are presented in the results section. Diffractograms from every sample analyzed are available for viewing in JPEG format on the attached CD, Appendix A. For ease in comparison in this study, all end member minerals and structural variants identified in analysis are grouped by general mineral type in the results. Thus, "albite" may be high or low. "Muscovite" includes paragonite and 2M1, 2M1 ammonia polytypes. "Biotite" refers to biotite 6H, phlogopite and siderophyllite. "Chlorite" refers to a large group of minerals, including clinoclore (with chromium and magnesium righ variants, as well as different polytypes), chamosite and chlorite-serpentine. "Kaolinite" describes kaolinite-montmorillonite and several polytypes. Section 2.2.3 has already addressed the uncertainties involved in this aspect of mineral identification.

3.1 Whole Rock XRD Analysis

Each rock analyzed (green and grey phyllite, white and red sandstone, dolerite, conglomerate, and three carbonates) had a distinct mineral composition; these data are summarized in Table 3.1. The green and grey phyllite samples both contained quartz, albite, muscovite, chlorite and calcite. In addition, the grey phyllite contained dolomite. The white sandstone and conglomerate were exclusively quartz; the red sandstone consisted of quartz and clinoferrosilite. The dolerite was comprised of quartz, laboradorite/andesine, enstatite, augite and ilmenite. Carbonate 1 contained quartz, calcite, dolomite and rutile. Carbonate 2 consisted of calcite, dolomite, ankerite and graphite. Carbonate 3 was comprised of quartz, dolomite and ankerite.

	jpeg file name	quartz	albite	muscovite	biotite	chlorite	calcite	dolomite
green phyllite	*grnphyll*	x	x	x		x	x	
grey phyllite	*greyphyll*	x	x	x	x	x	x	x
white sandstone	*whtsstn*	x						

	jpeg file name	quartz	labradorite/ andesite	calcite	dolomite	ankerite	clinoferrosilite	graphite	rutile	enstatite	augite	ilmenite
dolerite	*dolerite*	x	x							x	x	x
carbonate 1	*carb1*	x		x	x				x			
carbonate 2	*carb2*	x		x	x	x		x				
carbonate 3	*carb3*	x			x	x						
red sandstone	*redsstn*	x					x					
conglomerate	*conglom*	x										

Table 3.1 Summary XRD Results of Mineral Composition of Source Rock Samples
A jpeg file of each diffractogram is located in Appendix A

3.2 Pebble Counts

The percent of each lithology present in the cobble and boulder fraction is shown in Table 3.2. The west shore is dominated by sandstone (76.5%), with phyllite and quartz making up the remainder of the cobbles and boulders. "Quartz" refers to pure quartz pebbles, generally derived from veins in the Hecla Hoek (phyllite) formation, as distinguished from the highly quartzitic sandstone. The cirque glacier fan is characterized overwhelming by phyllite (88.9%), while Linneélva lithologies are more equally mixed, with 30.3% sandstone, 48.5% phyllite and 19.2% quartz. The five east side sources are dominated by carbonates (limestones and dolerites were not distinguished from each other in identification), with percents ranging from 83 on the northeast fan to 56.3 and 54.3 on the north twin and east central fans (respectively). Most of the remainder of the boulders and cobbles on the east side are dolerite and sandstone. The dolerite fan has the highest amount of dolerite (18.4%) and the south twin fan the lowest (7.9%). The north twin fan has the highest amount of sandstone (23.8%), while the northeast fan has the lowest (3.4%). The results are represented visually in Figure 3.1. The figure demonstrates that broadly, the west shore sources (west shore, cirque glacier fan) and Linnéelva are characterized by the dominance of sandstone and phyllite, although which of these lithologies dominates in the boulder and cobble fraction of a given source varies. The east shore sites are characterized by a dominant carbonate fraction (50-80% of total), with significant portions of the remaining boulders and cobbles deriving from sandstone (3-23%) and dolerite (8-18%).

Location	sandstn.	phyllite	carbon.	conglom.	dolerite	shale	quartz	other	n
West Shore	182	34	1	2			18	1	238
%	*76.5*	*14.3*	*0.4*	*0.8*	*0.0*	*0.0*	*7.6*	*0.4*	
Cirque Glacier Fan	6	136					11		153
%	*3.9*	*88.9*	*0.0*	*0.0*	*0.0*	*0.0*	*7.2*	*0.0*	
Linneelva Fan	60	96		1			38	3	198
%	*30.3*	*48.5*	*0.0*	*0.5*	*0.0*	*0.0*	*19.2*	*1.5*	
Dolerite Fan	17		104	3	28				152
%	*11.2*	*0.0*	*68.4*	*2.0*	*18.4*	*0.0*	*0.0*	*0.0*	
South Twin Fan	26		111	3	12			0	152
%	*17.1*	*0.0*	*73.0*	*2.0*	*7.9*	*0.0*	*0.0*	*0.0*	
North Twin Fan	36		85	9	18			3	151
%	*23.8*	*0.0*	*56.3*	*6.0*	*11.9*	*0.0*	*0.0*	*2.0*	
East Central Fan	35		107	11	23	9		12	197
%	*17.8*	*0.0*	*54.3*	*5.6*	*11.7*	*4.6*	*0.0*	*6.1*	
Northeast Fan	7		169		22	5			203
%	*3.4*	*0.0*	*83.3*	*0.0*	*10.8*	*2.5*	*0.0*	*0.0*	

Table 3.2 Number and Percent of Each Lithology Present at Source: Boulders and Cobbles

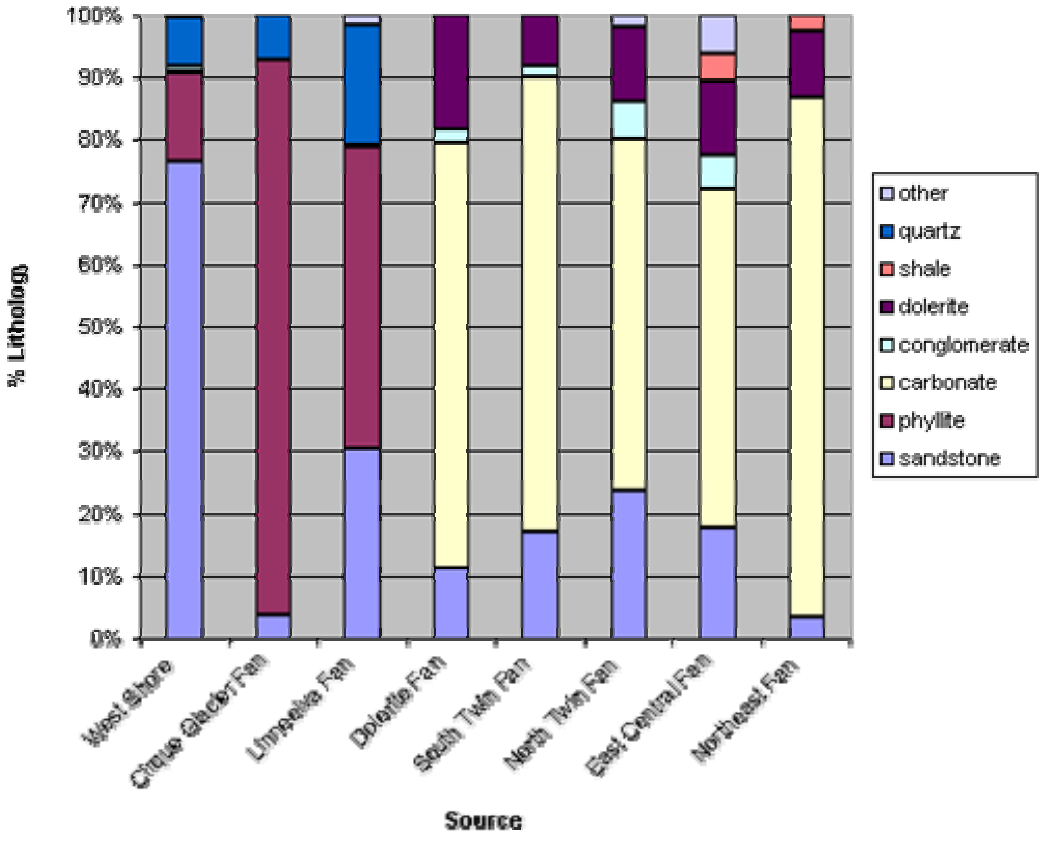

Figure 3.1 Percent Lithology Present at Source: Boulders and Cobbles

3.3 Surficial Sediment Analysis

3.3.1 Grain Size Analysis

The percent of each size fraction (gravel >2mm, sand between 2mm and 63μm, fines <63μm) for every surficial sample is shown in Table 3.3; fraction weights can be found in Appendix B, Table B.1. The measurement error associated with weighing the sand and gravel fractions is ±.05g, which is equivalent to between ±.1 to .2% error in percent composition of each size fraction in all of the surficial samples. Determination of this error can be found in Appendix B. Mean amount and standard deviation for each size fraction are calculated for the samples at each source. The west solifluction, west shore, dolerite, north and south twin, east central and northeast fans all show high standard deviations in all size fractions, in most cases at least half that of the mean. The cirque glacier fan and Linnéelva samples have lower standard deviations. Overall, gravel comprises between .4 and 8.8% at the Linnéelva and dolerites fan, respectively. Sand comprises between 37.6 (south twin fan) and 56.8% (dolerite fan) of the total sediment. Percent clay composition is the most variable, ranging from 14.1% in the dolerite fan to 41.8% of sediment in the northeast fan. Figure 3.2 is a ternary diagram showing the grain size distributions of the samples from each source. The diagram illustrates a lack of clustering either for samples from the same site, or from samples with similar transport mechanism (e.g. the solifluction lobes of the west shore do not cluster together). The exceptions to this scattered data are the samples from the two outwash fans: Linnéelva and the cirque glacier. The Linnéelva fan samples cluster between 50 and 75% sand with no gravel, and the cirque glacier fan samples cluster at about 50% sand and 30% clay.

location	% gravel	% sand	% fines	
West Solifluction	*15.5*	*53.1*	*31.3*	*mean*
	7.6	*26.5*	*26.0*	*stdev*
	0.1	*0.1*		*error*
West Shore	*13.6*	*41.7*	*52.2*	*mean*
	9.2	*27.2*	*26.3*	*stdev*
	0.1	*0.1*		*error*
Cirque Glacier Fan	*14.4*	*52.1*	*33.6*	*mean*
	9.4	*10.0*	*6.0*	*stdev*
	0.1	*0.1*		*error*
Linneelva Fan	*0.1*	*65.1*	*34.8*	*mean*
	0.0	*13.7*	*13.7*	*stdev*
	0.1	*0.1*		*error*
Dolerite Fan	*29.1*	*56.9*	*14.1*	*mean*
	9.7	*1.6*	*8.1*	*stdev*
	0.2	*0.2*		*error*
S. Twin Fan	*21.0*	*37.6*	*41.4*	*mean*
	22.0	*16.5*	*27.8*	*stdev*
	0.2	*0.2*		*error*
N. Twin Fan	*19.6*	*37.8*	*42.6*	*mean*
	10.0	*14.9*	*23.8*	*stdev*
	0.2	*0.2*		*error*
East Central Fan	*22.2*	*48.8*	*29.0*	*mean*
	12.0	*31.2*	*21.4*	*stdev*
	0.1	*0.1*		*error*
Northeast Fan	*4.8*	*53.4*	*41.8*	*mean*
	2.0	*28.0*	*26.7*	*stdev*
	0.2	*0.2*		*error*

Table 3.3 Grain Size Analysis of Surficial Sediments by Location

See Figure 3.2

3.3.2 Gravel Lithology

The results of the gravel identification of the surficial sediment samples are compiled in Table 3.4. The west solifluction sample is dominated by phyllite (53.6%), with signifcant amounts of sandstone (17.1%) and quartz (15.5%). The west shore sample has an even greater amount of phyllite (79.4%), with lesser amounts of sandstone (8.8%). The cirque glacier fan is overwhelming dominated by phyllite (98.2%). Other minor constituent lithologies identified on the west side include carbonate, dolerite and conglomerate. Linnéelva also shows a high amount of phyllite (83.3%) with dolerite comprising the remainder (16.7%). However, it should be noted that n=6 for this sample, due to the well sorted nature of the Linnéelva sediments and probably should not be regarded as a representative fan sample. The five east shore samples are characterized by high amounts of carbonate. The east central fan has the highest percent carbonate (70.4) while the north and south twin fan samples have the lowest (50 and 50.5, respectively). The second most abundant constituent of these five samples is dolerite, with the highest amount found in the dolerite fan (37.9%) and the lowest in the north twin fan sample (23.6%). Sandstone is a much less abundant lithology in the gravel fraction on the east shore; it ranges from 15% on the north twin fan to 1.9% in the east central fan sample. Minor amounts of Hecla Hoek quartz and phyllite were all also identified in the east shore samples. These results are displayed in Figure 3.3. The graph shows that generally, the west shore samples (west solifluction and west shore) can be characterized as dominated by phyllite with lesser amounts of sandstone and quartz, while the cirque glacier fan sample is almost exclusively phyllite. Gravel for the Linnéelva fan is not well represented by the samples collected. The east shore samples are dominated by

Location	sandstn.	phyllite	carbon.	conglom.	dolerite	Hecla Hoek	quartz	other	n
West Solifluction	85	280	0	1	35	11	77	8	497
%	*17.1*	*56.3*	*0.0*	*0.2*	*7.0*	*2.2*	*15.5*	*1.6*	
West Shore	47	413	8	0	22	0	19	11	520
%	*8.8*	*79.4*	*1.5*	*0.0*	*4.2*	*0.0*	*3.7*	*2.1*	
Cirque Glacier Fan	2	497	0	0	1	0	5	1	506
%	*0.4*	*98.2*	*0.0*	*0.0*	*0.2*	*0.0*	*1.0*	*0.2*	
Linneelva Fan	0	5	0	0	1	0	0	0	6
%	*0.0*	*83.3*	*0.0*	*0.0*	*16.7*	*0.0*	*0.0*	*0.0*	
Dolerite Fan	18	1	186	3	132	0	4	4	348
%	*5.2*	*0.3*	*53.4*	*0.9*	*37.9*	*0.0*	*1.1*	*1.1*	
South Twin Fan	10	10	151	5	97	10	14	2	299
%	*3.0*	*3.3*	*50.5*	*1.7*	*32.4*	*3.3*	*4.7*	*0.7*	
North Twin Fan	44	5	146	17	69	0	11	0	292
%	*15.0*	*1.7*	*50.0*	*5.8*	*23.6*	*0.0*	*3.8*	*0.0*	
East Central Fan	7	2	254	0	94	0	2	2	361
%	*1.9*	*0.6*	*70.4*	*0.0*	*26.0*	*0.0*	*0.6*	*0.6*	
Northeast Fan	6	0	74	0	33	0	0	1	114
%	*5.3*	*0.0*	*64.9*	*0.0*	*28.9*	*0.0*	*0.0*	*0.9*	

Table 3.4 Number and Percent of Each Lithology Present in Surficial Source Sediments: Gravel

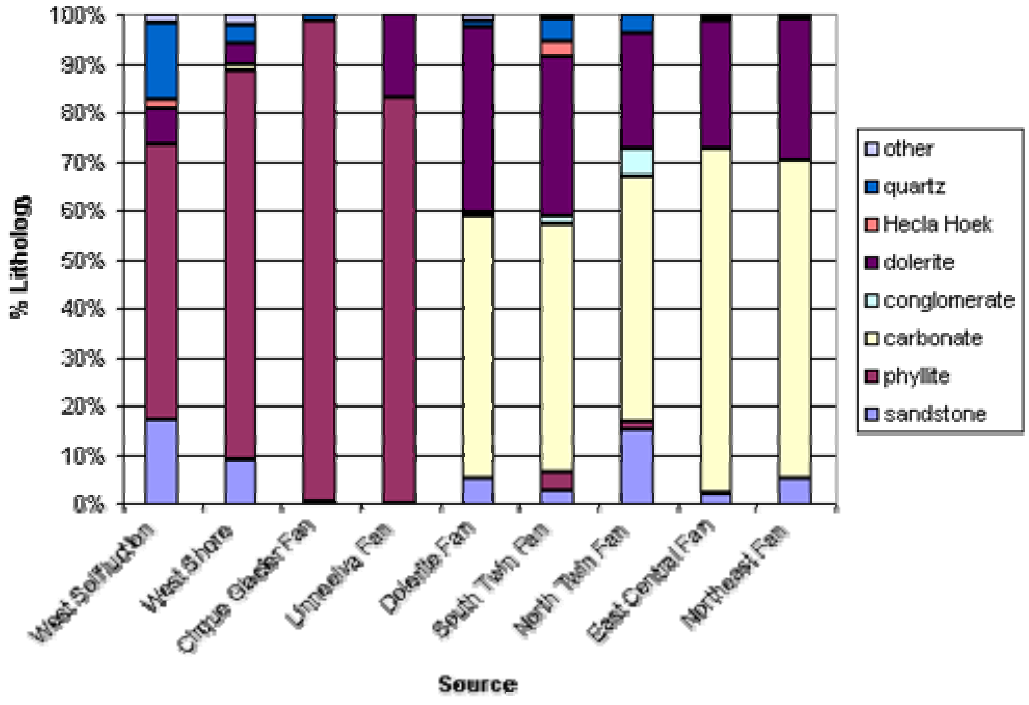

Figure 3.3 Percent of Each Lithology in Surficial Source Sediments: Gravel

carbonates (50-70%), with much of the remaining lithology deriving from the dolerite (27-38%).

3.3.3 XRD Analysis of Sand, Silt and Clay

The results of the XRD analysis identifying the minerals present in each size fraction from each sediment source studied are summarized in Table 3.5a-g. In the west solifluction, west shore and cirque glacier samples, quartz, muscovite, chlorite and kaolinite are present in all size fractions. The west solifluction and west shore samples have albite in the sand and silt fraction. The cirque glacier fan sample shows albite in all size fractions. In addition, the west solifluction and cirque glacier samples have lepidocrocite in the clay fraction. The west shore sample has calcite in the sand fraction, and dolomite and calcite in the silt fraction. In contrast, the cirque glacier fan has calcite and dolomite in the sand fraction and dolomite in the silt fraction. Generally, the west shore samples are characterized by the consistent presence of muscovite, chlorite and kaolinite in all size fractions, as well as the presence of albite in the sand and silt fractions.

The Linnéelva sample contains quartz, muscovite, chlorite and kaolinite in all size fractions. Albite is present in the sand and silt fractions of the fan. Additionally, calcite and dolomite are present in the sand fraction, with dolomite remaining in the silt fraction. Lepidocrocite is present in the clay-sized particles. On the basis of mineral presence and absence, sediments from Linnéelva are not ready distinguishable from the west shore sediments.

a. West Solifluction

	sand	silt	clay - air	clay - ethylene glycol	clay - 300C	clay - 550C
jpeg file name	*1sand*	*1silt*	*wstfolf1*	*wstsolf2*	*wstsolf3*	*wstsolf4*
quartz	x	x	x	x	x	x
albite	x	x				
muscovite	x	x	x	x	x	x
biotite					x	x
chlorite	x	x	x	x	x	x
kaolinite		x	x	x	x	
calcite						
dolomite						
lepidocrocite			x			

b. West Shore

	sand	silt	clay - air	clay - ethylene glycol	clay - 300C	clay - 550C
jpeg file name	*2sand*	*2silt*	*wstshor1*	*wstshor2*	*wstshor3*	*wstshor4*
quartz	x	x	x	x	x	x
albite	x	x				
muscovite	x	x	x	x	x	x
biotite	x				x	
chlorite	x	x	x	x	x	x
kaolinite		x	x	x	x	
calcite	x	x				
dolomite		x				

c. Cirque Glacier Fan

	sand	silt	clay - air	clay - ethylene glycol	clay - 300C	clay - 550C
jpeg file name	*3sand*	*3silt*	*cirque1*	*cirque2*	*cirque3*	*cirque4*
quartz	x	x	x	x	x	x
albite	x	x	x			
muscovite		x	x	x	x	x
biotite	x					x
chlorite	x	x	x	x	x	x
kaolinite			x	x	x	
calcite	x					
dolomite	x	x				
lepidocrocite			x			

d. Linnéelva Fan

	sand	silt	clay - air	clay - ethylene glycol	clay - 300C	clay - 550C
jpeg file name	*4sand*	*sandsiltclay4*	*linelva1*	*linelva2*	*linelva3*	*linelva4*
quartz	x	x	x	x	x	x
albite	x	x				
muscovite	x	x	x	x	x	x
biotite			x		x	x
chlorite	x	x	x	x	x	x
kaolinite			x	x	x	
calcite	x					

dolomite	x	x				
lepidocrocite			x	x		

Table 3.5 Summarized XRD Results of Mineral Composition of Surficial Sediment Samples
A jpeg file of each diffractogram is located in Appendix A

e. Twin Fans

	sand	silt	clay - air	clay - ethylene glycol	clay - 300C	clay - 550C
jpeg file name	*5sand*	*5silt*	*twins1*	*twins2*	*twins3*	*twins4*
quartz	x	x	x	x	x	x
muscovite	x	x	x	x	x	x
biotite			x			
chlorite						
kaolinite		x	x	x	x	
calcite	x	x				
dolomite	x	x				
ankerite	x	x				
enstatite						
rutile	x					
hematite	x			x		x

f. East Central Fan

	sand	silt	clay - air	clay - ethylene glycol	clay - 300C	clay - 550C
jpeg file name	*6sand*	*6silt*	*ec1*	*ec2*	*ec3*	*ec4*
quartz	x	x	x	x	x	x
muscovite		x	x	x	x	x
biotite			x		x	x
chlorite			x	x	x	x
kaolinite		x	x	x	x	
calcite	x	x	x		x	x
dolomite	x	x	x	x	x	x
ankerite	x					
enstatite		x				
kanoite		x				

g. Northeast Fan

	sand	silt	clay - air	clay - ethylene glycol	clay - 300C	clay - 550C
jpeg file name	*7sand*	*7silt*	*ne1*	*ne2*	*ne3*	*ne4*
quartz	x	x	x	x	x	x
muscovite		x	x	x	x	x
biotite			x	x	x	x
chlorite			x	x	x	x
kaolinite			x	x	x	
calcite	x	x				
dolomite	x	x	x			
ankerite	x	x				
enstatite						
rutile	x	x				

Table 3.5 (cont.) Summarized XRD Results of Mineral Composition of Surficial Sediment Samples
A jpeg file of each diffractogram is located in Appendix A

All three of the east shore samples (twin fans, east central fan and northeast fan) contain quartz in all the size fractions. The twin fans also contain muscovite in all size fractions, while in the east central and northeast fans, muscovite only shows up in the silt and clay fractions. Kaolinite is present in the silt and clay fractions of the twin fans; chlorite is absent. Kaolinite and chlorite show up only in the clay fractions of the east central and northeast fans. Calcite and dolomite are consistently present in the sand and silt fractions at the three eastern sites. Both are also present in the clay fraction on the east central fan; only dolomite shows up in the clay fraction of the northeast fan. In addition, ankerite is present in the sand and silt fractions of the twin and northeast fans. Hematite is present in the sand and clay fractions of the twin fans sample. Enstatite and another Mg-Fe pyroxene, kaolinite, are present in the silt fraction of the east central fan. Rutile is present in the sand fraction of the twin and northeast fans, and in the silt of the latter. In summary, the east shore samples are unique in the consistent presence of calcite and dolomite in the sand and silt fractions, the lack of chlorite (which is present only in the clay fraction), and the presence of accessory minerals such as enstatite and rutile.

Quantitative analysis of the percent of each mineral present in the different grain size fractions at each source shows further differences in the composition of source sediments. Although it is possible to distinguish relative amounts of kaolinite and chlorite in quantitative analysis (Curry and Grimley, 2006), this study did not undertake this analysis. Thus, the percent composition of chlorite presented represents a mixture of kaolinite and chlorite. The results of the quantitive XRD analysis for the sand fraction of the surficial sediments are presented in Table 3.6. In addition, Figures 3.4a and 3.4b display these results graphically. The quartz comprises between 60 and 75% of the total

	West Solifluction (%)	+/-	CEV	West Shore (%)	+/-	CEV	Cirque Glacier Fan (%)	+/-	CEV	Linnéelva Fan (%)	+/-	CEV
quartz	74.8	46.0	61.5	60.3	13.6	22.6	60.8	5.9	9.7	72.8	11.6	15.9
albite	17.3	10.6	61.3	30.9	7.0	22.7	7.8	0.8	10.3	2.9	0.5	17.2
chlorite/kaolinite	2.8	1.7	60.7	3.0	0.7	23.3	11.3	1.1	9.7	5.0	0.8	16.0
muscovite	5.1	3.2	62.7	4.6	11.0	239.1	20.2	2.0	9.9	19.2	3.1	16.1
calcite				1.5	0.3							
dolomite												
rutile												

	Twin Fans (%)	+/-	CEV	East Central Fan (%)	+/-	CEV	Northeast Fan (%)	+/-	CEV
quartz	77.1	23.3	30.2	69.4	3.2	4.6	65.0	6.0	9.2
albite									
chlorite/kaolinite									
muscovite	8.1	2.4	29.6						
calcite	4.3	1.3	30.2	11.3	0.5	4.4	10.6	1.0	9.4
dolomite	10.5	3.2	30.5	19.3	0.9	4.7	13.7	1.3	9.5
rutile							10.6	1.0	9.4

Table 3.6 Quantitative Analysis of Source Sediments: Sand
All percent (%) values are given as weight percent normalized
+/- is the error associated with the percent value, calculated by the quantitative analysis program
CEV is the coefficient of variance, which evaluates the magnitude of the error relative to the amount of the mineral present

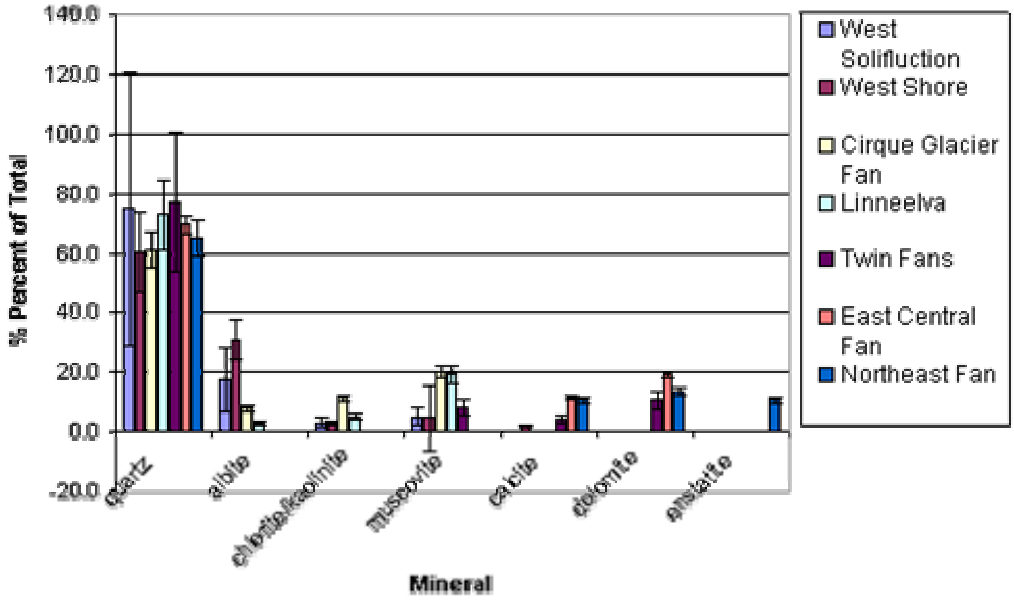

Figure 3.4a Percent Mineralogy of Source Sediments: Sand

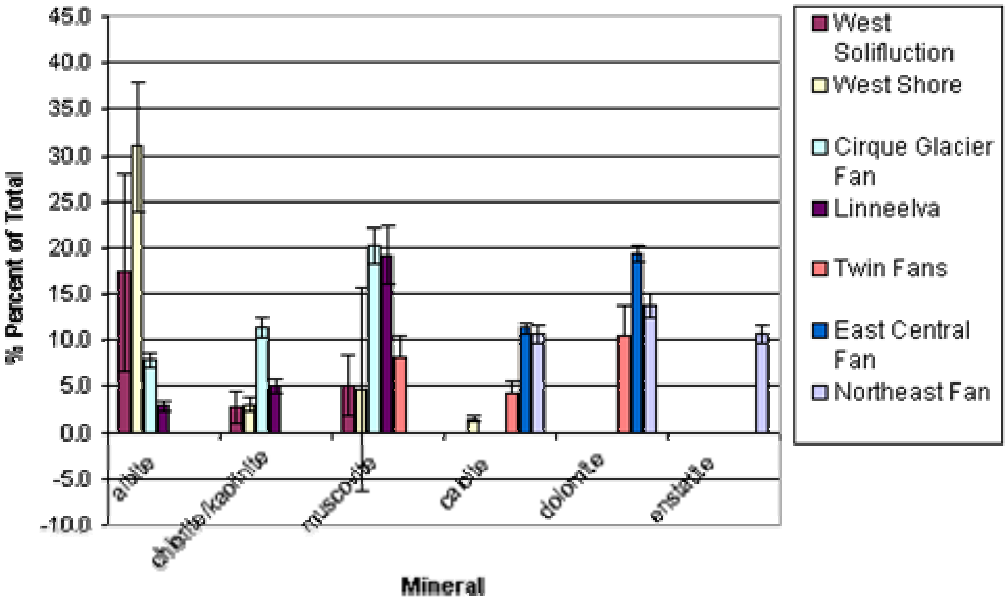

Figure 3.4b Percent Mineralogy of Source Sediments without Quartz: Sand

sand fraction at all the sites. No east-west trend for the quartz data exists (e.g. higher on one shore vs. the other). The west solifluction (74.8% ±46), west shore (60.3% ±13.6), Linnéelva (72.8% ±11.6) and twin fans (72.8% ±23.3) have very high standard deviations and coefficients of variance. The relatively low intensities of all other mineral peaks, compared to quartz, and subsequent low resolution of these peaks may be responsible for the high standard deviation observed. Heterogeniety of grain size in the powdered sample may also be a problem. Nonetheless, quartz can be identified as the mineral constituent with the proportionally highest concentration in the sand-size fraction in all samples despite the uncertainty related to its absolute quantity.

Albite is present in all three west shore samples, as well as on the Linnéelva fan; the quantitative analysis shows that it is present in greater amounts in the west shore sample (30.9% vs. 7.8 and 2.9% at the cirque glacier and Linnéelva fans, respectively) notwithstanding the standard deviation (±7) of the west shore sample. The high standard deviation (17.3% ±10.6) of the west solifluction albite casts uncertaintity on the absolute quantity of albite present in sample. Nonetheless, it is proportionally the second most important mineral in this sample. Thus, while absolute amounts of albite present in the west samples are not comparable, the west shore has relatively more albite than the cirque glacier fan. Additionally, in all three west samples, albite is the second most abundant mineral and is present in greater amounts than exist in the Linneélva sample. Chlorite/kaolinite is also present in all four of these samples; it is more abundant at the cirque glacier fan (11.3% ±1.1) than in the west solifluction (2.8% ±1.7), west shore (4.6% ± .7) and Linnéelva (5% ± .8) samples. Muscovite, present in the three west samples, Linnéelva and twin fans, comprises nearly 20% of the total sand in the cirque

glacier and Linnéelva fan samples. The high standard deviations and CEVs associated with the west solifluction (5.1% ±3.2, CEV=62.7) and west shore (4.6% ±11.0, CEV=239.1) preclude significant quantitative comparisons between these samples and the outwash fans. In summary, the relatively low amount of albite in the sand fraction in the Linnéelva fan distinguishes it from the three west sources, while the cirque glacier fan can be distinguished from the west shore and west solifluction sources by the higher amount of chlorite present.

The east shore sediments also differ from each other on the basis of relative amounts of carbonates and the presence/absence of enstatite. The twin fans sample has less calcite and dolomite in the sand size fraction (4.3% ±1.3 calcite, 10.5% ±3.2 dolomite) compared to the east central and northeast fans (11.3% ±.5, 19.3% ±.9 and 10.6% ±1, 13.7% ±1.3, respectively). The northeast fan is distinguished from the east central fan by the presence of enstatite.

Quantitative analysis of the silt size fraction of surficial sediments shows less prominent but still distinct differences between sources. Table 3.7 shows the results of the quantitative analysis of the silt-size fraction; Figures 3.5a and b graphically depict these results. The standard deviations associated with all the minerals in the twin fans and east central samples are very high; thus they are not considered for further analysis. The high error in these analyses are likely relately to the poor resolution of the sheet silicates. In addition, heterogeniety of grain size can not be ruled out.

The amount of quartz present in the silt-size fraction is more variable than that seen in the sand-size fraction. Amounts range from 30.5% ± 7.2 (northeast fan) and 32% ± 5.7 (cirque glacier fan) to 71.9% ± 7.4 (Linnéelva). Albite is present in the the west

	West Solifluction (%)	+/-	CEV	West Shore (%)	+/-	CEV	Cirque Glacier Fan (%)	+/-	CEV	Linnéelva Fan (%)	+/-	CEV
quartz	58.0	7.0	12.1	52.1	6.0	11.5	32.0	5.7	17.8	71.9	7.4	10.3
albite	13.4	1.6	11.9				23.6	4.2	17.8			
chlorite/kaolinite	9.2	1.1	12.0	9.8	1.1	11.2	13.9	2.4	17.3	4.3	0.4	9.3
muscovite	19.4	2.3	11.9	27.8	3.2	11.5	28.0	5.0	17.9	19.6	2.0	10.2
calcite				4.3	0.5	11.6						
dolomite				6.1	0.7	11.5	2.6	0.5	19.2	4.2	0.4	9.5

	Twin Fans (%)	+/-	CEV	East Central Fan (%)	+/-	CEV	Northeast Fan (%)	+/-	CEV
quartz	61.3	174.4	284.5	39.8	78.6	197.5	30.5	7.2	23.6
albite									
chlorite/kaolinite				3.2	6.1	190.6			
muscovite	10.7	30.5	285.0	5.0	9.8	196.0	5.6	1.3	23.2
calcite	2.4	6.8	283.3	13.2	26.0	197.0	3.6	0.9	25.0
dolomite	20.9	59.4	284.2	24.8	49.0	197.6	52.6	12.3	23.4

Table 3.7 Quantitative Analysis of Source Sediments: Silt
All percent (%) values are given as weight percent normalized
+/- is the error associated with the percent value, calculated by the quantitative analysis program
CEV is the coefficient of variance, which evaluates the magnitude of the error relative to the amount of the mineral present

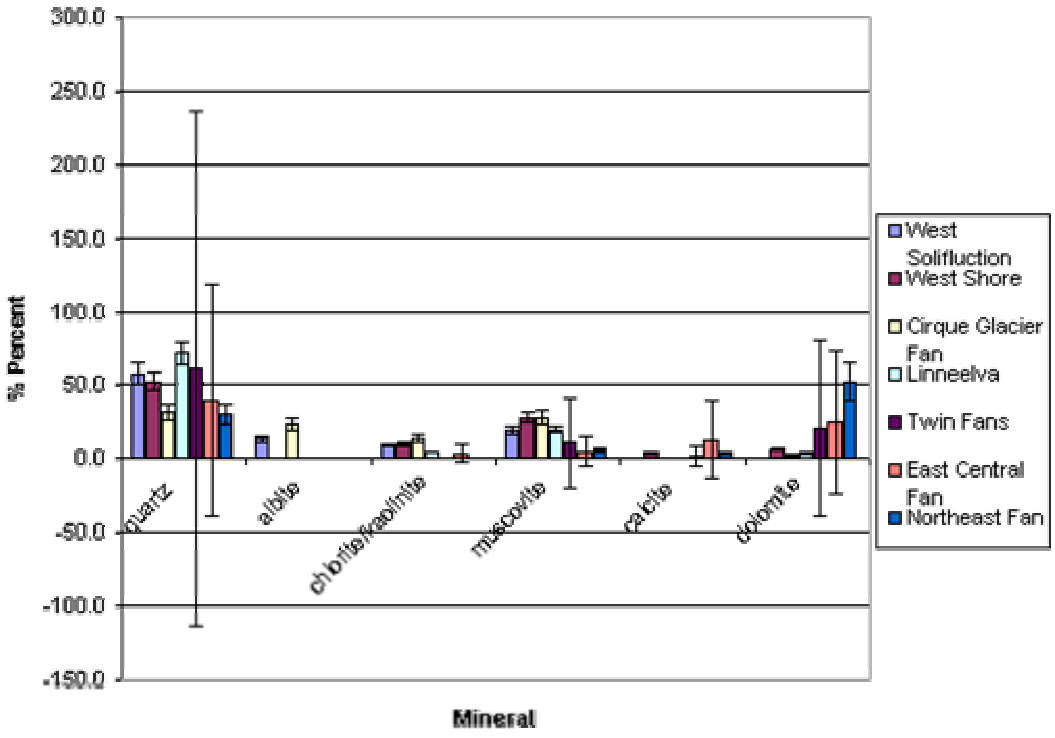

Figure 3.5a Percent Mineralogy of Source Sediments: Silt

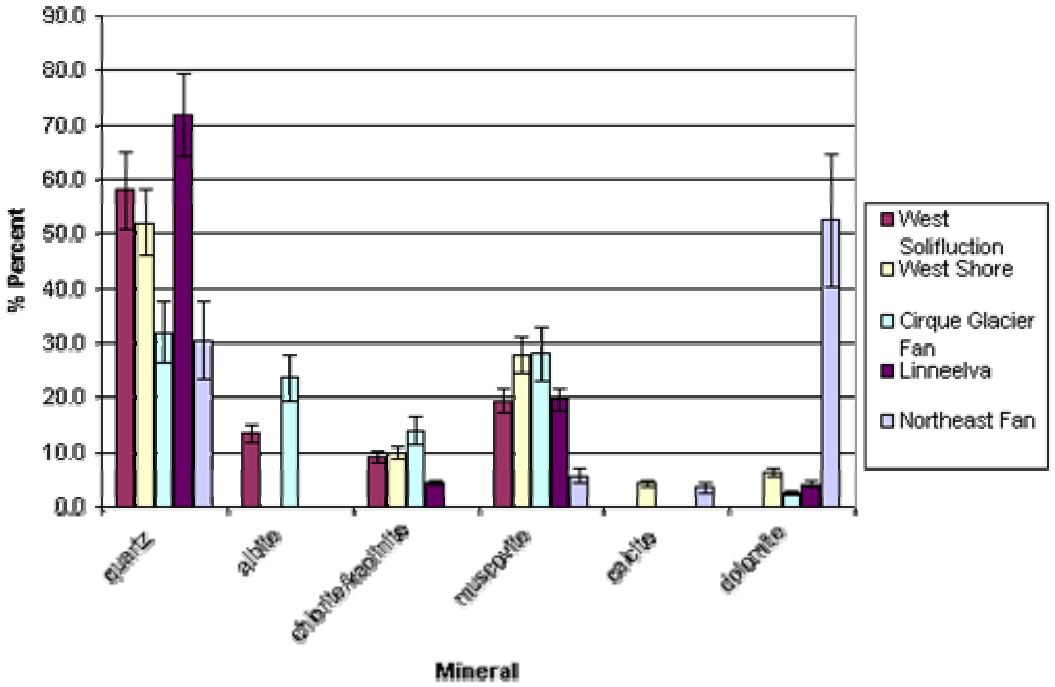

Figure 3.5b Percent Mineralogy of Source Sediments without Twin and East Central Fans: Silt

solifluction (13.4% ± 1.6) and cirque glacier fan (23.6% ± 4.2) samples. Higher amounts of chlorite/kaolinite (9.2-13.9%) in the three western samples distinguish them from the Linnéelva (4.3%) sample. Likewise, higher amounts of muscovite (19.4-28%) in the western and Linnéelva samples separate them from the northeast fan sample (5.6%). Calcite in the west shore and northeast fan samples shows similar values (4.3% ±.5 and 3.6% ± .9), but dolomite in the silt of the northeast fan (52.6% ± 12.3) is significantly greater than that found in west shore, cirque fan and Linnéelva samples (2.6-6.1%), notwithstanding the associated error. In summary, in the silt-sized fraction the three western sources are distinguished from Linnéelva and the northeast fan by higher amounts of chlorite/kaolinite. The relatively high amounts of albite in the cirque glacier fan and dolomite in the northeast fan make these sources unique.

The results from the quantitive analysis for the clay-sized fraction of the surficial sediments are summarized in Table 3.8. In addition, these results are graphically depicted in Figures 3.6a and b. The errors and CEVs associated with the quantity of minerals present in the Linnéelva sample (quartz 3.9% ± 5, CEV=128.2; chlorite/kaolinite 11.5% ± 14.5, CEV=126.1; muscovite 83.9% ± 105.8, CEV=126.1) precludes the significance of this data. The poor resolution seen in this diffractogram is likely due to a combination of not enough sample and variations in mineral composition.

In the clay fraction, sediments from different sources are close to indistinguishable. Quartz levels in all the samples (excluding Linnéelva) range from .8% ± .1 (east central fan) to 8.5% ± .6 (west solifluction). Based on the initital identification of sample composition, all sites must be assumed to be a mixture and chlorite and kaolinite, except the twins fans which contain only kaolinite. The highest levels of

	West Solifluction (%)	+/-	CEV	West Shore (%)	+/-	CEV	Cirque Glacier Fan (%)	+/-	CEV	Linnéelva Fan (%)	+/-	CEV
quartz	8.5	0.6	7.1	5.3	1.0	18.9	4.2	0.3	7.1	3.9	5.0	128.2
chlorite/kaolinite	25.6	2.0	7.8	35.4	6.5	18.4	42.8	2.6	6.1	11.5	14.5	126.1
muscovite	65.8	5.0	7.6	59.3	11.0	18.5	53.0	3.3	6.2	83.9	105.8	126.1
dolomite												

	Twin Fans (%)	+/-	CEV	East Central Fan (%)	+/-	CEV	Northeast Fan (%)	+/-	CEV
quartz	5.0	0.3	6.0	0.8	0.1	12.5	4.5	0.3	6.7
chlorite/kaolinite	17.1	1.0	5.8	34.3	2.5	7.3	12.5	0.8	6.4
muscovite	77.9	4.7	6.0	64.9	4.7	7.2	82.9	5.1	6.2
dolomite							0.6	0.4	66.7

Table 3.8 Quantitative Analysis of Source Sediments: Clay
All percent (%) values are given as weight percent normalized
+/- is the error associated with the percent value, calculated by the quantitative analysis program
CEV is the coefficient of variance, which evaluates the magnitude of the error relative to the amount of the mineral present

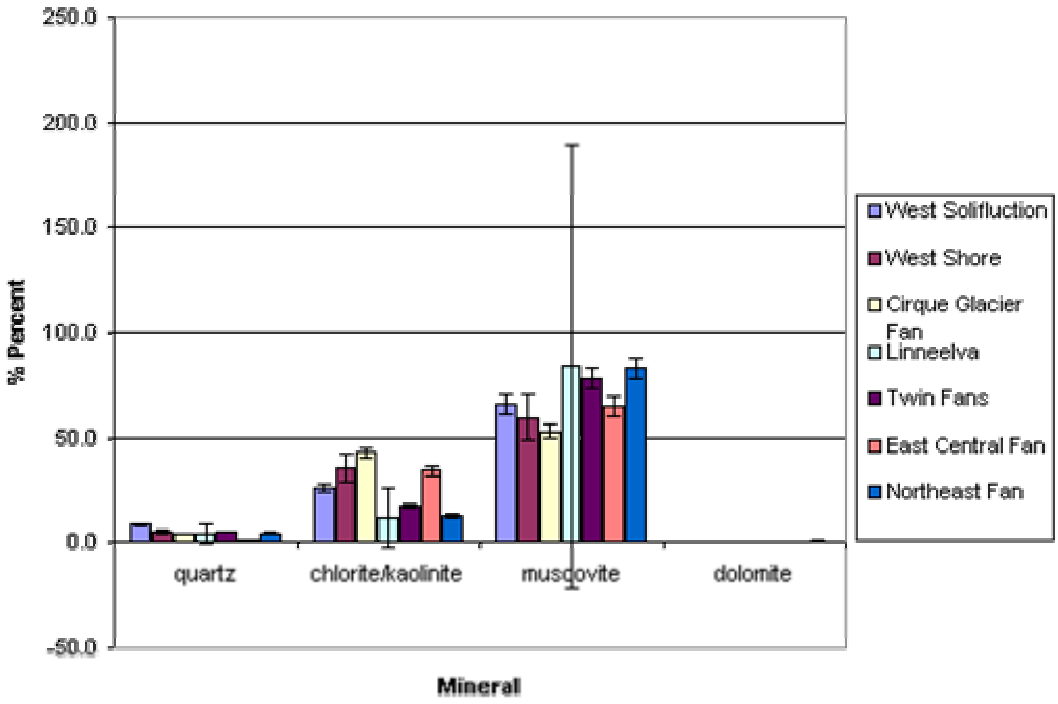

Figure 3.6a Percent Mineralogy of Source Sediments: Clay

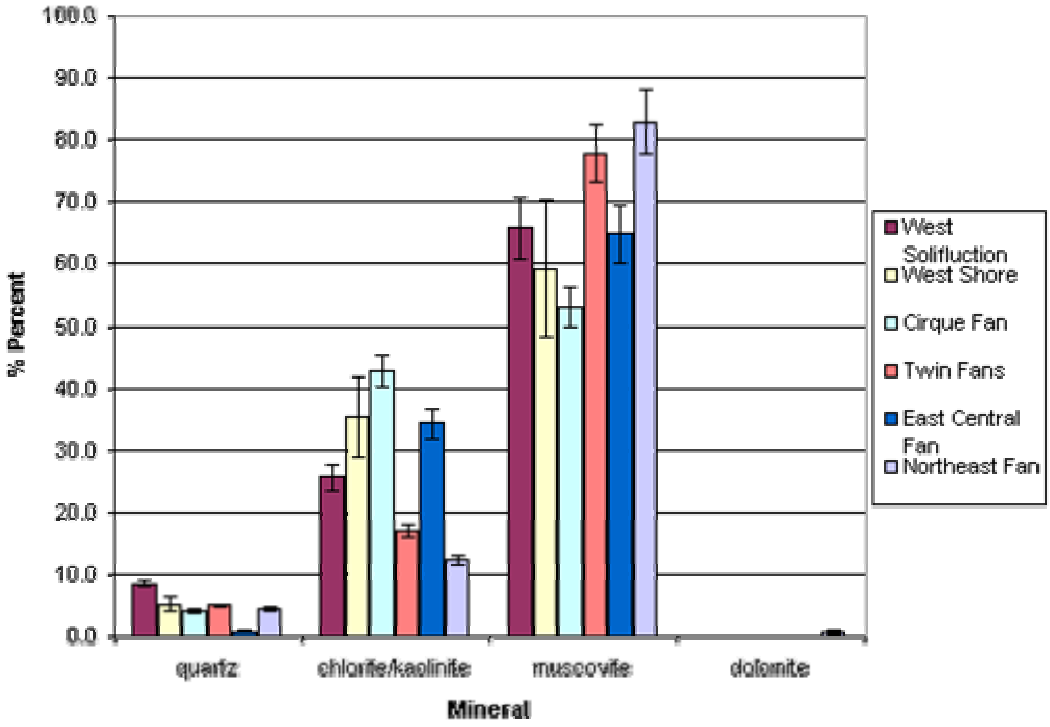

Figure 3.6b Percent Mineralogy of Source Sediments without Linnéelva: Clay

chlorite/kaolinite are present in the cirque glacier fan (42.8% ± 2.6); the west solifluction, west shore, and east central fans also high amounts of chlorite/kaolinite, ranging from 25.6% ± 2 (west solifluction) to 35.4% ± 6.5 (west shore). The remaining samples (twin and northeast fans) are comprised of less than 15% chlorite/kaolinite. The northeast fan is the only sample still containing carbonate in the clay-sized fraction (dolomite .6% ± .4) but the high error and CEV relative to the very minor amount present make it an unreliable indicator for provenance. In summary, high amounts of chlorite/kaolinite (25-43%) paired with lower amounts of muscovite (53-66%) separate the west side souces from the twin fans and northeast sediments (12-17% chlorite/kaolinite, 78-83% muscovite) but can not distinguish between the west sources and the east central fan (34% chlorite/kaolinite, 65% muscovite).

3.4 Sediment Core Analysis

3.4.1 Stratigraphy

Core 6 was obtained from 12m depth in the southeast basin of the lake. Figure 3.7 shows the location of recovered cores on a bathymetric map. The retrieved core is 13cm in length. Laminae are consistently diagonal, indicating that the core tube entered the sediment at an angle rather than perpendicular to the sediment surface. Depths were therefore taken from the center of the core half. Figure 3.8 is a diagram of core stratigraphy next to a digital photograph of the core. The core is continuously and well laminated from 0-12cm. The units from 0-4cm and 6.5-12cm contain alternating light brownish grey(Munsell® 2.5Y 6/2) and dark (2.5Y 5/2 greyish brown) layers. The unit

See Figure 3.7

See Figure 3.8

from 4-6.5cm is characterized by a darker dark layer (2.5Y 4/1, dark grey). From 12-13cm, the sediment is massive greyish brown (2.5Y 5/2) but it is likely that this stratigraphy was disturbed as a result of sediment loss and/or the tilted core tube.

Core 8 was retrieved from the southwest basin at 10.5m depth. The core is 25cm long with well preserved, detailed stratigraphy that is depicted in Figure 3.9. Distinctive units of strong, yellowish tan laminae occur throughout the core. Sediments from 0-2.5 are ~1mm, described as pale yellow (2.5Y 7/3) alternating with dark grey layers. From 2.5-5cm, laminae are also pale yellow alternating with dark grey, but are wider, approaching 2mm. The unit from 5 to 7.5cm is finely laminated, consisting of alternating greyish brown (2.5Y 5/2) and dark grey layers. From 7.5 to 9cm, sediments are similar to those at the top of the core: finely laminated with pale yellow and dark grey layers. Sediments from 9 to llcm are less distinctly yellow (2.5Y 6/3 light yellowish brown) alternating with dark grey and approach 2mm in width. The unit from 11-13.5cm is diffusely laminated, greyish brown and dark grey. Sediments from 13.5 to 14.5cm are finely laminated, pale yellow grading to light yellowish brown (alternating with dark grey). Yellowish layers are absent from 14.5 to 15cm. From 15 to 17.5cm, sediments are finely laminated with pale yellow grading downwards to light yellowish brown (alternating with dark grey). At 19.5cm a distinctive pale yellow lamina (2.5mm wide) occurs. Below this sharp boundary, from 19.5 to 25cm, sediments are diffusely laminated, alternating greyish brown and dark grey.

Core 12 was retrieved from a depth of 27m in the main north basin, north of the east central fan, and at 38cm in length is the longest core recovered. Stratigraphy is illustrated in Figure 3.10. The topmost unit, from 0 to 8.5cm, is finely laminated, with

See Figure 3.9

See Figure 3.10

alternately light olive brown (2.5Y 5/3) and dark grey (2.5Y 4/1) layers. From 8.5 to 12cm, sediment is diffusely laminated, greyish brown (2.5Y 5/2) and dark grey in color. The unit from 15-18cm is visibly coarser grained, characterized by thicker laminations (~2-3mm) and light yellowish brown color (10YR 6/4) and greyish brown color. The bottom unit, from 18 to 38cm, is finely laminated (>1mm), and with light yellowish brown and greyish brown laminae, characterized by the periodic wider (~1mm) light layers.

Core 11, was also recovered from the main north basin, south of the northeast fan at a depth of 24m, and is 24cm long. Depicted in Figure 3.11, its stratigraphy correlates well to that seen in core 12. The topmost unit, from 0 to 5cm, is finely laminated, with alternating light greyish brown (10YR 6/2) and dark grey (10YR 4.1) layers. A diffusely laminated unit occurs from 5-7cm, light greyish brown and dark grey in color. From 7-10cm, sediments are finely laminated, with alternating layers of light greyish brown and dark grey. The unit from 10-12cm is characterized by thicker laminae that are visibly coarser and lighter (brownish yellow 10YR 6/6, alternating with dark grey). From 12 to 24cm, the bottom unit, sediments dark grey and light greyish brown, finely laminated with periodic wider (~1mm) light layers.

3.4.2 Grain Size Analysis

The results of the continuous grain size analysis for core 6 are summarized in Table 3.9. Grain size fraction weights can be found in Appendix B, Table B.2. Sand sample 6-1 was lost during processing. The silt percent (and therefore clay percent) of sample 6-3 are erroneous and not included in mean or standard deviation calculation.

See Figure 3.11

sample	sand %	% silt	% clay	
0	2.7	97.1	0.2	
1		82.1	17.9	
3	2.8	*104.0*	*-6.9*	
4	7.3	88.2	4.5	
5	1.1	96.1	2.9	
6	2.1	86.8	11.2	
7	1.4	91.6	7.1	
8	1.8	76.6	21.6	
9	1.9	95.8	2.3	
10	5.8	79.2	15.0	
11	2.8	70.9	26.2	
12	3.9	77.9	18.2	
	3.1	*85.7*	*11.5*	*mean*
	1.9	*8.9*	*8.8*	*st dev.*
		1.3		*error*

Table 3.9 Core 6 Continuous Grain Size Analysis
Erroneous numbers are indicated by italics and are not
included in mean or standard deviation calculations

The values are likely due an error in either initial weight or initial transciption in the lab notebook. The error associated with weighing the silt fraction is ±.05g, which is equal to between ±1 to 3%. Silt is the dominant size fraction, ranging from 70-97% of the core, with a mean composition of 85.7%. Sand comprises between 1.5-7% of the sediment, averaging 3.1%. Clay composition ranges widely from .2-26.6%, with a mean value of 11.5%. A plot of the grain size is shown in Figure 3.12. Samples at 4 and 10cm show the largest amounts of sand, 7.3 and 5.8% respectively. These increases do not correspond to increases in the silt fraction, which show close to average compositions (88.2 and 79.2% respectively). The highest values of silt are observed at 0cm (97.1%), 5cm (96.1%), 7cm (91.6%) and 9cm (95.8%). The highest clay values occur at 8cm (21.6%), and between 10 and 12 cm (15.0-26.2%). As seen in Figure 3.12, this high percent clay layer correlates to the massive unit. Higher sand values (beginning at 4cm) coincide with lighter colored lamina.

Grain size analysis results for core 8 are presented in Table 3.10. Grain size fractions weights are presented in Appendix B, Table B.3. The silt (and therefore clay) fractions or samples 8-8, 8-11, 8-13, 8-15, 8-18, 8-21 and 8-23 are erroneous and not included in the mean or standard deviation calculations. Errors in samples 8-8, 8-11, 8-15 and 8-21 are related to errors in either initial weight or initial transciption into the lab notebook. The <63μm fraction of samples 8-13, 8-18 and 8-23 were lost to the lab bench during processing. The standard weighing error associated with the silt fraction is ±.05g, or ±1.8%. The silt fraction comprises the majority of the sediment present, ranging from 30.3-97.4%, with an average value of 76.5%. The amount of sand is less than that present in core 6; the sand fraction ranges from .2-2.8% and has a mean value of .9%.

See Figure 3.12

sample	sand %	% silt	% clay	
0	1.0	84.0	15.0	
1	0.8	84.6	14.6	
2	1.1	66.3	32.7	
3	1.0	84.4	14.6	
4	0.3	62.5	37.1	
5	0.5	73.0	26.5	
6	0.5	81.4	18.2	
7	0.8	97.0	2.2	
8	0.7	*100.6*	*-1.3*	
9	0.6	97.4	1.9	
10	1.2	90.5	8.3	
11	1.7	*178.9*	*-80.7*	
12	2.8	76.6	20.6	
13	0.5	*77.4*	*22.1*	
14	0.7	71.4	27.9	
15	1.8	*240.7*	*-142.5*	
16	0.2	30.3	69.5	
17	0.6	67.1	32.3	
18	1.0	*13.3*	*85.7*	
19	0.5	66.3	33.2	
20	0.5	79.8	19.7	
21	0.9	*370.3*	*-271.2*	
22	1.2	85.6	13.2	
23	1.8	*17.3*	*80.9*	
24	1.1	76.4	22.5	
25	0.6	79.7	19.7	
	0.9	*76.5*	*22.6*	*mean*
		15.0	*15.1*	*st dev*
		1.8		*error*

Table 3.10 Core 8 Continuous Grain Size Analysis
Erroneous numbers are indicated by italics and are not
included in mean or standard deviation calculations

Clay values range from 1.9-69.5%, averaging 22.6%. Figure 3.13 shows the continuous grain size plot for core 8. The highest sand values occur at 11cm (1.7%), 12cm (2.8%), 15cm (1.8%) and 23cm (1.8%). Broad increases in the amount of sand present occur between 0-3cm, 10-13cm, and 21-24cm. The latter two peaks correspond to the diffuse units observed from 11-13.5cm and 19.5-23cm in the core stratigraphy. Silt peaks occur at 7cm (97.0%), 9cm (97.4%), and 22cm (85.6%). A drastic increase in the clay fraction occurs at 17cm. With the exception of 3cm (14.6%), a general increase in the clay-size fraction is observed between 2 and 6cm (ranging from 26.5 to 37.1%). This increase in clay roughly corresponds with a unit of the distinctive yellow lamina from 0-5cm. Likewise, the high clay peak at 17cm is bracketed by a general increase in the percent clay present between 14 and 19 cm (ranging between 27.9 and 33.2%), and broadly correlates to a unit of yellow laminae from 13.5-17.5cm and the distinct yellow layer at 19.5cm. In contrast, the broad silt peak observed at 7-10cm (range of 90-97%) corresponds to a distinctive yellow unit at 7.5-11cm.

Table 3.11 shows the results of the core 12 grain size analysis. Grain size fraction weights are in Appendix B, Table B.4. The error associated with weighing the silt is ±.05g, or ±2.9%. Silt and clay values are unavaible for sample 8-15 due to either an error in the initial weight or in the initial transcription of values in the lab notebook. Sample 12-36 was lost during sample processing. Silt comprises the majority of the sediment with an average percent composition of 73.4 but varies significantly, from 42.4 to 97.5%. The clay fraction represents an average of 26.4% of the total sediment and ranges from 1.9-57.5%. Sand makes up an average of only .3% of the total sediment, with a range of .1 to 2%. The plot of the grain size results is shown in Figure 3.14. The peak sand

See Figure 3.13

sample	sand %	% silt	% clay	
0	0.5	92.5	7.0	
1	0.4	81.6	18.0	
2	0.3	79.8	20.0	
3	0.3	91.3	8.4	
4	0.5	97.0	2.5	
5	2.0	46.3	51.7	
6	0.2	42.4	57.5	
7	0.1	80.5	19.4	
8	0.1	88.3	11.6	
9	0.2	73.1	26.7	
10	0.1	50.4	49.5	
11	0.2	73.4	26.4	
12	0.2	86.6	13.2	
13	0.1	96.2	3.7	
14	0.6	74.7	24.9	
15	*0.6*	*124.0*	*-24.6*	
16	0.5	63.5	36.2	
17	0.4	84.1	15.5	
18	0.1	85.0	14.8	
19	0.4	86.4	13.2	
20	0.5	97.5	1.9	
21	0.3	78.7	21.1	
22	0.4	80.0	19.7	
23	0.3	73.2	26.4	
24	0.1	69.9	29.9	
25	0.1	71.4	28.4	
26	0.1	92.4	7.4	
27	0.1	79.9	19.9	
28	0.2	44.5	55.3	
29	0.2	44.7	55.0	
30	0.3	87.0	12.7	
31	0.2	53.7	46.1	
32	0.1	59.4	40.4	
33	0.1	67.9	32.0	
34	0.1	52.4	47.5	
35	0.1	49.1	50.8	
36	n/a	n/a	n/a	
37	0.1	65.8	34.1	
	0.3	*73.4*	*26.4*	*mean*
	0.3	*16.6*	*16.6*	*st. dev*
		2.9	*2.3*	*error*

Table 3.11 Core 12 Continuous Grain Size Analysis
Erroneous numbers are indicated by italics and are not
included in mean or standard deviation calculations

See Figure 3.14

composition (2%) occurs at 5cm and corresponds to a particularly low silt value (46.3%) and has no distinct stratigraphic corrollary. A second sand peak (.6%) at 15 and 16cm corresponds to below average silt composition (63.5%). These low silts values, in addition to two high silt values (85 and 86.4%) at 18 and 19cm, correspond to the visibly coarser, lighter unit observed between 15 and 18cm. Peaks in percent clay composition (range of 47.5-57.5%) occur at 5-6, 10, 28-29 and 34-35cm.

The summarized results of the core 11 grain size analysis are seen in Table 3.12. Grain size fraction weights are presented in Appendix B, Table B.5. The silt and clay percent fractions are erroneous for sample 11-0. This is due to an error in the initial weight or the initial transcription to the lab notebook. The weighing error for the silt fraction is ±.05g, which is equal to ±2.2%. In core 11, the silt-size fraction comprises the majority of the sediment (75.9% mean, with a range of 48.1-87.3%). Clay represents an average of 23.2% and ranges from 11.8-51.6%. The sand-size fraction accounts for an average of .9% of the total sediment and ranges from .2 to 5.9%. Excluding the 5.9% peak, the mean sand composition is .7%. Figure 3.15 graphically depicts the grain size results alongside the stratigraphy for core 11. The peak sand composition (5.9%) occurs at 10cm and correlates well with the observed coarse unit at 10-12cm and a silt peak of 82.5%. Slightly heightened sand values at 0-1cm, 13cm and 17cm (1, 1.1 and .9%) are coupled with elevated amounts of silt (77.7, 85.4 and 87.3%). Heightened sand values at 12 and 15cm (.7 and 1.1%) are decoupled from silt trends (76.2 and 72.9%). Consistently high clay values (ranging from 30.4-33.7%) between 5 and 7cm correspond to the diffusely laminated stratigraphic unit.

sample	sand %	% silt	% clay	
0	1.0	*119.8*	*-20.8*	
1	1.0	77.7	21.3	
2	0.5	65.7	33.8	
3	0.65	71.7	27.7	
4	0.5	82.3	17.2	
5	0.3	65.9	33.7	
6	0.40	67.9	31.7	
7	0.2	69.3	30.4	
8	0.4	48.1	51.6	
9	1.1	75.0	23.9	
10	5.95	82.5	11.6	
11	0.8	75.6	23.6	
12	0.7	76.2	23.0	
13	1.1	85.4	13.4	
14	0.6	86.6	12.8	
15	1.08	72.9	26.0	
16	0.4	78.1	21.5	
17	0.9	87.3	11.8	
18	0.6	85.6	13.8	
19	0.52	82.3	17.2	
20	0.3	75.8	23.8	
21	0.7	82.0	17.2	
	0.9	*75.9*	*23.2*	*mean*
	1.2	*9.3*	*9.6*	*st. dev.*
		2.2		*error*

Table 3.12 Core 11 Continuous Grain Size Analysis
Erroneous numbers are indicated by italics and are not
included in mean or standard deviation calculations

See Figure 3.15

3.4.3 XRD Analysis of Core Sediments: Silt and Clay

The mineral composition of the core 6 sediment samples can be seen in Table 3.13a-e. Samples are labeled according to core number and sample depth (e.g. core 6, 0cm is written 6-0). Quartz, muscovite, chlorite and kaolinite are present in both the silt and clay fractions for all five of the core 6 samples. Dolomite occurs in the silt fraction of all five samples. In addition, Sample 6-0 contains iron oxide (lepidocrocite, hematite) in the clay fraction. At 3cm, core 6 has both calcite and dolomite in the silt fraction and dolomite and iron oxide (lepidocrocite, magnetite) in the clay fraction. In sample 6-5, only lepidocrocite shows up in the clay fraction. At a depth of 7cm in core 6, dolomite and lepidocrocite occur in the clay fraction. Finally, sample 6-9 contains lepidocrocite in the clay fraction.

The results of the quantitative analysis of core 6 silt and clay samples are summarized in Table 3.14 and displayed graphically in Figure 3.16. Sample 6-3 is not included in the analysis because of a high coefficient of variance, likely resulting from compositional variations causing low resolution in the diffractogram for the minor mineral constituents in the diffractogram. The amount of quartz in the silt size fraction ranges from 34.6 ± 2.6 to 48.6% ± 9.1 in samples 6-9 and 6-0, respectively. Based on the magnitude of error and CEVs, sample 6-9 has relatively less quartz than the other four samples, which are not significantly different. Muscovite quantities range from 40.8 ± 2.3 to 50.6% ± 3.8 (6-0 and 6-3). Thus, sample 6-3 has relatively more muscovite, and remaining four samples are comparable in quantity. The amount of chlorite varies from 9% ± .5 in 6-0 to 10.6% ± .8 at 6-7; changes in chlorite quantity are not considered large

a. Sample 6-0

	silt	**clay - air**	**clay - 550C**
jpeg file name	*6-0S*	*6-0A*	*6-0H*
quartz	x	x	x
muscovite	x	x	x
biotite	x	x	
chlorite	x	x	x
kaolinite		x	
calcite			
dolomite	x		
lepidocrocite		x	
hematite			x

b. Sample 6-3

	silt	**clay - air**	**clay - 550C**
jpeg file name	*6-3S*	*6-3A*	*6-3H*
quartz	x	x	x
muscovite	x	x	x
biotite			x
chlorite	x	x	x
kaolinite	x	x	
calcite	x		
dolomite	x	x	
lepidocrocite		x	
magnetite			x

c. Sample 6-5

	silt	**clay - air**	**clay - 550C**
jpeg file name	*6-5S*	*6-5A*	*6-5H*
quartz	x	x	x
muscovite	x	x	x
biotite			x
chlorite	x	x	x
kaolinite	x	x	
calcite			
dolomite	x		
lepidocrocite		x	
hematite			

d. Sample 6-7

	silt	**clay - air**	**clay - 550C**
jpeg file name	*6-7S*	*6-7A*	*6-7H*
quartz	x	x	x
muscovite	x	x	x
biotite	x		x
chlorite	x	x	x
kaolinite	x	x	
calcite			
dolomite	x	x	
lepidocrocite		x	
hematite			

e. Sample 6-9

	silt	**clay - air**	**clay - 550C**
jpeg file name	*6-9S*	*6-9A*	*6-9H*
quartz	x	x	x
muscovite	x	x	x
biotite	x		x
chlorite	x	x	x
kaolinite	x	x	
calcite			
dolomite	x		
lepidocrocite		x	
hematite			

Table 3.13 Mineralogy of Core 6 Samples: Silt and Clay
A jpeg file of each diffractogram is in Appendix A

a. Silt

sample	quartz (%)	+/-	CEV	muscovite (%)	+/-	CEV	chlorite (%)	+/-	CEV	lepidocrocite (%)	+/-	CEV	dolomite (%)	+/-	CEV	
0	43.6	2.5	6.0	40.8	2.3	4.7	9	0.5	5.3				6.7	0.4	7.3	
3	*48.6*	*9.1*	*21.9*	*64.8*	*6.5*	*13.2*	*8*	*1.5*	*16.0*				*7.6*	*1.4*	*25.5*	
5	42.1	2.9	7.0	43.5	2.9	5.9	9.3	0.6	6.4				5.1	0.3	5.5	
7	39	3.9	9.4	47.2	3.5	7.1	10.6	0.8	8.5				3.2	0.2	3.6	
9	34.6	2.6	6.3	50.6	3.8	7.7	10	0.8	8.5				4.7	0.4	7.3	
	41.6			49.4			9.4						5.5			mean

b.
Clay

sample	quartz (%)	+/-	CEV	muscovite (%)	+/-	CEV	chlorite (%)	+/-	CEV	lepidocrocite (%)	+/-	CEV	dolomite (%)	+/-	CEV	
0	*4.2*	*0.8*	*12.5*	*61.8*	*11.1*	*19.2*	*32.4*	*5.8*	*16.8*	*1.6*	*0.3*	*25.0*				
3	*13.5*	*2.7*	*42.2*	*50.8*	*10.1*	*17.5*	*35.3*	*7.1*	*20.5*	*0.4*	*0.1*	*8.3*				
5	*3.9*	*3.9*	*60.9*	*60.8*	*0*	*0.0*	*35.1*	*0*	*0.0*	*0.1*	*0*	*0.0*				
7	*6.7*	*2*	*31.3*	*58.1*	*17*	*29.4*	*33.3*	*9.7*	*28.0*	*1.9*	*0.6*	*50.0*				
9	*3.8*	*0.4*	*6.3*	*57.4*	*5.9*	*10.2*	*36.9*	*3.8*	*11.0*	*1.9*	*0.2*	*16.7*				
	6.4			57.8			34.6			1.2						mean

Table 3.14 Core 6 Mineralogy: Quantitative Analysis
All percent (%) values are given as weight percent normalized
+/- is the error associated with the percent value, calculated by the quantitative analysis program
CEV is the coefficient of variance, which evaluates the magnitude of the error relative to the amount of the mineral present
Italics indicate a CEV greater than 10%

See Figure 3.16

enough to be significant. Dolomite ranges from 3.2% ± .2 at a depth of 7cm to 6.7% ± .4 at 0cm; these changes are also not considered significant.

In the clay-sized fraction, all samples exhibit high coefficient of variance values. The large uncertainty is due to the poor peak resolution and low intensity of the clay diffractograms, which in turn is likely caused by a low concentration of sample material and probable differences in mineral composition. Quartz compositions range from 3.8% ± 6.3 (6-9) to 13.5% ± 2.7 (6-3). Thus sample 6-3 contains a relatively high amount of quartz. The amount of muscovite present varies from 50.5% ± 10.1 to 61.8% ± 11.1 in samples 6-3 and 6-0, respectively. Given the magnitude of error and substantiated by high CEV values, these shifts are not considered significant. Chlorite values change only slightly between samples, from 32.4% ± 5.8 in sample 6-0 to 36.9% ± 3.8 in sample 6-9. Like, the amount of lepidocrocite present varies little, from .1 to 1.9%.

The presence of calcite in sample 6-3 is associated with average sand composition, but the high amount of muscovite in the silt fraction and quartz in the clay fraction can not be related to silt and clay amounts due to the loss of this sample during processing. The relatively low amount of quartz in sample 6-9 corresponds to an increase in the amount of silt present.

The results of the XRD analysis for core 8 sediments are displayed in Table 3.15a-e. Samples at all depths contain quartz, muscovite, chlorite and kaolinite in both the silt and clay-sized fractions, and dolomite in the silt fraction. In addition, samples 8-1, 8-6 and 8-10 contain dolomite in the clay-sized fraction. In samples 8-6, 8-10 and 8-21, lepidocrocite occurs in the clay fraction. Sample 8-6 also contains hematite.

a. Sample 8-1

	silt	**clay - air**	**clay - 550C**
jpeg file name	*8-1S*	*8-1A*	*8-1H*
quartz	x	x	x
albite			
muscovite	x	x	x
biotite	x		x
chlorite	x	x	x
kaolinite		x	
calcite			
dolomite	x	x	
lepidocrocite			
hematite			

b. Sample 8-6

	silt	**clay - air**	**clay - 550C**
jpeg file name	*8-6S*	*8-6A*	*8-6H*
quartz	x	x	x
albite			
muscovite	x	x	x
biotite	x		
chlorite	x	x	x
kaolinite		x	
calcite			
dolomite	x	x	
lepidocrocite		x	
hematite			x

c. Sample 8-10

	silt	**clay - air**	**clay - 550C**
jpeg file name	*8-10S*	*8-21A*	*8-21H*
quartz	x	x	x
albite	x		
muscovite	x	x	x
biotite			x
chlorite	x	x	x
kaolinite		x	
calcite			
dolomite	x	x	
lepidocrocite		x	
hematite			

d. Sample 8-15

	silt	**clay - air**	**clay - 550C**
jpeg file name	*8-15S*	*8-15A*	*8-15H*
quartz	x	x	x
albite			
muscovite	x	x	x
biotite			x
chlorite	x	x	x
kaolinite		x	x
calcite			
dolomite	x		
lepidocrocite			
hematite			

e. Sample 8-21

	silt	**clay - air**	**clay - 550C**
jpeg file name	*8-21S*	*8-21A*	*8-21H*
quartz	x	x	x
albite			
muscovite	x	x	x
biotite	x		
chlorite	x	x	x
kaolinite		x	
calcite			
dolomite	x		
lepidocrocite		x	
hematite			

Table 3.15 Mineralogy of Core 8 Samples: Silt and Clay
A jpeg file of each diffractogram is in Appendix A

Table 3.16 summarizes the results of the sand and silt quantitative mineral analyses for core 8. In the silt-size fraction, samples 8-10, 8-15 and 8-21 have high coefficients of variance. Some fronting is seen in the muscovite and chlorite/kaolinite peaks in these diffractograms, possibly indicating composition variations. Resolution may also be affected by heterogeniety of grain size, a result of insufficient grinding during sample preparation. The amount of quartz ranges from 24.1% ±7.4 to 42.8% ±4.0 in samples 8-15 and 8-1. Overall, sample 8-15 has relatively low amounts of quartz. Muscovite content varies very slightly from 42.2% ±4 in sample 8-1 to 52.6% ± 16.2 in sample 8-15. The high errors and CEVs associated with these values precludes the significance of these shifts in quantity. The amount of chlorite present ranges from 12.2% ±1.2 to 21.6% ± 6.7 (8-1 and 8-15). This variation, given the range of error and CEV values, is not great enough to consider shifts significant. Dolomite concentrations vary from 1.7% ± .05 (8-21) to 3.6% ± .3 (8-6), a difference which is not considered important.

In the clay fraction, all samples have high CEV values. The error associated with these samples can be attributed to poorly resolved peaks. In samples 8-10 and 8-21 in particular, the muscovite peaks are extraordinarily broad and the major quartz peak at 26.6 two-theta – which is also a secondary peak for muscovite – also shows poor resolution. Thus in these samples it's likely that a significant composition difference in muscovite, or the presence of a clay mineral with similar peaks, is the primary contributor to overall poor resolution. Sample concentration is not thought to be a major factor because the intensities approach 1000 counts. Percent mineral composition varies little for muscovite and quartz. Quartz quantities have a maximum range of 6.4 to 9.0%

a. Silt

sample	quartz (%)	+/-	CEV	muscovite (%)	+/-	CEV	chlorite (%)	+/-	CEV	lepidocrocite (%)	+/-	CEV	dolomite (%)	+/-	CEV	
1	42.8	4.0	11.6	42.2	4.0	8.6	12.2	1.2	7.3				2.7	0.3	11.5	
6	39.2	3.2	9.3	42.9	3.5	7.5	14.3	1.2	7.3				3.6	0.3	11.5	
10	*33.4*	*3.8*	*11.0*	*44.1*	*5.0*	*10.8*	*19.3*	*2.2*	*13.3*				*3.1*	*0.4*	*15.4*	
15	*24.1*	*7.4*	*21.5*	*52.6*	*16.2*	*34.9*	*21.6*	*6.7*	*40.6*				*1.7*	*0.5*	*19.2*	
21	*32.5*	*8.6*	*25.0*	*50.6*	*13.4*	*28.8*	*15.1*	*4.0*	*24.2*				*1.7*	*0.5*	*19.2*	
	34.4			46.5			16.5						2.6			mean

b.
Clay

sample	quartz (%)	+/-	CEV	muscovite (%)	+/-	CEV	chlorite (%)	+/-	CEV	lepidocrocite (%)	+/-	CEV	dolomite (%)	+/-	CEV	
1	*9.0*	*1.6*	*21.6*	*61.7*	*10.7*	*16.7*	*28.4*	*4.9*	*16.7*				*0.9*	*0.2*	*33.3*	
6	*7.1*	*1.4*	*18.9*	*62.7*	*12.3*	*19.2*	*28.3*	*5.5*	*18.8*	*2.0*	*0.4*	*21.1*				
10	*7.1*	*2.8*	*37.8*	*64.4*	*25.8*	*40.4*	*28.3*	*11.3*	*38.6*				*0.3*	*0.1*	*16.7*	
15				*63.6*	*2.1*	*3.3*	*36.4*	*1.2*	*4.1*							
21	*6.4*	*0.7*	*9.5*	*66.9*	*7.4*	*11.6*	*25.0*	*2.8*	*9.6*	*1.8*	*0.2*	*10.5*				
	7.4			63.9			29.3			1.9			0.6			mean

Table 3.16 Core 8 Mineralogy: Quantitative Analysis
All percent (%) values are given as weight percent normalized
+/- is the error associated with the percent value, calculated by the quantitative analysis program
CEV is the coefficient of variance, which evaluates the magnitude of the error relative to the amount of the mineral present
Italics indicate a CEV greater than 10%

(samples 8-21 and 81, respectively) white muscovite varies from 61.7% in sample 8-1 to 66.9% in 8-21. Quartz is present in sample 8-21 but was removed from the original quantitative analysis due to high associated error. The amount of chlorite shifts from 25.0 to 36.4% in 8-21 to 8-15. While sample 15 thus has relatively more chlorite than sample 21, significant comparisons can not be drawn to the other three depths due to high error in those samples. Lepidocrocite and dolomite occur only in very small amounts (<2%) in select samples; thus shifts are not thought to be important.

Graphs of the change in percent mineral composition down core, plotted against grain size, can be seen in Figure 3.17. The presence of dolomite in the clay fraction in samples 8-1 and 8-10 correspond to peaks in the silt size fraction. Low quartz quantity in silt sample 8-15 occurs with an increase in percent sand and just above a major peak in clay content.

The mineralogy of core 12 sediment samples are summarized by Table 3.17. All of the samples from core 12 have quartz, muscovite, chlorite and kaolinite in the silt and clay fractions. Additionally, each sample contains iron oxide (lepidocrocite and hematite) in the clay-sized fraction. Samples 12-5, 12-15, 12-22 and 12-30.5 contain dolomite in the silt-sized fraction. In addition, orthopyroxene occurs in the silt fraction in samples 12-15 and 12-30.5.

The results of the quantitative analysis of the silt and clay fractions of core 12 sediments are displayed in Table 3.18. The amount of quartz in the silt-size fraction ranges from 28.7% ± 2.3 (12-30.5) to 39.5% ± 1.9 (12-22). Thus sample 12-5 and 12-22 have relatively more quartz than 12-10, 12-15 and 12-30.5. Muscovite shows no significant variations, with values ranging from 45.3% ± 4.3 to 51.3% ± 2.3 in samples

See Figure 3.17

a. Sample 12-5

	silt	**clay - air**	**clay - 550C**
jpeg file name	*12-5S*	*12-5A*	*12-5H*
quartz	x	x	x
muscovite	x	x	x
biotite			
chlorite	x	x	x
kaolinite	x	x	
calcite			
dolomite	x		
orthopyroxene			
lepidocrocite		x	
hematite			

b. Sample 12-10

	silt	**clay - air**	**clay - 550C**
jpeg file name	*12-10S*	*12-10A*	*12-10H*
quartz	x	x	x
muscovite	x	x	x
biotite			
chlorite	x	x	x
kaolinite	x	x	
calcite			
dolomite			
orthopyroxene			
lepidocrocite		x	
hematite			x

c. Sample 12-15

	silt	**clay - air**	**clay - 550C**
jpeg file name	*12-15S*	*12-15A*	*12-15H*
quartz	x	x	x
muscovite	x	x	x
biotite			
chlorite	x	x	x
kaolinite	x	x	
calcite			
dolomite	x		
orthopyroxene	x		
lepidocrocite		x	
hematite			x

d. Sample 12-22

	silt	**clay - air**	**clay - 550C**
jpeg file name	*12-22S*	*12-22A*	*12-22H*
quartz	x	x	x
muscovite	x	x	x
biotite			
chlorite	x	x	x
kaolinite	x	x	
calcite			
dolomite	x		
orthopyroxene			
lepidocrocite		x	
hematite			x

e. Sample 12-30.5

	silt	**clay - air**	**clay - 550C**
jpeg file name	*12-30.5S*	*12-30.5A*	*12-30.5H*
quartz	x	x	x
muscovite	x	x	x
biotite			
chlorite	x	x	x
kaolinite	x	x	
calcite			
dolomite	x		
orthopyroxene	x		
lepidocrocite		x	
hematite			x

Table 3.17 Mineralogy of Core 12 Sediment Samples: Silt and Clay
A jpeg file of each diffractogram is in Appendix A

a. Silt

sample	quartz (%)	+/-	CEV	muscovite (%)	+/-	CEV	chlorite (%)	+/-	CEV	lepidocrocite (%)	+/-	CEV	dolomite (%)	+/-	CEV	
5	38.5	1.9	5.5	46.2	2.3	4.8	15.3	0.8	4.9							
10	31.7	1.4	4.1	51.3	2.3	4.8	17.0	0.8	4.9							
15	33.0	3.1	9.0	45.3	4.3	9.0	18.8	1.8	11.0				2.9	0.3	8.8	
22	39.5	1.9	5.5	46.8	2.2	4.6	13.7	0.7	4.3							
30.5	28.7	2.3	6.7	50.3	4.1	8.5	17.1	1.4	8.5				3.9	0.3	8.8	
	34.3			48.0			16.4						3.4			mean

b.
Clay

sample	quartz (%)	+/-	CEV	muscovite (%)	+/-	CEV	chlorite (%)	+/-	CEV	lepidocrocite (%)	+/-	CEV	dolomite (%)	+/-	CEV	
5	*6.1*	*0.7*	*11.5*	*62.5*	*6.8*	*10.8*	*28.6*	*3.1*	*10.7*	*2.8*	*0.3*	*15.0*				
10	*6.7*	*0.6*	*9.8*	*62.6*	*5.8*	*9.2*	*28.5*	*2.6*	*8.9*	*2.2*	*0.2*	*10.0*				
15	*6.4*	*0.9*	*14.8*	*63.6*	*9.3*	*14.8*	*28.3*	*4.1*	*14.1*	*1.7*	*0.2*	*10.0*				
22	*5.0*	*0.7*	*11.5*	*59.1*	*7.9*	*12.6*	*34.2*	*4.6*	*15.8*	*1.6*	*0.2*	*10.0*				
30.5	*6.1*	*0.7*	*11.5*	*66.2*	*8.1*	*12.9*	*26.0*	*3.2*	*11.0*	*1.7*	*0.2*	*10.0*				
	6.1			62.8			29.1			2.0						mean

Table 3.18 Core 12 Mineralogy: Quantitative Analysis
All percent (%) values are given as weight percent normalized
+/- is the error associated with the percent value, calculated by the quantitative analysis program
CEV is the coefficient of variance, which evaluates the magnitude of the error relative to the amount of the mineral present
Italics indicate a CEV greater than 10%

12-15 and 12-10, respectively. Likewise, chlorite concentrations vary only slightly, from 13.7% ± .7 at 22cm to 18.8% ± 1.8 at 12-15. Dolomite amounts range from 2.9-3.9%, a change that is not considered important.

All samples in the clay size fraction are poorly resolved and therefore have high coefficients of variance. Like the clay samples in core 8, the muscovite peaks are consistently broad and exhibit fronting, potentially indicating the presence of composition variants and/or other clay mineral that are impossible to identify or verify without further analyses. The quartz peaks in the samples show tailing and/or shoulders to the right, indicating the presence of other minerals. This is likely, given that pyroxene, rutile and plagioclase all have peaks around 27° two-theta. Overall sample quality is not thought to have affected resolution because peak intensities approach 1200 counts. The amount of quartz ranges from 5.0 to 6.1% (12-22 and 12-5). Muscovite varies from 59.1% ± 7.9 in sample 12-22 to 66.2% ± 8.1 in sample 12-30.5. Amounts of chlorite shift from 26.0% ± 3.2 (12-30.5) to 34.2% ± 4.6 (12-22). Lepidocrocite varies only slightly, from 1.6 to 2.8%. None of these changes in the quantity of minerals present in samples downcore are considered significant in light of the magnitude of error and CEVs associated with the samples.

Figure 3.18 shows the concentration of minerals downcore against the core 12 grain size analysis plot. The presence of dolomite and low quartz in the silt-size fraction in at 15cm corresponds with a peak in sand-size fraction, decoupled from silt which is at a minimum. These trends are also coincident with the presence of orthopyroxene in the silt fraction and a stratigraphic unit with wider laminae. The dolomite and orthopyroxene present 12-30.5 occur with a relatively low amount of quartz and correspond with a peak

See Figure 3.18

in silt composition. Higher amounts of quartz in sample 12-5 occurs with a peak in sand composition and in 12-22 with a peak in silt. Low amounts of quartz in 12-10 correspond with a peak in clay and the diffuse stratigraphic unit.

Summarized results from the XRD analysis of core 11 sediments are seen in Table 3.19. Samples from all depths contain quartz, muscovite, chlorite and kaolinite in the silt and clay fractions. Samples from 3 and 10cm deep contain dolomite in the silt-sized fraction. Core samples 11-3, 11-6 and 11-10 contain lepidocrocite in the clay fraction; in samples 11-16 and 11-19, iron oxides (lepidocrocite and hematite) occur in the clay-sized fraction. Calcite shows up in the silt-size fraction of sample 11-10, and sample 11-16 contains orthopyroxene in the silt fraction.

Table 3.20 displays the results of the quantitative analysis of the silt and clay fractions for core 11. In the silt-size fraction, samples 11-3 and 11-10 have high coeffecients of variance. Some fronting on the muscovite peaks is observed in the diffractograms, but minerals are otherwise relatively well resolved and have reasonable intensities. Thus, composition variations and/or heterogeneity of sample size have likely affected the quantitative analysis. The amount of quartz ranges from 27.2% ±1.2 (11-19) to 43.9% ± 7.9 (11-10). Samples 11-10 and 11-16 therefore have relatively more quartz than samples 11-6 and 11-19 but can not be said to be significantly different from each other. Muscovite varies from 37.7% ± 6.8 at 10cm to 54.7% ±2.5 at 19cm. Given the error and CEV values, samples can not be quantified as significantly different from each other. The amount of chlorite present ranges from 11.3% ± 2.1 to 20.1% ± 1 in samples 11-10 and 11-6, respectively. Thus 11-6 has relatively more chlorite than 11-10, but

a. Sample 11-3

	silt	**clay - air**	**clay - 550C**
jpeg file name	*11-3S*	*11-3A*	*11-3H*
quartz	x	x	x
muscovite	x	x	x
biotite			
chlorite	x	x	x
kaolinite		x	
calcite			
dolomite	x		
orthopyroxene			
lepidocrocite		x	
hematite			

b. Sample 11-6

	silt	**clay - air**	**clay - 550C**
jpeg file name	*11-6S*	*11-6A*	*11-6H*
quartz	x	x	x
muscovite	x	x	x
biotite		x	x
chlorite	x	x	x
kaolinite	x	x	
calcite			
dolomite			
orthopyroxene			
lepidocrocite		x	
hematite			

c. Sample 11-10

	silt	**clay - air**	**clay - 550C**
jpeg file name	*11-10S*	*11-10A*	*11-10H*
quartz	x	x	x
muscovite	x	x	x
biotite			x
chlorite	x	x	x
kaolinite		x	
calcite	x		
dolomite	x		
orthopyroxene			
lepidocrocite		x	
hematite			

d. Sample 11-16

	silt	**clay - air**	**clay - 550C**
jpeg file name	*11-16S*	*11-16A*	*11-16H*
quartz	x	x	x
muscovite	x	x	x
biotite			
chlorite	x	x	x
kaolinite	x	x	
calcite			
dolomite			
orthopyroxene	x		
lepidocrocite		x	
hematite			x

e. Sample 11-19

	silt	**clay - air**	**clay - 550C**
jpeg file name	*11-19S*	*11-19A*	*11-19H*
quartz	x	x	x
muscovite	x	x	x
biotite			
chlorite	x	x	x
kaolinite	x	x	
calcite			
dolomite			
orthopyroxene	x		
lepidocrocite		x	
hematite			x

Table 3.19 Mineralogy of Core 11 Sediment Samples: Silt and Clay
A jpeg file of each diffractogram is in Appendix A

a. Silt

sample	quartz (%)	+/-	CEV	muscovite (%)	+/-	CEV	chlorite (%)	+/-	CEV	lepidocrocite (%)	+/-	CEV	dolomite (%)	+/-	CEV	
3	*33.1*	*3.5*	*10.4*	*48.2*	*5.1*	*10.6*	*16.1*	*1.7*	*10.4*				*2.6*	*0.3*	*7.1*	
6	28.5	1.5	4.5	51.3	2.6	5.4	20.1	1.0	6.1							
10	*43.9*	*7.9*	*23.5*	*37.7*	*6.8*	*14.1*	*11.3*	*2.1*	*12.9*				*5.9*	*1.1*	*25.9*	
16	35.4	1.8	5.4	48.8	2.4	5.0	15.8	0.8	4.9							
19	27.2	1.2	3.6	54.7	2.5	5.2	18.0	0.8	4.9							
	33.6			48.1			16.3						4.3			mean

b.
Clay

sample	quartz (%)	+/-	CEV	muscovite (%)	+/-	CEV	chlorite (%)	+/-	CEV	lepidocrocite (%)	+/-	CEV	dolomite (%)	+/-	CEV	
3	*6.0*	*0.6*	*9.5*	*51.0*	*5.4*	*9.0*	*40.6*	*4.3*	*13.1*	*2.3*	*0.2*	*10.0*				
6	*6.1*	*0.7*	*11.1*	*61.8*	*7.1*	*11.8*	*29.2*	*3.4*	*10.3*	*2.9*	*0.3*	*15.0*				
10	*6.1*	*1.5*	*23.8*	*56.5*	*13.9*	*23.1*	*36.5*	*9.0*	*27.4*	*1.0*	*0.2*	*10.0*				
16		*0.0*	*0.0*	*66.0*	*9.6*	*16.0*	*32.3*	*4.7*	*14.3*	*1.8*	*0.3*	*15.0*				
19	*6.9*	*0.9*	*14.3*	*65.1*	*8.8*	*14.6*	*26.1*	*3.5*	*10.6*	*1.9*	*0.3*	*15.0*				
	6.3			60.1			32.9			2.0						mean

Table 3.20 Core 11 Mineralogy: Quantitative Analysis
All percent (%) values are given as weight percent normalized
+/- is the error associated with the percent value, calculated by the quantitative analysis program
CEV is the coefficient of variance, which evaluates the magnitude of the error relative to the amount of the mineral present
Italics indicate a CEV greater than 10%

these quantities are not appreciably different from the other three samples. Dolomite ranges from 2.6 to 5.9%; this absolute change is not considered significant.

Qualitative analysis of the clay-size fraction produced high coefficients of variance in all samples due to poorly resolved diffractograms. Muscovite peaks with significant fronting, chlorite/kaolinite peaks with broad bases, and general poor peak resolution is likely due to significant compositional variations. Quartz amounts vary little, from 6.0 to 6.9%. The amounts of muscovite exhibit a maximum of shift from 51.0% ± 5.4 in sample 11-3 to 66.0% ± 9.6 in sample 11-16. Chlorite ranges from 26.1% ± 3.5 to 40.6% ± 4.3 at 19 and 3cm depths, respectively. Besides the presence of relatively more chlorite at 3cm than at 19cm, error and CEV associated with the chlorite values render differences nearly indistinguishable. The amount of lepidocrocite is minor and varies little, from 1.0-2.9%.

Percent mineral composition in core 11 is plotted against grain size in Figure 3.19. The presence of dolomite in samples 11-3 occurs corresponds to an increase in the clay composition and percent chlorite (clay-size) of the sediment. The presence of dolomite and calcite in sample 11-10 occurs with the highest sand peak and an increase in silt and a relative decrease in silt-sized chlorite. These trends correspond to the stratigraphic unit with increased lamina width (10-12cm). A decrease in the amount of quartz present in the silt fraction and chlorite in the clay fraction at 19cm correspond to elevated silt composition and the presence of orthopyroxene in the silt-size fraction.

A general trend in mineral quantity was observed for the suite of cores. Core 6 had relatively higher amounts of quartz in the silt fraction (average 41.6%), comparable amounts of muscovite (average 49.4%) and chlorite (average 9.4%) than the over three

See Figure 3.19

cores. Cores 8, 11 and 12 had less quartz (~34%), comparable muscovite (46.5-48%) and more chlorite (~16.5%). Clay compositions were nearly identical, with quartz representing between 6 and 7.5%, muscovite ranging from 58% (core 6) to 64% (core 8), and chlorite 30% (core 12) to 34% (core 6).

Chapter 4. Discussion

4.1 From Bedrock to Coarse Sediment Lithology

The dominant lithologies in the gravel fractions of the surficial sediments at each site show generally good correspondence with the underlying lithology. Figure 4.1 visually depicts the amount of the major lithologies present in both size fractions at each site. The west shore samples show a significant change in dominant lithology between size fractions, from 76% sandstone in the boulders and cobbles fraction to 68% phyllite in the gravel fraction. This trend corresponds well with the field observation that clasts of cobble size and larger were predominately sandstone, while smaller clasts tended to be phyllites. However, the solifluction sheets and lobes of the western shore are situated almost entirely on sandstone with the phyllite located topographically higher to the west, so the predominance of phyllite in the matrix sediments of the lobes is perhaps unexpected. Two explanations for this trend are considered: the preferential transportation of a particular clast shape and the relative weathering rates of the two lithologies.

Phyllite clasts throughout the valley located in a variety of geomorphic settings were observed to be discoid or blade-like (after the Zingg categorization of clast shape, 1955, in Engelhardt, 1977). In contrast, sandstone clasts were much blockier and spheroid. Bertran et al. (1997) found that solifluction lobes in southern France exhibited relatively high fabric strength, with the long axis of clasts oriented parallel to the slope direction. In addition, the solifluction deposits showed increasingly compact-shaped clasts further down slope, indicating slight preferential transportation of this shape. Based on this study, it would be expected that the spheriodal sandstone clasts might show

See Figure 4.1

preferential transportation and therefore higher abundance in all size fractions. However, this is not the case in Linnédalen.

Instead, the higher concentration of phyllite in the gravel fraction is attributed to the higher weathering rate of phyllites and subsequently greater production of finer grain sizes. This finding is substantiated by a study on the weathering rates of rocks by Andre (2002) in a postglacial landscape in Lapland (68ºN). The study described weathering rates between .8 and 1.5mm ka^{-1} for a suite of biotite-rich crystalline rocks (which included a sericite-rich phyllite), compared to rates of .1 to .3 mm ka^{-1} for the more resilient crystalline rocks (which included quartzitic rocks). Due to the highly quartzitic nature of the sandstone in Linnédalen, the weathering rate of the crystalline rock is considered to be a good approximation of the weathering rate of the sandstone. The relatively high rates of phyllite weathering observed by Andre supports the conclusion that in Linnédalen the predominance of phyllite in smaller grain sizes indicates heightened weathering relative to the sandstone. Therefore, the high amounts of phyllite found in the gravel fraction of the west shore samples likely reflect the high break down rates of phyllite rather than the preferential transportation of disc-shaped clasts via solifluction. This further implies that the weathering rate and movement of phyllite is great enough to result in the predominance of phyllite even in samples which are directly underlain by the sandstone.

On the cirque glacier fan, phyllite dominates in both the boulders and cobbles and gravel fractions, with the percent phyllite present increasing by 10% in the gravel fraction (Figure 4.1). This increase is attributed to the higher weathering rate of phyllite relative to the quartzitic sandstone and pure quartz (the latter being derived from veins in the

phyllite formation). Nonetheless, like the west shore samples, a higher amount of sandstone might be expected in both size fractions because the melt water stream from the cirque runs primarily over exposed sandstone bedrock. The contact between the phyllite and sandstone was observed in the field to lie somewhere under or inside the terminal cirque moraine, a contact which is corroborated by the geologic map (refer back to Figure 4.1, or Figure 1.3). The cirque itself (and hence the former glacier) primarily overlies phyllite. The almost complete dominance of phyllite in the cobble and gravel fractions of the outwash fan sediments point to the fact that the primary sediment source is the glacial sediments, with little contribution from the bedrock lying between the cirque and the lake edge. Thus, not only do the phyllites chemically weather more readily, but a mechanism for greater physical weathering also exists for the phyllites.

As a general consideration before proceeding, weathering in arctic and other cold regions has traditionally been considered to occur mainly by physical processes, with temperature limiting chemical weathering. This paradigm has specifically been called into question by a number of studies showing the importance of chemical weathering in arctic environments (Darmody et al., 1987; White and Blum, 1995; Hall et al., 2002; Dixon et al., 2002; Anderson et al., 1997). Several of these studies indicate that the presence or absence of moisture is a more critical precondition of chemical weathering than temperature (Darmody et al., 1987; Hall et al., 2002; Anderson et al., 1997). The absolute and relative rate of chemical weathering in cold regions still needs to be determined, but Dixon et al. (2002) and Darmody et al. (1987) demonstrate that appreciable chemical weather has occurred on rocks and moraines exposed only for the duration of the Holocene. Furthermore, the weathering rates of specific rock types do not

follow temperature gradients either. Andre (2002) showed that the weathering rates of crystalline rocks from southern Europe to Canada and the Arctic were comparable, and that while the dissolution rate of carbonate rocks was substantially lower on Spitsbergen ($< 3mm\ ka^{-1}$) than in temperate or equatorial zones, this trend followed a gradient of higher vs. lower precipitation rather than temperature control. Thus the discussion of both physical and chemical weathering is highly relevant to the transport and alteration of rocks and minerals in Linnédalen.

The east shore fans all have carbonate as the dominant lithology in both the boulders and cobbles and the gravel size fraction (Figure 4.1). With the exception of the east central fan (which shows the opposite trend), the carbonates decrease in percent from the coarser to the finer fraction. Conversely, the amount of dolerite present on all the fans increases in the finer fraction. These changes in dominance are proposed to be the product of differential weathering and to reflect the relative activity of the fans. The relative reaction rate of minerals generally decreases according to the following series: carbonates > mafic silicates > feldspars > quartz (White and Blum, 1995; Blatt, 1982). In addition, the increasing reactivity of grains with decreasing size (and therefore increasing surface area) is well documented (Darmody et al., 1987; Fairchild et al., 1994; Anderson et al., 1997). Thus it would be expected that greater chemical weathering occurs with decreasing grain size, and that carbonate minerals (and hence carbonate bearing rocks) would weather more quickly in smaller grain sizes than mafic silicate bearing rocks (such as the dolerite). Where this trend is not observed – on the east central fan – it is proposed that this fan is more recently and/or currently active and that carbonates are therefore still abundant in all grain sizes. This hypothesis about fan activity is supported in part by

field observation because the east central fan was the only alluvial fan observed to have any stream flow (albeit it was very low). The activity of this fan is further supported by the presence of calcite and dolomite in the silt and clay fractions of the surficial sediments, as will be discussed in greater detail later.

At the east shore sites, sandstone diminishes in amount from the coarser to finer fraction. As on the west shore, this is attributed to the lower weathering rate of this quartzitic rock. Therefore, while both dolerite and sandstone are more resistant to weathering than the carbonate, the dolerite is in turn less resistant than the sandstone. This is evidenced by the increased presence on dolerite in the gravel fraction; it is weathered easily enough to be present in the smaller grain sizes (unlike the sandstone) but not easily enough to diminish in quantity in this grain size (like the carbonates).

Given the mixed east-west catchment of Linnéelva, it would be expected that the sediments at the outwash fan contain a mixture of carbonates, phyllite and sandstone. To some extent, this is the case (see Figure 4.1). The boulders and cobbles fraction is dominated by the same lithologies as the western sources (phyllite, sandstone and quartz) but notably, the abundance of phyllite is less and sandstone more than what is present at the west source sites. This may indicate increased transport of sandstone (spheroid) clasts in the fluvial system and/or increasing source contribution of sandstone.

The former hypothesis is supported by the work of Komar and Li (1986) who show that the entrainment of a clast is affected by its pivoting angle. The pivoting angle is a parameter describing the rollability and angularity of a clast. Thus in series of spheres, smooth ellipsoids, angular grains and imbricated ellipsoids, each subsequent shape requires increasing threshold values (e.g. need higher flow for entrainment).

Demir and Walsh (2005), studying the bedload transported in streams during winter storm events in South Wales, found that smooth beds favor the movement of clasts that roll (rods and spheres), while rough beds favor the transport of flat clasts (blades and discs). Based on field observation, Linnéelva is unlikely to be categorized as either entirely smooth bedded or entirely rough, given the significant changes in channel morphology and bedform exhibited over its length. Thus, preferential transport of one clast over the other can not be invoked to explain the dominance of one lithology over another in Linnéelva.

Instead, the length of Linnéelva (~8km from glacier to lake), sitting primarily on sandstone, may explain the more equitable distribution of phyllite and sandstone and the lack of carbonates. The long fluvial pathway lends itself to long-term clast exposure and hence extensive breakdown of the carbonates. Blatt (1982) notes that the dipolar nature of water is such an effective agent of chemical weathering as to make the effects of physical weathering trivial in comparison. The long pathway also enables more time and a more extensive mechanism for the breakdown of the resilient (and more proximal) sandstone. The west wall of the valley is characterized throughout by the presence of formerly glaciated cirques lying on phyllite whose melting remnant ice continue to supply abundant phyllite to Linnéelva. In contrast, no comparable fluvial or erosive mechanism exists to deliver carbonates from the east side of the valley to Linnéelva.

As was noted in the results section, only six pieces of gravel were present in the Linnéelva sample and thus the distribution of lithologies present in the gravel fraction is not considered a representative sample of gravel lithology. Nonetheless, this fraction

appears to indicate, to some extent, the weatherability of phyllites and the input of the more resistant dolerite (relative to the carbonate) from the east side.

As a final remark about the distribution of coarse lithologies in the valley, clasts representing all the types of bedrock in valley were present on both the east and west shores in minor amounts (e.g. dolerite occurred on the west side, phyllite on the east). This may indicate the presence on the valley floor of glacial sediments from the last glacial maximum on Svalbard, which is the last time Linnédalen was entirely glaciated. Alternately, clasts could have been transported as ice-rafted debris during the breakup of winter ice in the lake, a mechanism observed by O'Reilly (1995). However, given the presence of boulders and cobbles of distal lithology present 20-30m from the lake shore, glaciation is considered the more likely mechanism for the emplacement of these clasts.

4.2 Relation of Mineralogy to Lithology: Whole Rock Analysis

The mineral identification from the XRD analysis of whole rock hand samples agrees well with the published geology (Dallmann et al. 1992). The areno-argillaceous phyllites, described by Dallmann et al. (1992) as having a strong cleavage of sericite, chlorite and opaque minerals, has a primarily siliceous matrix with some localized calcite and dolomite cements. This corresponds well with the occurrence of quartz, albite, muscovite, chlorite, calcite and dolomite in the hand samples. No opaque minerals were detected in the two hand samples analyzed. It is possible that those minerals were present in such small amounts as to be indistinguishable from background noise on the diffractogram. The absence of these minerals may be an effect of either inhomogeneous mineral content of the rocks (and thus the hand samples selected had only minor amounts

of the opaque minerals) or, more likely, the minerals are simply present in very small amounts throughout the unit. Given the argillaceous nature and low-metamorphic grade of the rock, it is also suggested that detrital kaolinite may be present. This is discussed in greater detail later, in the discussion of surficial sediment composition.

The two sandstone samples, white and red (of the Orustdalen and Vegard Formations, respectively), are dominated by quartz. This is in good agreement the Dallman et al. publication (1992), which describes a quartzitic sandstone that contains numerous plant fragments. The red color of the latter sandstone is attributed to the clinoferrosilite present. The identification of this mineral is tenuous due to its very minor amount and subsequently poorly developed peak pattern on the diffractogram. Regardless of the limit of positive identification, the presence of an iron-bearing mineral is likely. Given the coal seams of this formation, the presence of carbon might be expected. Numerous diffractogram search-match analyses from surficial and core sediment samples did in fact indicate the presence of graphite in the samples, although analysis of the rock samples did not. The presence of a graphite (C) peak in a sample could represent coal (Allen, pers. comm., 2005). However, the positive identification of graphite was never made because the major graphite peaks are coincident with quartz peaks and thus the two minerals are indistinguishable by the techniques used in this study.

The three carbonate samples analyzed contained different assemblages of calcite, dolomite and potentially ankerite (which could not be resolved from dolomite). On the basis of mineral assemblage, carbonate 3 can be identified as a dolomite, while carbonates 1 and 2 could be limestones or dolomites. These lithologies are consistent

with the arenaceous and silicified dolomites and limestones and dolomitic sandstones of the Nordenskiöldbreen Formation and the dolomites and argillaceous limestones of the Gipshuken Formation. The silicified to arenaceous nature of the carbonates is consistent with the quartz identified in the samples. The description of the Gipshuken limestones as argillaceous lends credibility to the finding of detrital rutile in carbonate 1. Rutile, which is highly resistant to weathering, is a common detrital mineral in sediments (Engelhardt, 1977; Deer et al., 1992).

The identified constituents of the dolerite (quartz, labradorite/andesite, enstatite, augite and ilmenite) are consistent with the standard pyroxene and plagioclase composition of dolerite. This analysis produced a complex diffractogram; the identification of end member minerals was not conclusive but for the scope of this study, the detection of the presence of plagioclase, mafic and calcic pyroxenes and ilmenite is sufficient.

4.3 Grain Size Analysis and Sediment Transport

The results of the grain size analysis of surficial sediments reflects the different mechanisms of sediment transport in the valley. Samples from the alluvial fans and solifluction sites are characterized by marked heterogeneity of grain size distribution (see Figure 3.2). The process of solifluction involves the slow mass movement of soils under the force of gravity and is promoted by freeze-thaw action (Matsuoka 2001). It occurs most commonly in soils with sandy to silty texture because such soils have low liquid and plastic limits (Harris, 1989 *in* Matsuoka, 2001). Thus, while grain size affects movement,

the mass movement nature of the transport does not produce sorting of sediment and hence a heterogeneous fine matrix would be expected.

Likewise, the heterogeneous nature of the alluvial fan sediments is thought to reflect the nature of sedimentation on the fans. It is proposed that the main mechanism of sediment transportation and deposition on the alluvial fans is rainfall events in conjunction with mass sediment movements, generating low frequency – high magnitude fluvial and sedimentation events. Fan morphology, observed in the field, is characterized by freshly scoured channels (up to one meter deep) and older, less distinct channels and vegetated surfaces. With the exception of the east central fan which had very low but constant stream flow, no flowing water was observed on any of the fans. Therefore channel development must have occurred under different climatic conditions than those observed during the summer of 2005. The lack of vegetation on some of the channels suggests that development is continuing to occur, supporting the idea that fluvial movement is occurring intermittently.

The mechanisms of transport and deposition on Arctic alluvial fans are rarely directly addressed. Boggs (2001) provides the general definition of debris-flow dominated fans: fans formed by a combination of debris flow and fluvial processes and that are characterized by poorly sorted sediment ranging from large boulders to muddy matrix. Stream flow processes including the deposition of stream-channel and sheet flood debris may also occur on these fans. This type of alluvial fan best describes the fans observed in Linnédalen. As in any climate systems, the sedimentation on high arctic alluvial fans is controlled by hydrologic activity. Numerous studies have shown that the spring snowmelt is the most important hydrologic and sediment transfer event of the year

(Woo and Sauriol, 1980; Kane et al., 1992; Beylich, 2004; Forbes and Lamoureux, 2005 etc.). However, the source area of each of the fans studied is quite small, representing only a fraction of the total watershed (refer to Figure 2.1, and aerial photograph of the Linnédalen). Thus, while some fluvial activity associated with spring snowmelt may occur on the alluvial fans, it is unlikely that this is the dominant mechanism of sedimentation on the fans. As fieldwork took place in late July and early August, well after annual spring melt (June), this conclusion can not be supported by field observations. However, Humlum (pers. comm., 2005) has observed that heavy rainfall events occuring in the late summer sometimes produce high discharge events on the fans.

After the active layer of an arctic watershed thaws, freeing previously frozen sediment, mass movement and sediment erosion can occur. Åkerman (1996) records the onset of mass movement (in the form of hill slope and solifluction lobe activity) around Kapp Linné after the annual thawing of the active layer for a period of twenty two years. Numerous studies have documented the importance of sediment inputs to fluvial or lacustrine systems that occur only after the active layer has thawed; examples include channel slumping (Hammer and Smith, 1983; Lewis et al., 2005) debris flows (Sletten et al., 2003) and overland flow (Forbes and Lamoureux, 2005). Such events may occur in conjunction with rainfall events (Sletten et al., 2003; Lewis et al., 2005; Forbes and Lamoureux, 2005) or in the course of normal fluvial activity (Sletten et al., 2003). Lewis et al. (2005) observed that in a high Arctic watershed on Ellesmere Island, a standard rainfall event in conjunction with a saturated active layer resulted in a mass sediment movement upstream that produced 32% of the total seasonal sediment deposited in the lake. A conjoining of the debris-flow alluvial fan described by Boggs (2001) with the

low frequency – high magnitude events observed by Lewis et al. (2005) forms a picture of sediment transport and deposition in Linnédalen. It is proposed that sediment transportation and deposition on the alluvial fans in Linnédalen occurs after the thawing of the active layer as a result of rainfall events mobilizing sediments from a saturated active layer and producing debris flows.

In contrast to the mass flow mechanisms of the solifluction lobes and alluvial fans, the outwash fans associated with the cirque glacier and Linnéelva are streamflow systems and thus exhibit more extensive grain size sorting (Boggs 2001). This is demonstrated by the Linnéelva and cirque glacier fan sediment samples, which fall into clusters of grain size distribution (refer to Figure 3.2)

4.4 Mineral Transport in Surficial Sediments

Figure 4.2 is a schematic diagram of the composition and relative abundance of minerals entering the lake from each source. The size of the arrows represents the amount of the mineral present in the sand and silt fractions at each source. Quartz is present in amounts greater than 50% in at least the sand fraction of all the surficial sediment samples. Given the ubiquity of quartz, its resistance to weathering, its presence in all of the bedrock hand samples analyzed, and that its terminal mode occurs in the fine to medium sand-sized fraction (Dreimanis and Vagners, 1969), this abundance of quartz is not unexpected.

On the west shore of the lake, quartz, albite, muscovite, chlorite and kaolinite are present in all the surficial sediment samples. The presence of all of these minerals is consistent with the composition of the phyllite. The phyllite was shown to be the major

See Figure 4.2

component of the gravel size fraction of sediments at each of the three western shore sources, which was explained by the more rapid weathering experienced by phyllite. Likewise, this faster rate of weathering is appropriate to explain the dominance of phyllite mineralogy in the sand and silt fractions. The consistently higher amounts of albite and muscovite (between 10 and 50%) relative to the other minerals in the three west side sources may indicate that these two minerals are present in greater amounts in the phyllite.

The quantity of albite in the sand and silt fractions in the west shore samples reflects different weathering effects. In the sand-size fraction, the west shore has a relatively higher amount of albite than the other two samples, which likely reflects a balance of between shorter transportation distance (than the west solifluction sample) and less intense physical weathering (than the cirque glacier fan sample). The west solifluction sample is the farthest north and located farthest from source phyllite. It is suggested that this increased transportation distance allows time for more of the albite to break down, resulting in the low amount observed.

The cirque fan is located most proximal to the phyllite source and the major source of sediments is glacial debris. Anderson et al. (2003) note that the physical breakdown of a mineral promotes chemical weathering. However, while there is relatively less albite in the sand-size fraction of the cirque glacier sediments, there is relatively more in the silt fraction. Given this, relationship and the greater reactivity of smaller grains, increased chemical weathering is an implausible explanation for the lower amounts of albite in the sand sized fraction. Instead, the higher amounts of albite in the silt fraction points to the idea of terminal mode put forth by Dreimanis and Vagners in

their study of till mineralogy (1969). Terminal mode represents the smallest size that minerals physically weather to before dissolution. The study does not give a terminal mode for albite, but suggests that mineral hardness is an indication of terminal mode. Dolomite's terminal mode (hardness 3.5-4) is in coarse to medium silt, while quartz (hardness 7) has a terminal mode in medium to fine sand; thus albite (hardness 6-6.5) likely falls between these two members, possibly in the fine sand to coarse silt fraction. If this estimate of terminal mode is to be accepted, the increased presence of albite in the silt fraction of the cirque glacier fan sediments suggests intense physical weathering of albite but less chemical weathering.

The higher amount of chlorite in the sand-size fraction of the cirque glacier sample may to be a product of proximity to source. This implies increased physical weathering of chlorites on longer transport paths (i.e. to the west shore solifluction lobes). Chlorite generally breaks down to vermiculite (Blatt 1982), a mineral which was not identified in the sediments and thus the chemical weathering of chlorite is not indicated. The presence of calcite and dolomite in the cirque glacier fan and west shore sediments indicates proximity to source (phyllite) because the higher weathering rates of carbonates compared to silicate minerals make it relatively unstable in sediments (Fairchild et al., 1994; White and Blum, 1995; Andre 2002). It's unlikely that the lack of iron oxide in the west shore sediment sample relates to any significant source, weathering or transportation difference because this sample is neither most proximal nor most distal to the phyllite source. More likely it was present in the sample but in smaller amounts than could be distinguished from background noise. Iron oxide is presumed to occur throughout the

valley as a weathering product resulting from the break down of any one of the numerous iron-bearing silicates.

In the three east side sources, muscovite, kaolinite, calcite and dolomite are present in all samples (refer to Figure 4.2). The mineralogy and chemical weathering of the east side rocks and sediments is more complex because several of the minerals present in the sediments were not identified as constituents of the east shore rocks. The presence of unstable calcite and dolomite in greater amounts in the northwest and east central fan samples indicate more recent deposition compared to the twin fans. Likewise, the presence of dolomite in greater amounts than calcite on all of the fans is due to the lower solubility of dolomite relative to calcite and hence slower weathering rates (Fairchild et al., 2004). The presence of pyroxene in the east central fan sediments suggests that sedimentation on this fan is more recent relative to the northeast or twins fans. The iron oxide seen exclusively in the twin fans sediment may relate to a localized outcrop of red sandstone and associated red-stained sediments observed between the fans in the field.

The presence of rutile on only the northeast and twin fans poses a dilemma for interpretation; equal distribution of rutile would be expected on all three of the east fans because weathering rate does not limit its occurrence. The irregular presence of rutile may therefore reflect heterogeneous distribution of minerals throughout the fan sediments, resulting in either the over representation of rutile in the twin and northeast fan samples or the under representation of the mineral in the east central fan sediments. Alternately, given the highly stable nature of rutile (Engelhardt, 1977; Deer et al., 1992), it is possible that the older deposition of sediments on the northeast and twins fans

(inferred by the presence/absence of calcite, dolomite and pyroxene) have relatively increased concentrations of the mineral. However, because the amount of calcite and dolomite present on the east central and northeast fans (indicating equitable amounts of weathering), this explanation seems unlikely.

The possibility of misidentification can not be ruled out for this sample, given that the major peaks for rutile and pyroxene (specifically, enstatite) are located at about 30° two-theta. The dominance of quartz and the carbonates in the sand size fraction of these samples diminishes the resolution of minor peaks; thus positive identification based on the unique minor peaks of rutile and pyroxene is more difficult. Of the two samples, it is more likely that pyroxene is present in the northeast fan sample (in place of rutile) because the east central sample displays a distinct peak for kanoite at 27.5° two-theta and the presence of a minor enstatite peak at 24° two-theta. If the identified rutile in the northeast fan sample was truly enstatite, this would suggest similar activity levels on these two fans, an interpretation which is substantiated by similar amounts of carbonate. Therefore this latter interpretation of misidentification is favored over the alternative - concentration of rutile in the northeast and twin fan sediments relative to the east central fan sediments.

To explain the presence of the sheet silicates (specifically, kaolinite, muscovite and chlorite) in the east shore sediments requires a discussion of clay mineral formation because these minerals were not identified in the whole rock analysis. The expected weathering product of pyroxenes is calcium-sodium montmorillonite (Blatt 1982). Subsequent weathering of montmorillonite produces kaolinite (Blatt 1982). Thus if the pyroxenes were weathering to produce kaolinite, montmorillonite would be expected in

the samples (indicated by a peak at 18° two-theta shifting to 15.5° two-theta after glycolation). This peak, representing an intermediate step of the pyroxene-montmorillonite-kaolinite weathering series, was absent in all diffractograms, indicating that this weathering reaction is not occurring and an alternative mechanism for the formation of kaolinite must be considered.

Although potassium feldspar and muscovite are most commonly cited as weathering to kaolinite (Blatt, 1982; Deer et al., 1992; Nesse, 2000 etc.), White and Blum (1995) provide a reaction for albite weathering directly to kaolinite:

$$[NaAlSi_3O_8]\text{albite} + 1.5H_20 + CO_2 \rightarrow$$

$$0.5[Al_2SiO_2O_5(OH)_4]\text{kaolinite} + Na^+ + HCO_3^- + 2H_4SiO_4$$

Given the marked absence of plagioclase feldspars in the east shore sediment samples (which is unexpected given their presence in the dolerite), it is suggested that the kaolinite is derived directly from the weathering of the plagioclase feldspars.

However, if this reaction series is to be applied to the east shore samples, it must be applied to the west shore samples as well. The continued presence of albite in the west shore samples then must reflect comparatively greater abundance of albite such that it remains in significant amounts in the sediments despite the weathering of some albite into kaolinite. This is explained by considering the amount of phyllite vs. dolerite present in the valley: phyllite is a major lithological unit, whereas the dolerite is an intrusion ~10m in width. However, it should be noted that the presence of pyroxene and the absence of feldspars in the east shore samples stands in contrast to a number of studies stating that pyroxenes weather more rapidly than feldspar in surficial samples (White and Blum, 1995; McCarroll 1978). McCarroll suggests that the chelates produced from rock-

encrusted lichens preferentially attack iron-bearing pyroxenes, contributing to their higher weathering rates. It is therefore possible that a lack of lichen cover (relative to McCarroll's study site in an alpine zone in southern Norway) on the dolerite outcrops in Linnédalen results in lower weathering rates of pyroxenes relative to plagioclase at this site.

Muscovite occurs in minor amounts in all three east side sources; chlorite occurs only in the east central and northeast fans. Both minerals are common detrital constituents of sedimentary rocks. However, if this is the origin of the minerals then they are present in such minor amounts in the parent rocks that they were not identifiable in the whole rock diffractograms. Alternately, it is possible that the chlorite represents the weathered product of biotite (Blatt, 1982), or the degradation of other ferro-magnesian minerals (Deer et al., 1992). As discussed earlier, anywhere that muscovite is identified biotite must be assumed to be present because of the difficulty in distinguishing between the two minerals. In any case, chlorite is a common detrital mineral and weathering bi-product and could have been produced by any number of weathering reactions. Furthermore, the possibility of glacial sediments contributing to the minerals found in the surficial sediments on either side of the lake can not be discounted.

As in the lithological analysis of Linnéelva, the surficial sediment analysis demonstrates a mixture of mineral sources that most closely resembles the western samples (see Figure 4.2). The lower amount of albite present (relative to the western sources) is likely due to increased physical and chemical weathering occurring over the length of the river combined with a more distal phyllite source. Likewise, the presence of calcite and dolomite in minor amounts indicates the balance between source proximity

and weathering. The relatively higher amounts of muscovite in this sample compared to albite and dolomite points to the relative resistance of muscovite to physical weathering and thus its continued presence in high amounts despite a potentially long tranportation path (Dreimanis and Vagners, 1969).

The generalized mineralogical composition by grain size for the east and west sides and Linnéelva is depicted schematically in Figure 4.3. The organization of the data this way implicates differences in the origins of minerals. The presence of the sheet silicates (muscovite, chlorite and kaolinite) in all grain size fractions supports their lithologic origin (in the phyllite). In contrast, the kaolinite and chlorite on the east side only enter the sediments in the clay sized fraction, suggesting that these minerals are the alteration products of primary minerals. The presence of dolomite and calcite in all grain size fractions in the east shore samples indicates their proximal source and more concentrated source and hence their proportionally greater importance to the overall sediment composition. The loss of albite from the clay fraction in the Linnéelva sample suggests the increased weathering of this mineral, likely due to a longer period of entrainment. Similarly, the presence of calcite only in the sand fraction and dolomite in the sand and silt fractions point to the balance between carbonate source location and rapid weathering.

Generally, the clay fraction of the surficial sediments from different sources looks very similar. This is due in large part to the predominance of the phyllosilicates (namely muscovite, chlorite and kaolinite) in this size fraction, a trend which is mirrored in numerous studies dealing with fluvial systems (Wall and, Wilding 1976; Wall et al., 1978; Chakrapani, 1996). The most likely cause of this concentration of phyllosilicates

See Figure 4.3

in the clay-sized fraction pertains to terminal mode. While quartz, dolomite and calcite all reach terminal mode in the sand and silt-size fractions, phyllosilicates achieve terminal mode in the clay-sized fraction (Dreimanis and Vagners, 1969).

4.5 Mineral Deposition in Lake Sediments

Basic principles of fluvial sediment transport state that higher flow rates produce an increase in entrained sediment grain size, provided sediments are unconsolidated. Conversely, an increase in high flow rates may also yield an increase in the amount of entrained fine sediments if the clays and silts are consolidated (Hjulström's diagram, in Boggs, 2001). Assuming unconsolidated sediments, an increase in grain size in lake sediments may be interpreted to represent a period of higher flow rates, a relationship many studies have used to interpret climate change from lake sediments records (e.g. Francus et al., 2002; Lewis et al., 2002). Østrem et al. (1967) demonstrates that in Decade River on Baffin Island, suspended sediment concentration does not necessarily increase with an increase in river discharge, but the total sediment flux does proportionally increase. Thus, higher flow rates may also produce higher rates of lacustrine sedimentation, as numerous studies have interpreted (e.g. Retelle and Child, 1996; Lamoureux and Gilbert, 2004). However, in Arctic watersheds, exhuastion of sediment supply can sometimes produce high discharge events with no corresponding peak in grain size or sediment deposition (e.g. Hammer and Smith, 1983; Forbes and Lamoureux, 2005). Differences in and controls on the contribution of sediment from proglacial rivers, fluvial systems, and hill slope activity must be considered and understood to accurately interpret lake sediment records (e.g. Jansson et al., 2005).

Core 6, retrieved from the southeast basin, represents sedimentation proximal to Linnéelva. Table 4.1 and Figure 3.16 summarize the significant changes in mineral content and quantity and correlated changes in grain size for core 6. The occurrence of higher amounts of sand (relative to the amount present in cores 11 and 12) is consistent with the proximity of core 6 to a major sediment source (Linnéelva), as is the occurrence of wider laminae and hence a higher rate of deposition.

The presence of quartz, muscovite, chlorite and kaolinite in all the silt and clay fractions of all the core sediment samples is consistent with the presence of these minerals in the Linnéelva fan sediments, as is the occurrence of dolomite in the silt fraction. The occurrence of calcite in the silt fraction is not correlated with an increase in sand amount but coincides with the presence of dolomite in the clay fraction and an increase in the relative amount of muscovite and quartz in the silt and clay fractions (respectively). The irregular occurrence of the relatively unstable carbonate minerals in the core sediments suggests changes in the depositional regime to favor or disadvantage the preservation of these minerals in the sediment. The presence of carbonates could indicate a period of increased discharge and sedimentation, resulting in the rapid transport and deposition of sediments and thus the preservation of carbonates due to minimal exposure time (period of weathering). If increased sediment flux and deposition occurred, a relative increase in the amount of silt present would be expected, but this can't be verified in sample 6-3 due to incomplete grain size data. However, increased amounts of silt in samples 6-0, 6-5 and 6-7, and high percent silt in sample 6-9 do not show higher amounts of carbonates, as would be expected according to the above model of increased deposition and carbonate preservation. Thus it must be concluded that no

Table 4.1 Core 6 Summarized Downcore Mineralogy Trends and Grain Size Correlations

sample	silt content	silt qualitative	clay content	clay qualitative	grain size
6-0					more silt
6-3	Ca	more Mu	Do	more Qu	ave. sand, no silt or clay data
6-5					more silt, low sand
6-7			Do		more silt, low sand
6-9		less Qu			high silt

*All samples have Qu (Quartz), Mu (Muscovite), Chl (Chlorite), and Ka (Kaolinite) in silt and clay fractions, Do (Dolomite) in silt, and Fe (Iron Oxide) in clay fraction

+More, less, high and low are descriptors given relative to the average percent grain size

clear correlation between grain size and either mineral composition or quantity exists in this limited data set. Alternative explanations for the variations in mineral content might include heterogeneous distribution of minerals in the source sediments or changes in sediment delivery up valley (i.e. increased or decreased input from Linnébreen or changes in east wall activity).

Core 8, taken from the southwest basin, is interpreted as representing a mixture of sediment input from Linnéelva and the cirque glacier fan on the basis of its distinctively colored laminae and the lack of stratigraphic correlation with southeast basin cores (Snyder et al., 2000). Table 4.2 and Figure 3.17 display the summarized trends in mineral content and quantity trends with corresponding grain size for core 8. All of the subsamples contain quartz, muscovite, chlorite and kaolinite in the silt and clay fractions and dolomite in the silt fraction, which is consistent with the presence of these minerals in the cirque glacier fan sediments. The occurrence of dolomite in the clay fraction does not correlate to grain size changes or with the presence of iron oxide. Relatively less quartz in the silt-size fraction and more chlorite in the clay-size fraction in sample 8-15 correlate to an increase in the amount of sand present and a distinctly yellowish tan stratigraphic unit.

The yellowish laminae observed only in west basin cores has been interpreted as sediments derived from the cirque glacier fan (Snyder, et al. 2000). Field observations of the sediment plume flowing from the cirque outwash stream and laboratory observations of surficial sediment samples support that sediments derived from this source are noticeably lighter and yellowish tan in color (Werner, pers. comm. 2006). It is likely that this lighter sediment color is due to an abundance of phyllosilicates, and in particular,

Table 4.2 Core 8 Summarized Downcore Mineralogy Trends and Grain Size Correlations

sample	silt content	silt qualitative	clay content	clay qualitative	grain size
8-1			Do		ave. sand, silt and clay
8-6			Do, Fe		ave. sand, silt and clay
8-10			Do, Fe		more sand and silt
8-15		less Qu		more Chl	more sand, no silt or clay data
8-21			Fe	less Chl	ave. sand, no silt or clay data

*All samples have Qu (Quartz), Mu (Muscovite), Chl (Chlorite), and Ka (Kaolinite) in silt and clay fractions, and Do (Dolomite) in silt

+More, less, high and low are descriptors given relative to the average percent grain size

chlorite; this abundance is verified by the surficial sediment analysis of the cirque glacier fan. An increase in the amount of sand present, such as that seen in sample 8-15, may reflect an increase in local source contribution (i.e. the cirque stream). This interpretation is supported by a proportional increase in the amount of chlorite present (recall that cirque glacier fan sediments contained the most chlorite in the clay fraction at 43%). Thus, sample 8-15 shows a good correlation between stratigraphy (yellowish tan sediment), an increase in percent sand, and a distinctive cirque glacier fan signal (high amounts of chlorite in the clay fraction). This sample therefore gives some mineralogical support to the suggestion that the light laminae represent sediments derived from the cirque glacier. Lending support to this interpretation, the occurrence of less clay-sized chlorite in sample 8-21 coincides with a brown, diffusely laminated unit. However, higher resolution sampling is needed to definitively identify the light laminae as a signal of cirque glacier sedimentation.

The significant trends in down core mineralogy and corresponding grain size changes for core 12 are summarized in Table 4.3 and Figure 3.18. All samples contain quartz, muscovite, chlorite and kaolinite in the silt and clay fractions and iron oxide in the clay fraction. This composition is consistent with the mineralogy of both the Linnéelva and east central fan surficial sediments. The presence of dolomite in sample 12-5 occurs with higher silt-sized quartz and higher sand content, decoupled from the silt (which is present in lesser amounts). Likewise, the presence of dolomite and orthoclase in the silt fraction in sample 12-30.5 coincides with an average amount of sand decoupled from the silt (present in low amounts). The decoupling of the percent sand and silt trends may indicate the input of sand from a source other than Linnéelva. Jansson (2005) notes that

Table 4.3 Core 12 Summarized Downcore Mineralogy Trends and Grain Size Correlations

sample	silt content	silt qualitative	clay content	clay qualitative	grain size
12-5	Do	more Qu			high sand, low silt
12-10					ave. sand, high clay
12-15	Do, Orth	more Chl			high sand, no silt or clay data
12-22	Do	more Qu, less Chl			ave.sand, more silt
12-30.5	Do, Orth				ave. sand, low silt/high clay

*All samples have Qu (Quartz), Mu (Muscovite), Chl (Chlorite), and Ka (Kaolinite) in silt and clay fractions, and Fe (Iron Oxide) in clay fraction

+More, less, high and low are descriptors given relative to the average percent grain size

the occurrence of larger clasts in lake sediments can indicate the contribution of rapid slope processes to lake sedimentation. Thus, the decoupling of the silt and sand trend proximal to an alternative sediment source (the east central fan), combined with the presence of local source minerals (orthopyroxene, potentially dolomite) may indicate the activity and contribution of east fan sediments.

However, such an interpretation must be treated with caution. An increase in the course sand fraction in lake sediments has been attributed to increased niveo-aeolian activity (Lewis et al., 2002; Lamoureux and Gilbert, 2004). Such a trend could also appear as decoupled from changes in the silt fraction and may or may not reflect local mineralogy. Additionally, during a period of lower sedimentation rates but standard winter aeolian activity, the sand in a given volume of sediment would appear to be more concentrated because the total annually deposited sediment would decrease while the volume of annually deposited coarse sand remained the same. Nonetheless, the presence of orthopyroxene suggests relatively rapid deposition due to the high weathering rate of this mineral.

The presence of dolomite in the core 12 sample presents a dilemma for interpretation because both Linnéelva and east central fan sediments consistently contain dolomite in the silt fraction. Bøyum and Kjensmo (1980) suggest that the low magnesium and calcium content of the upper 300cm of sediments from Linnévatnet may be caused by the low sedimentation rate in Linnévatnet enabling prolonged contact between sediment and water and thus enabling leaching of magnesium and calcium to occur as equilibrium conditions between the ionic content of water and sediment are achieved. Thus it may be speculated that dolomite originating on the Linnéelva fan may

dissolve during transportation in the lake, and thus that any dolomite found in sediments in the deep is may reflect a more proximal sediment source and/or rapid deposition. However, without further information on the rate of this dissolution reaction, dolomite must still conservatively be considered to come from either the eastern fans or Linnéelva.

The significant trends in mineral quantity and assemblage, correlated with grain size changes, for core 11 are summarized in Table 4.4 and Figure 3.19. Quartz, muscovite, chlorite and kaolinite are present in the silt and clay fractions of all samples; iron is present in the clay fraction. Dolomite and calcite in the silt fraction of sample 11-10 coincide with high sand and higher than average silt composition. In addition, relatively more quartz and less chlorite occur in the silt fraction of this sample. The presence of calcite in this sample is unique in the deep basin samples and interpreted as representing rapid deposition and hence preservation of calcite. The presence of dolomite and orthoclase in samples 11-3 and 11-16 (respectively) with low corresponding sand amounts and average silt and clay is puzzling. If the presence of these minerals indicate sediment input from the northeast fan, either the amount of sediment contributed was too small relative to the input from other sources to cause a discernible signal in the grain size, or the grain size distribution of this input was similar to that of the other contributing sources. Alternatively, the lack of correspondence between the presence of dolomite and orthoclase and the grain size distribution might simply indicate heterogeneity of source material and hence the irregular appearance of minerals in the sediment record.

Overall, phyllosilicates were present in increased quantities in the silt fraction of cores 8, 11 and 12 relative to the amount seen in core 6. Little variation in mineral

Table 4.4 Core 11 Summarized Downcore Mineralogy Trends and Grain Size Correlations

	silt content	silt qualitative	clay content	clay qualitative	grain size
11-3	Do			more Chl	low sand, ave. silt and clay
11-6		more Chl			low sand, less silt
11-10	Do, Ca	more Qu, less Chl			high sand, more silt
11-16	Orth	more Qu			low sand, ave. silt and clay
11-19				less Chl	low sand, more clay

*All samples have Qu (Quartz), Mu (Muscovite), Chl (Chlorite), and Ka (Kaolinite) in silt and clay fractions,
and Fe (Iron Oxide) in clay fraction
+More, less, high and low are descriptors given relative to the average percent grain size

quantity was observed in the clay-sized fraction. The difference in the composition of the silt fraction is attributed to the dynamics of sediment transport. Non-platy minerals (e.g. quartz) preferentially settle in low flow regimes such as lakes while platy minerals (e.g. phyllosilicates) remain in suspension (Wood, 1978). Thus it would is expected that greater quantities of phyllosilicates are contained in sediments deposited farther from the inlet.

Diagenesis refers to processes affecting physical or chemical alteration of sediments after deposition; these changes occur in an essentially closed system (Engelhardt, 1973). The main concern for diagenesis in fluvially deposited sediments is the alteration of clay minerals, a problem encountered in submarine deposition (Engelhardt, 1973; Naidu and Mowatt 1983) but not discussed in Arctic lacustrine sediments. No minerals were identified in the core sediments that were not also present in the surficial sediments. Therefore, diagenesis following deposition and burial is not thought to affect mineral assemblages in Linnévatnet sediments studied in this project.

Interpretation of mineral content and quantity in all the cores is severely limited by the relatively few samples analyzed. In addition, the sand fraction of the cores was not analyzed for mineral content because the quantity was too small to do XRD analysis and the time and experience of the author were too limited to identify minerals in grain mounts. Trends between stratigraphic units, grain size and mineralogy may become apparent with smaller sampling intervals and full analysis of each size fraction. In particular, the analysis of the sand and silt-sized sediments is likely to be the most useful because the biggest and most definitive differences in source sediments were observed in these fractions. The difficulty in obtaining quantitative analysis with acceptable amounts

of error for the clay composition of core sediments, combined with the fact that the clay-sized fraction of different sources did not vary significantly, make this size fraction less useful for determinations of provenance.

4.6 Core Grain Size and Stratigraphy: Climatic and Temporal Considerations

As core 6 does not demonstrate any distinctive changes in stratigraphy, no correlations between stratigraphy and changes in grain size are made (refer to Figure 3.12 to see stratigraphy and grain size). Cesium 137 dating (Werner, pers. comm. 2006) of a core located close to core 6 yielded a date of 1963-4 at 18cm and thus a sedimentation rate of 4.5mm/yr is calculated for the southeast basin. By applying this sedimentation rate to core 6 (see Table 4.5), the bottom of core (13cm) is dated to 1976.

Core 8 displays the most distinctive changes in stratigraphy (see Figure 3.13). On the basis of field and laboratory observation and previous work by Snyder et al. (2000), the stratigraphic units characterized by yellowish tan laminae (0-5, 9-11, 13.5-17.5 and 19.5cm) are interpreted here as periods of higher sedimentation. The first unit (0-5cm) is characterized by higher amounts of sand and variable amounts of silt and clay, the second unit (9-11cm) has high to medium silt values, and the third unit (13.5-17.5cm) has generally high amounts of clay. These differences in dominant grain size are likely related to differences in sediment transport and deposition in the fluvial and/or glacial systems. The presence of coarser grain size indicates higher flow, but higher flow may result from either more precipitation in general (a fluvial signal) or warmer summer temperatures (resulting in higher temperature and thus a glacial signal) or a mixture of the two. Likewise, finer sediments suggest lower flow, which may result from decreased

Table 4.5 Core 6 Age and Depth Correlations

dating method	Cesium 137 (Werner, pers. Comm.)	
sed. rate (mm/yr)	**4.5**	
depth (cm)	yrs B.P.	calendar yrs.
0	0	2005
4	9	1996
6.5	14	1991
13	29	1976
*18**	*41*	*1963-4*

*indicates the age and depth of ^{137}Cs, from Werner's core

precipitation (fluvial signal) or colder summer temperatures (low ablation, a glacial signal) or a mixture of the two. In addition, advancing vs. retreating glaciers may produce different sedimentary signals. Jansson (2005) suggests that the sedimentation from an advancing glacier is less than that from a retreating glacier because that latter exposes ample sediment for entrainment and deposition. Conversely, Larsen and Stalberg (2004) interpreted three units in a proglacial lacustrine record as representing a glacial advance (thick, coarse laminae), glacial maximum (diffuse lamination) and glacial retreat (laminae, not as regular as during the advance), effectively saying that advancing glaciers produce more sediment.

The two periods of diffuse, dark laminations (from 11-13.5 and 19.5-25cm) correspond with general increases in the amount of sand present. Underdeveloped laminae are often interpreted to represent periods of lower sediment. Increases in the amount of sand present have been correlated to increased niveo-aeolian deposition (Lewis et al.; 2002). The units combining diffuse laminae and increased sand deposition are thus tentatively interpreted as representing dry and/or cold periods with increased windiness.

An approximate chronology was developed for the core 8 stratigraphy by correlating the position of this core to the dated cores from Snyder et al. (2000). Figure 4.4 illustrates the core locations and the age-depth model developed for core 8. Snyder et al.'s core 02 was taken from a depth and location comprable to the location of core 8 from this study. The previous study obtained a ^{14}C maximum age of 470 yrs. B.P. at a depth of 69cm in a core proximal to the cirque glacier outwash fan (core 04, by Snyder et al.'s nomenclature). Utilizing the stratigraphic correlation between cores 04 and 02

See Figure 4.4

(90cm in 04 = 29cm in 02), a depth of 22cm in core 04 was calculated as corresponding to the dated horizon at 69cm in core 02 (see Figure 4.4). A sedimentation rate for core 02 was then calculated : (22cm/470yrs) = .47mm/yr. In comparison, this rate is significantly lower than the rates calculated using the annual sediment collected in deployed sediment traps in the west basin during 2004 (1.3mm/yr) and 2005 (.9mm/yr) (Motley, pers. comm., 2006). Because of the proximal location of core 02 to core 8, the sedimentation rate is applied directly to core 8 to obtain a maximum age at the bottom (25cm) of 532 yrs. B.P. Table 4.6 displays the ages associated with the stratigraphic boundaries of core 8. These ages should be regarded as maximums because the radiocarbon age used represents a maximum age.

Snyder et al. (2000) state that the onset of glaciation in the cirque occurred within the last six centuries (possibly within the last four) based on radiocarbon ages and the absence of yellowish tan laminae prior to this. Thus the bottom glacial unit (13.5-17.5cm) in core 8, corresponding to the period from approximately 1633 to 1718 A.D., is interpreted here to represent a period of glacial growth. The higher amounts of clay present in this unit may reflect colder summer temperatures dictating the fluvial regime by limiting ablation and thus limiting coarse sediment transport. Such a temperature decrease is plausible given that a precondition for glacier growth is lower summer temperatures, in addition to higher winter precipitation.

The dates provided by modeling for this period of glacial growth are relatively young, and at the minimum of Snyder et al.'s (2000) postulated period of cirque glaciation. In a review of scientific literature on the intitiation and termination of the Little Ice Age in the North Atlantic, Grove (2001) suggests a two-phase Little Ice Age in

Table 4.6 Core 8 Age and Depth Correlations

dating method	Snyder et al. 2000 (^{14}C dates)	
sed. rate (mm/yr)	**0.47**	
depth (cm)	yrs B.P.	calendar yrs.
0	0	2005
2.5	53	1952
5	106	1899
7.5	160	1845
9	191	1814
11	234	1771
13.5	287	1718
14.5	309	1696
15	319	1686
17.5	372	1633
19.5	415	1590
*22**	*470*	*1535*
25	532	1473

*corresponds to the horizon, in core 8, correlated to the ^{14}C from core 02, Snyder et al. (2000)

Spitsbergen and Greenland. Oxygen isotope analysis on an ice plateau in east-central Spitsbergen indicates colder periods between A.D. 1180 and 1500 and between A.D. 1700 and 1900, with a general warming in the 16th century (Gordiyenko et al., 1980) in Grove, 2001). Thus the bottom yellow unit of core 8, interpreted here as increased glacial activity, is not considered the onset of cirque glaciation because it is likely that glaciation occurred earlier in the Little Ice Age.

The second yellow unit, tentatively dated as occurring between 1771 and 1814 A.D., likely represents another period of glacial growth during the Little Ice Age related to increased winter precipitation and warmer summer temperatures. Such conditions would be conducive to both increased glacier growth and summer ablation, resulting in increased discharge and deposition, which is consistent with the wide laminae and coarse sediment peak in this unit of core 8. Nesje and Dahl (2003) propose that similar conditions - increased winter precipitation and temperature - promoted glacier advances in Norway in the 18th century.

The tentative dating of the onset of the final period of increased glacial activity is ~1889 A.D., which is roughly synchronous with the end of the Little Ice Age and onset of warming in the Northern Hemisphere (Mann et al., 1998). This date for glacial retreat is earlier than those reported for many North Atlantic glaciers (e.g. Nesje and Dahl, 2003; Bakke et al., 2005), and earlier than the date (1930 A.D.) proposed for this cirque by Snyder et al. (2000). It is possible that the wider laminae of this unit (from 2.5-5cm) correspond to a period of greater glacial activity, with increased summer ablation corresponding to increased temperatures but winter accumulation holding the glacier in

balance. The finer laminae may then correspond to the period of glacier decay, with summer ablation outpacing winter accumlation.

By extrapolation using the age model for core 8, the diffuse units correspond (in total) to the period spanning from 1473 to 1771 A.D. Giraudeau et al. (2004) interpreted the Little Ice Age (defined in that paper as 1400-1800 A.D.) as a period with increased intensity of the westerly winds in the North Atlantic based on variations in coccolith and benthic foraminifera populations in marine sediments from the North Iceland shelf. Further evidence of increased windiness and/or lower precipitation from Spitsbergen and the North Atlantic would help to constrain this interpretation.

As noted in the results section, the general stratigraphy of cores 11 and 12 correlate well, although the relative positions of the coarse grained layers reflect a difference in sedimentation rates between the two sites (Figures 3.14 and 3.15). Given the more distal location of core 11 from the main source of sediment to the lake (Linnéelva), a lower sedimentation rate for this core would be expected, as is evidenced by the higher stratigraphic location of the coarse layer (10cm deep, as opposed to 15cm in core 12). The presence of local mineralogy (dolomite, calcite, and orthopyroxene) and increased sand indicates that the deposition of this coarser unit may be related to, or at least synchronous with, east shore fan activity. Alternately, this visibly coarser layer could be interpreted as a turbidite, particularly in core 11 where the sand content represents a 600% increase (from representing an average of 1% of the total sediment to 6% in the 10cm sample). Core 11 was extracted from a location with fairly gradual bathymetric slope but was located proximal to an extremely steep bathymetric gradient just south of the northeast fan (refer back to Figure 3.7 for the locations of the cores on a

bathymetric map). Thus the occurrence of a turbidite in this location would not be unexpected.

However, the presence of this layer in both cores indicates a change in the conditions controlling sedimentation that affected at least the deep basin. The layer (3cm in core 12 and 2cm in core 11) thins with distance from Linnéelva, supporting the idea that the layer represents sedimentation from both Linnéelva and the east shore. Given the proposed mechanism for sediment transport on these fans (precipitation paired with mass movement), increased fan activity may indicate a period of relatively warmer temperatures (promoting thawing of the active layer and hence mass movement) and wetter conditions (promoting the fluvial action that mobilizes sediment). Numerous studies have indicated that warmer temperatures increase the size of the active layer (Anisimov et al., 1997; Åkerman, 1996; Kane et al., 1992), and combined with more precipitation, promote increased mass movement on all levels, from solifluction lobes (Matsuoka, 2001) to debris flows (Sletten et al., 2003). If the layer in core 11 is in fact a turbidite, then it may have been triggered by a debris flow resulting from a shift in climatic conditions. Nonetheless, the possibility of the turbidite occurring as a random event can not be discounted. Finally, an increase in precipitation, whether in the form of rain or snow, would be expected to increase discharge and hence sediment flux from Linnéelva as well. Thus, increased east slope activity is not proposed as supplanting sedimentation from Linnéelva but rather contributing to overall deposition in the main basin.

The diffuse unit observed in both cores 11 and 12, similar to the diffuse units of the core 8, is thought to represent a period of overall lower sedimentation in the valley.

In contrast to the units in core 8, there is no sand peak associated with this layer in the deep basin cores.

Obtaining temporal constraint for the deep basin cores was more challenging because no previous studies on Linnévatnet have dated, or even studied, cores from the deep basin. Thus radiocarbon dates and sedimentation rates obtained from cores taken in the southeast basin of the lake had to be extrapolated to develope an age-depth model for cores 11 and 12. Figure 4.5 schematically depicts this model. Svendsen and Mangerud (1997) calculate a maximum sedimentation rate of 1.2mm/yr from approximately 1400 A.D. to present for their core 15 by stratigraphically correlating a radiocarbon date (580 ±70) obtained in a study by Snyder (1994) to their cores. To extrapolate this date to cores 11 and 12, a proportional relationship between the sedimentation rates for locations of core 15 and cores 11 and 12 was established by using the isopach map of lacustrine sediment depths from Mangerud and Svendsen (1990). The base of the lacustrine sediment unit represents the marine/lacustrine boundary, which is dated to 9600 B.P. by Svendsen et al. (1989). Core 11 and 12 retrieval locations were identified on the isopach map by overlaying and resolving it with the bathymetric map of core locations in Adobe Illustrator. Core locations on the latter map were identified using ArcView and GPS coordinates taken during core retrieval. Core 15 was already located on the isopach map in Svendsen and Mangerud (1997). Core 11 was retrieved from 2m of lacustrine sediment, core 12 from 2.8m, and core 15 from 5m. The rate calculated by Svendsen and Mangerud (1997) was then multiplied by the ratio of total lacustrine sediment depth at the site of core 12 (1.2mm/yr*(2.8m/5m)) to obtain a sedimentation rate of .67mm/yr at for core 12. In the same manner (1.2mm/yr*(2m/5m)), a sedimentation rate of .48mm/yr

See Figure 4.5

was calculated for core 11. Tables 4.7 and 4.8 show the ages calculated for the stratigraphic unit boundaries for cores 12 and 11, respectively. The bottom of core 12 (38cm) has an age of 1438 A.D., while the bottom of core 11 (23cm) is given an age of 1526 A.D.

Using these calculations, the diffuse unit of lamination occurs between 1826 and 1878 A.D. in core 12 and between 1859 and 1901 A.D. in core 11. The period of increased sedimentation occurs between 1755 and 1797 A.D. in core 11 and between 1736 and 1781 A.D. in core 12. The offset of dates between the synchronous stratigraphic units in the cores indicates an error in the calculation of sedimentation rates for the two locations. One substantial source of uncertainty is using the isopach map with 1m contours to estimate sediment depth. Further compounding this problem is that the calculation of rate requires the assumption of continuous and linear sedimentation through time to achieve an average annual rate. Clearly this is a problematic assumption, as evidenced by the identification by this and many authors of periods of higher and lower sedimentation rates related to climatic changes. This source of error affects the age-depth models for all four cores.

A sedimentation rate for the middle of the deep basin was calculated using total annual sediment yields from sediment traps deployed in 2004 (.6mm/yr) and 2005 (.3mm/yr) (Motley, pers. comm. 2006). This trap is located approximately equidistant between where cores 11 and 12 were extracted. Therefore, the sedimentation rates calculated from Svendsen and Mangerud (1997) and the isopach map are on the same order of magnitude as current sedimentation. Thus, despite the limitations associated

Table 4.7 Core 12 Age and Depth Correlations

dating method	Svendson & Mangerud 1997 (C14 dates)	
sed. rate (mm/yr)	**0.67**	
depth (cm)	yrs. B.P.	calendar yrs.
0	0	2005
8.5	127	1878
12	179	1826
15	224	1781
18	269	1736
38	567	1438
*39**	*580*	*1425*

*corresponds to the hypothetical depth, in core 12, correllated to the ^{14}C age from core 15, Svendson and Mangerud (1997)

Table 4.8 Core 11 Age and Depth Correlations

dating method	Svendson & Mangerud 1997 (C14 dates)	
sed. rate (mm/yr)	**0.48**	
depth (cm)	yrs. B.P.	calendar yrs.
0	0	2005
5	104	1901
7	146	1859
10	208	1797
12	250	1755
23	479	1526
*29**	*580*	*1425*

*corresponds to the hypothetical depth, in core 11, correllated to the ^{14}C age from core 15, Svendson and Mangerud (1997)

with the calculated sedimentation rates, some interpretations can be made comparing stratigraphic trends in the deep basin cores to those seen in the west basin core.

The inferred period of lowered sedimentation in the deep basin, occurring between 1826 and 1901 A.D. (using the maximum and minimum ages between the two cores) is dated later than the upper unit of diffuse laminae in the west basin core (which occurred between 1718 and 1771 A.D.). The magnitude of the offset between these units indicates that the units are not synchronous. However, the diffuse unit in the deep basin cores does coincide with a unit of finely laminated dark sediments in core 8 (5-9cm, 1814-1889 A.D.). In core 8, the absence of yellowish tan laminae is taken to indicate decreased cirque glacier activity and thus an increase in the relative importance (but not necessarily rate) of sedimentation from Linnéelva. A period of cooler summer temperatures (and thus less glacier ablation) would diminish the input from the cirque glacier. However, any precipitation or input from spring snowmelt would still produce flow, particularly in Linnéelva which has much bigger catchment. In addition, such cold and dry conditions may diminish the depth of the active layer, resulting in less hill slope activity. The samples associated with the diffuse layers in the deep basin cores contained no local minerals (calcite, dolomite or orthopyroxene). While these two samples do not provide conclusive evidence that the hill slopes were less active, it does support this interpretation of lower overall sedimentation. Therefore, it is suggested that a period of lower summer temperatures and low precipitation in the 19th century may have reduced discharge from the cirque glacier and Linnéelva and hill slope activity, producing the dark, fine laminae seen in core 8 and the diffusely laminated sediment in the deep basin cores.

A second possibility for correlation between the deep and west basin cores exists. The deep basin unit, interpreted as representing higher overall sedimentation and increased eastern slope activity, is dated to the period from 1736 to 1781 A.D. in core 12. This unit in core 11 occurs between 1755 and 1797. These correlate reasonably well with the second yellow unit of the west core basin, dated from 1771 to 1814 A.D. and interpreted as representing increased glacial activity as a response to warmer and wetter winters. Thus, both the interpreted climatic conditions and the age correlate well between the cores and it is suggested that the second half of the 18th century was a relatively warm and wet period resulting in increased sedimentation throughout the basin.

Finally, the grain size plots of core 11 and 12 show an unexpected relationship. The average silt values are similar (75.9% in core 11, 73.4% in core 12) despite the significantly more distal location of core 11 from Linnéelva. Moreover, core 12 exhibits a much greater magnitude of variation in the silt and clay amounts. The dampened peaks exhibited in the grain size analysis for core 11 could be a function of a lower sedimentation rate, where a longer period of time is represented in a given volume and thus extremes in mean grain size may be averaged to produce an overall intermediate grain size. However, the slightly higher average silt amount seen in core 11 is still unexpected. Therefore it is suggested that an alternative sediment source may be contributing to the grain size distribution seen in core 11.

The majority of the solifluction sheets and lobes are located on the northwestern lake shores. The shoreline in contact with the water in this area was characterized by cobbles and few fines, with solifluction lobes ending in eroded scarps above the cobbles. The morphology of the shoreline suggests that wave action (and possibly ice) reworks

and suspends finer sediments supplied by the solifluction lobes, leaving the coarse lithology concentrated on the shore. A similar observation was made by O'Reilly (1995) on Sophia Lake, Cornwallis Island, where gelifluction lobes were observed to end at the edge of the lake in small erosional bluffs. Provided temperatures are warm enough for thawing of the active layer and an ice-free lake to occur, sediment input via wave action would be expected to be relatively constant. In a non-glacial lake on Axel Heiberg Island, Doran (1993, *in* Retelle and Child, 1996) estimated that between 15 and 30% of the annual sediment deposited in the lake is supplied by gelifluction. Given the pro-glacial character of Linnévatnet, it's unlikely that gelifluction would supply this high an amount of sediment to the lake. Nonetheless, the contribution of sediment from solifluction would be highest in the north end of the lake, while sediment input from Linnéelva would be lowest at this location.

The grain size analysis of the west shore and solifluction sources did not include separation of silt and clay. The total fines comprised anywhere from 5 to 80% of the total sediment present in the solifluction lobes. However, unconsolidated silts and clays are suspended equally at a given velocity (Hjulström's diagram, in Boggs, 2001); therefore silt should be suspended in equal or greater quantities than clay. Nonetheless, the great variability in the fines composition of the solifluction lobes prevents the identification of a particular grain size fingerprint from the lobes. This means that the grain size analysis of the surficial sediments can neither support nor refute the assertion that increased silt deposition seen in core 11 might be attributed to the reworking of sediments supplied by the solifluction.

Chapter 5. Conclusion

5.1 Conclusions

Sediments entering Linnévatnet from the east shore, west solifluction lobes, cirque glacier outwash fan and Linnéelva have unique mineralogical compositions that can be identified through paired x-ray diffractometer and quantitative analysis of the sand, silt and clay-sized fractions. East shore sediments are identified by the presence of rutile and pyroxene, and higher amounts of carbonate minerals (dolomite and calcite). West shore sediments can be recognized by higher amounts of muscovite and albite, and the presence of sheet silicates (chlorite/kaolinite and muscovite) in the sand and silt-size fractions. The cirque glacier fan is characterized by high amounts of chlorite/kaolinite in all size fractions and high amounts of albite in the silt fraction. Linnéelva sediments are recognized as containing high amounts of quartz and muscovite but lower amounts of carbonate, albite and chlorite/kaolinite relative to the east and west sources. The sand and silt fractions are most indicative of provenance; source sediments are nearly indistinguishable in the clay-size fraction even with quantitative analysis.

Source sediment composition reflects the underlying bedrock lithology and the relative weathering rates of different lithologies and minerals. The phyllite breaks down more rapidly than the sandstone and is thus a more significant contributor of sediments on the west shore. The high weathering rate of carbonate makes this lithology a less significant contributor to sediment on the east shore than was expected. Chemical weathering in Linnédalen appears to be less important than physical weathering based on the absence of clay minerals indicative of such weathering. Mineral composition of the different grain size fractions is primarily determined by the terminal mode of the minerals present and mechanism of deposition, with longer periods of transport or exposure

resulting in the absence of less stable minerals in the sediments. The grain size distribution of sediments at the different sources implicates transport mechanism. Heterogeneity of sediments on the alluvial fans and solifluction lobes indicates that sedimentation occurs primarily by mass movement processes. Relatively sorted sediments on the Linnéelva and cirque glacier outwash fans reflect the fluvial processes dominant at these locations.

Low sampling resolution limited down-core analysis of shifts in sediment sources. Significant shifts in grain size distribution suggest changes in sedimentation over time, potentially indicating climatic changes. Compositional and quantitative analysis of down core silt and clay mineralogy, paired with grain size analysis, suggests changes in the relative contribution of different sediment sources through time. In particular, an increase in the silt-size fraction in the west basin core, paired with relatively higher amounts of chlorite and distinctive stratigraphy, indicate a period of increased glacier activity. Increases in the sand-size fraction decoupled from the silt trend, paired with the presence of local mineralogy (orthopyroxene, calcite) may indicate periods of increased east fan activity. Age-depth modeling suggests that these periods of increased cirque glacier and east fan activity may be synchronous, suggesting wetter and warmer conditions in the second half of the eighteenth century, but better age constraint is necessary to support this interpretation. Differences in grain size distribution in cores 11 and 12 may implicate solifluction lobes as a significant contributor of sediment in the northern end of the deep basin.

5.2 Future Work

This study indicates that changes in the contribution of alternative sediment sources over time have likely occurred and may be indicators of climatic changes. With further study of the climatic controls and processes of transport and deposition associated with cirque glaciers and alluvial fans, a better interpretation of the long term record of climate contained in the Linnévatnet sediments will be made possible.

Continuous grain size analysis paired with continuous quantitative and compositional analysis of mineralogy down core may indicate changes in source contribution that either analysis individually can not. The separate analysis of the sand, silt and clay fractions is imperative to future provenance studies because the mineral composition of sediments changes significantly with grain size. Future studies might focus on the identification of accessory minerals (rutile, pyroxene) and plagioclase feldspars (albite and labradorite/andesite) because these minerals are highly source specific. It is expected that analysis of the sand-size fraction of the down core sediments may be particularly important because the greatest differences in source sediment composition was observed in this fraction. In addition, further study of the dissolution dynamics of dolomite is recommended to determine if the presence of this mineral in the deep basin sediments is indicative of proximal sources or not.

Previous studies of provenance have successfully utilized principle component and factor analysis statistics of mineral assemblages to determine the relative contribution of different sediment sources to a basin (Curry and Grimley, 2005; Kairyte et al., 2005). The application of such an analysis to the sediments of Linnédalen may also prove fruitful. Further study of the processes of sediment transport and deposition on the

alluvial fans is also recommended, potentially utilizing long term sediment traps in the deep basin placed proximal to the fans.

References Cited

Akerman, H.J., 1996, Slow mass movements and climatic relationship, 1972-1994, Kapp Linne, West Spitsbergen: Advances in Hillslope Processes, v. 2, p. 1219-1257.

Akerman, H.J., 2005, Relations between slow slope processes and active-layer thickness 1972-2002, Kapp Linné, Svalbard: Norsk Geografisk Tidsskrift, v. 59, p. 116-128.

Allen, D.B., 2006, personal communication.

Anderson, S.P., Drever, J.I., and Humphrey, N.F., 1997, Chemical weathering in glacial environments: Geology, v. 25, p. 399-402.

André, M.-., 2002, Rates of Postglacial rock weathering on glacially scoured outcrops (Abisko-Riksgränsen area, 68°N): Geografiska Annaler, Series A: Physical Geography, v. 84, p. 139-150.

Anisimov, O.A., Shiklomanov, N.I., and Nelson, F.E., 1997, Global warming and active-layer thickness: Results from transient general circulation models: Global and Planetary Change, v. 15, p. 61-77.

Bakke, J., Lie, Ø, Nesje, A., Dahl, S.O., and Paasche, Ø, 2005, Utilizing physical sediment variability in glacier-fed lakes for continuous glacier reconstructions during the Holocene, northern Folgefonna, western Norway: Holocene, v. 15, p. 161-176.

Bertran, P., Hétu, B., Texier, J.-., and Van Steijn, H., 1997, Fabric characteristics of subaerial slope deposits: Sedimentology, v. 44, p. 1-16.

Beylich, A.A., and Gintz, D., 2004, Effects of high - magnitude/low - frequency fluvial events generated by intense snowmelt or heavy rainfall in arctic periglacial environments in northern Swedish Lapland and northern Siberia: Geografiska Annaler, Series A: Physical Geography, v. 86, p. 11-29.

Blatt, H., 1982, Sedimentary Petrology: San Francisco, W. H. Freeman and Company, p. 564.

Boggs, S., 2001, Principles of Sedimentology and Stratigraphy: New Jersey, Prentice Hall, p. 726.

Boyum, A., J. Kjensmo, 1978, Physiography of Lake Linnevatn, Western Spitsbergen: Verh. Internaf. Verein Limnol., v. 20, p. 609-614.

Boyum, A., and Kjensmo, J., 1980, Post-glacial sediments in Lake Linnevatn, Spitsbergen: Arch. HydroBiol., v. 2, p. 232-249.

Carroll, D., 1970, Clay minerals : a guide to their X-ray identification: Boulder, Colorado, Geological Society of America, p. 80.

Chakrapani, G.J., Subramanian, V., Gibbs, R.J., and Jha, P.K., 1995, Size characteristics and mineralogy of suspended sediments of the Ganges River, India: Environmental Geology, v. 25, p. 192-196.

Connor, R., and Chmura, G.L., 2000, Dynamics of above- and belowground organic matter in a high latitude macrotidal saltmarsh: Marine Ecology Progress Series, v. 204, p. 101-110.

Craft, C., Broome, S., and Campbell, C., 2002, Fifteen years of vegetation and soil development after brackish-water marsh creation: Restoration Ecology, v. 10, p. 248-258.

Curry, B.B., and Grimley, D.A., 2006, Provenance, age, and environment of mid-Wisconsinan slackwater lake sediment in the St. Louis Metro East area, USA: Quaternary Research, v. 65, p. 108-122.

Dallman, W. K., A. Hjelle, A. Andresen, Y. Ohta, O. Salvigsen, 1992, Geological Map Svalbard 1:100,000. B9G Isfjorden: Oslo, Norsk Polarinstitutt, p. 52.

Dallman, W.K., 1999, Lithostratigraphic Lexicon of Svalbard. Upper Paleozoic to Quaternary bedrock. Review and recommendations for nomenclature use. Tromso, Norway, Norsk Polarinstitutt.

Darmody, R.G., Thorn, C.E., and Rissing, J.M., 1987, Chemical weathering of fine debris from a series of Holocene moraines: Storbreen, Jotunheimen, southern Norway: Geografiska Annaler, Series A, v. 69 A, p. 405-413.

Deer, W.A., Howie, R.A., and Zussman, J., 1992, An introduction tothe rock-forming minerals: Harlow, Essex, England, Longman Scientific & Technical, p. 696.

Demir, T., and Walsh, R.P.D., 2005, Shape and size characteristics of bedload transported during winter storm events in the Cwm Treweryn stream, Brecon Beacons, South Wales: Turkish Journal of Earth Sciences, v. 14, p. 105-121.

Dixon, J.C., Thorn, C.E., Darmody, R.G., and Campbell, S.W., 2002, Post-glacial rock weathering processes on a roche moutonnée in the Riksgra nsen area (68°N), northern Norway: Norsk Geografisk Tidsskrift, v. 56, p. 257-264.

Doran, P.T., 1993, Sedimentology of Colour Lake, a nonglacial High Arctic lake, Axel Heiberg Island, NWT, Canada: Arctic & Alpine Research, v. 25, p. 353-367.

Dreimanis, A., and Vagners, U.J., 1969, Lithologic relation of till to bedrock, *in* Wright, H.E., ed., Quaternary Geology and Climate: Washington D.C., National Academy of Sciences, p. 93-98.

Engelhardt, W.v., 1977, The Origin of Sediments and Sedimentary Rocks: New York, John Wiley & Sons, p. 359.

Fairchild, I.J., Bradby, L., and Baruch, S., 1994, Reactive carbonate in glacial systems: a preliminary synthesis of its creation, dissolution and reincarnation, *in* Deynoux, M. et al., ed., Earth's Glacial Record: Cambridge, Cambridge University Press, p. 176-192.

Field guide compiled by Gary Nichols based on work by Ida Lonne, 2004, AG 201: The Geology of Svalbard: v. Field Excursion, .

Forbes, A.C., and Lamoureux, S.F., 2005, Climatic controls on streamflow and suspended sediment transport in three large middle arctic catchments, Boothia Peninsula, Nunavut, Canada: Arctic, Antarctic, and Alpine Research, v. 37, p. 304-315.

Forman, S.L., Mann, D.H., and Miller, G.H., 1987, Late Weichselian and Holocene relative sea-level history of Broggerhalvoya, Spitsbergen. Quaternary Research, v. 27, p. 41-50.

Francus, P., Bradley, R.S., Abbott, M.B., Patridge, W., and Keimig, F., 2002, Paleoclimate studies of minerogenic sediments using annually resolved textural parameters: Geophysical Research Letters, v. 29, p. 59-1.

Giraudeau, J., Jennings, A.E., and Andrews, J.T., 2004, Timing and mechanisms of surface and intermediate water circulation changes in the Nordic Seas over the last 10,000 cal years: A view from the North Iceland shelf: Quaternary Science Reviews, v. 23, p. 2127-2139.

Gordiyenko, F.G., Kotlyakov, V.M., Punning, Y.-.M., and Vairmäe, R., 1980, Study of a 200-m core from the Lomonosov ice plateau on Spitsbergen and the paleoclimatic implications: Polar Geogr. Geol, v. 5, p. 242-251.

Grove, J.M., 2001, The initiation of the "Little Ice Age" in regions round the north atlantic: Climatic Change, v. 48, p. 53-82.

Gude, M., and Scherer, D., 1998, Snowmelt and slushflows: hydrological and hazard implications: Annals of Glaciology, v. 26, p. 381-384.

Hall, K., Thorn, C.E., Matsuoka, N., and Prick, A., 2002, Weathering in cold regions: Some thoughts and perspective: Progress in Physical Geography, v. 26, p. 577-603.

Hammer, K.M., and Smith, N.D., 1983, Sediment production and transport in a proglacial stream: Hilda Glacier, Alberta, Canada. Boreas, v. 12, p. 91-106.

Harris, C., 1989, Mechanisms of mass movement in periglacial environments, *in* Anderson, M.G. and Richards, K.S., eds., Slope Stability: Chichester, Wiley, p. 531-559.

Harvey, A.M., Foster, G., Hannam, J., and Mather, A.E., 2003, The Tabernas alluvial fan and lake system, southeast Spain: Applications of mineral magnetic and pedogenic iron oxide analyses towards clarifying the Quaternary sediment sequences: Geomorphology, v. 50, p. 151-171.

Hassol, S.J., 2004, Arctic Climate Impact Assessment: Impacts of a Warming Arctic: Cambridge, Cambridge University Press, p. 139.

Hestnes, E., 1998, Slushflow hazard - where, why and when? 25 years of experience with slushflow consulting and research: Annals of Glaciology, v. 26, p. 370-376.

Hjelle, A., and Lauritzen, O., 1982, Geological map of Svalbard 1:500 000 - Sheet 3G, Spitsbergen northern part. Norsk Polarinstitutt Skrifter, v. 154, p. 3-15.

Houghton, J.T., Jenkins, G.J., and Ephraums, J.J., 1990, Climate change: the IPCC scientific assessment: Climate Change: The IPCC Scientific Assessment.

Humlum, O., July 2005, personal communication.

Jackson, J. A. (editor), 1997, Glossary of Geology: Alexandria, Va., American Geological Institute, p. 769.

Jansson, P., Rosqvist, G., and Schneider, T., 2005, Glacier fluctuations, suspended sediment flux and glacio-lacustrine sediments: Geografiska Annaler, Series A: Physical Geography, v. 87, p. 37-50.

Kairyte, M., Stevens, R.L., and Trimonis, E., 2005, Provenance of silt and clay within sandy deposits of the Lithuanian coastal zone (Baltic Sea): Marine Geology, v. 218, p. 97-112.

Kane, D.L., Hinzman, L.D., Woo, M., and Everett, K.R., 1992, Arctic Hydrology and Climate Change, *in* F. Stuart Chapin III et al., ed., Arctic Ecosystems in a Changing Climate: an Ecophysiological Perspective: San Diego, Academic Press, Inc., p. 35-469.

Komar, P.D., and Zhenlin Li, 1986, Pivoting analyses of the selective entrainment of sediments by shape and size with application to gravel threshold. Sedimentology, v. 33, p. 425-436.

Konisky, R.A., and Burdick, D.M., 2004, Effects of stressors on invasive and halophytic plants of New England salt marshes: A framework for predicting response to tidal restoration: Wetlands, v. 24, p. 434-447.

Lamoureux, S.F., and Gilbert, R., 2004, A 750-yr record of autumn snowfall and temperature variability and winter storminess recorded in the varved sediments of Bear Lake, Devon Island, Arctic Canada: Quaternary Research, v. 61, p. 134-147.

Landvik, J.Y., Mangerud, J., and Salvigsen, O., 1987, The Late Weichselian and Holocene shoreline displacement on the west-central coast of Svalbard: Polar Research, v. 5, p. 29-44.

Larsen, E., and Stalsberg, M.K., 2004, Younger Dryas glaciolacustrine rhythmites and cirque glacier variations at Kråkenes, western Norway: Depositional processes and climate: Journal of Paleolimnology, v. 31, p. 49-61.

Lehman, S.J., and Forman, S.L., 1992, Late Weichselian glacier retreat in Kongsfjorden, west Spitsbergen, Svalbard: Quaternary Research, v. 37, p. 139-154.

Lewis, T., Braun, C., Hardy, D.R., Francus, P., and Bradley, R.S., 2005, An extreme sediment transfer event in a Canadian High Arctic stream: Arctic, Antarctic, and Alpine Research, v. 37, p. 477-482.

Lewis, T., Gilbert, R., and Lamoureux, S.F., 2002, Spatial and temporal changes in sedimentary processes at proglacial Bear Lake, Devon Island, Nunavut, Canada: Arctic, Antarctic, and Alpine Research, v. 34, p. 119-129.

Mangerud, J., et al., 1992, The Last Glacial maximum on Spitsbergen, Svalbard: Quaternary Research, v. 38, p. 1-31.

Mangerud, J., Dokken, T., Hebbeln, D., Heggen, B., Ingólfsson, O., Landvik, J.Y., Mejdahl, V., Svendsen, J.I., and Vorren, T.O., 1998, Fluctuations of the Svalbard-Barents sea ice sheet during the last 150000 years: Quaternary Science Reviews, v. 17, p. 11-42.

Mangerud, J., and Svendsen, J.I., 1990, Deglaciation chronology inferred from marine sediments in a proglacial lake basin, western Spitsbergen, Svalbard: Boreas, v. 19, p. 249-272.

Mann, D.H., Peteet, D.M., Reanier, R.E., and Kunz, M.L., 2002, Responses of an arctic landscape to lateglacial and early holocene climatic changes: The importance of moisture: Quaternary Science Reviews, v. 21, p. 997-1021.

Mann, M.E., Bradley, R.S., and Hughes, M.K., 1998, Global-scale temperature patterns and climate forcing over the past six centuries: Nature, v. 392, p. 779-787.

Matsuoka, N., 2001, Solifluction rates, processes and landforms: A global review: Earth-Science Reviews, v. 55, p. 107-134.

Motley, J.B., March 2006, personal communication.

Nesje, A., and Dahl, S.O., 2003, The 'Little Ice Age' - Only temperature? Holocene, v. 13, p. 139-145.

Nesse, W.D., 2000, Introduction to Mineralogy: New York, Oxford University Press, p. 442.

Newton, R.M., 1978, Stratigraphy and structure of some New England tills. Unpublished doctoral dissertation, University of Massachusetts, Amherst, Massachusetts: p. 241.

O'Reilly, B.S., 1995, Modern sedimentary processes and paleoenvironmental reconstruction from laminated lacustrine and marine sediments, Sophia Lake, N.W.T., Canada. Unpublished B. Sc. honors thesis, Bates College: p. 196.

Ostrem, G., Bridge, C.W., and and Rannie, W.F., 1967, Glacio-hydrology, discharge and sediment transport in the Decade Glacier area, Baffin Island, NWT: Geografiska Annaler, v. 49A, p. 268-282.

Pederson, J., Smith, G., and Pazzaglia, F., 2001, Comparing the modern, Quaternary, and Neogene records of climate-controlled hillslope sedimentation in southeast Nevada: Bulletin of the Geological Society of America, v. 113, p. 305-319.

Pollastro, R.M., 1982, A recommended procedure fro the preparation of oriented clay-mineral specimens for X-ray diffraction analysis: modifications to Drever's filter-membrane peel technique: Open-File Report 82-71, v. Open-file report 82-71, p. i-9.

Retelle, M.J., and Child, J.K., 1996, Suspended sediment transport and deposition in a high arctic meromictic lake: Journal of Paleolimnology, v. 16, p. 151-167.

Ritter, D.F., 1978, Process Geomorphology: Dubuque, Iowa, Wm. C. Brown Company Publishers, p. 603-463.

Ruikka, M., and Strand, K., 2002, Clay minerals in response to the Pleistocene climate change on the Yermak Plateau, Arctic Ocean (ODP, Site 911): Polar Record, v. 38, p. 241-248.

Scherer, D., Gude, M., Gempeler, M., and Parlow, E., 1998, Atmospheric and hydrological boundary conditions for slushflow initiation due to snowmelt: Annals of Glaciology, v. 26, p. 377-380.

Schiff, C., 2005, Unsustainable glacier ablation at 78°N latitude, Linnebreen, Svalbard: Geological Society of America Abstracts with Programs, v. 37, no. 1, p. 14.

Serreze, M.C., Walsh, J.E., Chapin III, F.S., Osterkamp, T., Dyurgerov, M., Romanovsky, V., Oechel, W.C., Morison, J., Zhang, T., and Barry, R.G., 2000, Observational evidence of recent change in the northern high-latitude environment: Climatic Change, v. 46, p. 159-207.

Siegert, M.J., Dowdeswell, J.A., Svendsen, J.-., and Elverhøi, A., 2002, The Eurasian Arctic during the last ice age: American Scientist, v. 90, p. 32-39.

Sletten, K., Blikra, L.H., Ballantyne, C.K., Nesje, A., and Dahl, S.O., 2003, Holocene debris flows recognized in a lacustrine sedimentary succession: Sedimentology, chronostratigraphy and cause of triggering: Holocene, v. 13, p. 907-920.

Smith, N.D., and Ashley, G.M., 1985, Proglacial lacustrine environment. Glacial Sedimentary Environments, p. 135-216.

Snyder, J.A., Werner, A., and Miller, G.H., 2000, Holocene cirque glacier activity in western Spitsbergen, Svalbard: Sediment records from proglacial Linnevatnet: Holocene, v. 10, p. 555-563.

Snyder, J.A., Miller, G.H., Werner, A., Jull, A.J.T., and Stafford Jnr, T.W., 1994, AMS-radiocarbon dating of organic-poor lake sediment, an example from Linnevatnet, Spitsbergen, Svalbard: Holocene, v. 4, p. 413-421.

Steel, R.J., and Worsley, D., 1984, Svalbard's post- Caledonian strata - an atlas of sedimentational patterns and palaeogeographic evolution. Petroleum Geology of the North European Margin. Proc. NEMS '83, Trondheim, 1983, p. 109-135.

Svendsen, J.I., and Mangerud, J., 1997, Holocene glacial and climatic variations on Spitsbergen, Svalbard: Holocene, v. 7, p. 45-57.

Svendsen, J.I., Mangerud, J., and Miller, G.H., 1989, Denudation rates in the Arctic estimated from lake sediments on Spitsbergen, Svalbard: Palaeogeography, Palaeoclimatology, Palaeoecology, v. 76, p. 153-168.

Thomas, E.K., 2005, Using Geochemical Evidence to Determine Provenance in a High Arctic Glacier-Fed Lake, Linné Valley, Svalbard, Norway. Unpublished B. Sc. Thesis, Smith College, Northampton, Massachusetts: p. i-58.

Viscosi-Shirley, C., Mammone, K., Pisias, N., and Dymond, J., 2003, Clay mineralogy and multi-element chemistry of surface sediments on the Siberian-Arctic shelf: Implications for sediment provenance and grain size sorting: Continental Shelf Research, v. 23, p. 1175-1200.

Wall, G.J., and Wilding, L.P., 1976, Mineralogy and related parameters of fluvial suspended sediments in Northwestern Ohio: Journal of Environmental Quality, v. 5, p. 168-173.

Wall, G.J., Wilding, L.P., and Smeck, N.E., 1978, Physical, chemical and mineralogical properties of fluvial unconsolidated bottom sediments in Northwestern Ohio: Journal of Environmental Quality, v. 7, p. 319-325.

Warren, R.S., and Niering, W.A., 1993, Vegetation change on a northeast tidal marsh: interaction of sea- level rise and marsh accretion: Ecology, v. 74, p. 96-103.

Werner, A., February 2006, personal communication.

Werner, A., 1988, Holocene glaciation and climatic change, Spitsbergen, Svalbard. University of Colorado unpublished thesis: p. 296.

Werner, A., 1993, Holocene moraine chronology, Spitsbergen, Svalbard: lichenometric evidence for multiple Neoglacial advances in the Arctic: Holocene, v. 3, p. 128-137.

White, A.F., and Blum, A.E., 1995, Effects of climate on chemical weathering in watersheds: Water-Rock Interaction. Proc. Symposium, Vladivostok, 1995, p. 57-60.

Woo, M.-., and Sauriol, J., 1980, Channel development in snow-filled valleys, Resolute, Northwest Territories, Canada. Geografiska Annaler Series A, v. 62, p. 37-56.

Wood, P.A., 1978, FINE-SEDIMENT MINERALOGY OF SOURCE ROCKS AND SUSPENDED SEDIMENT, ROTHER CATCHMENT, WEST SUSSEX. Earth Surf Processes, v. 3, p. 255-263.

Worsley, D., O. J. Aga, 1986, Evolution of an arctic archipelago. The Geological History of Svalbard. Statoil, Harstad, .

Appendices

location	sample	total wgt. (g)	gravel wgt. (g)	% gravel	sand wgt. (g)	% sand	fines wgt. (g)	% fines	
West Solifluction	72705-01	33.82	2.06	6.1	30.6	90.5	1.16	3.4	
	72705-02	39.17	4.43	11.3	15.9	40.6	18.84	48.1	
	72705-03	37.6	7.39	19.7	17.15	45.6	13.06	34.7	
	72705-04	39.14	10.08	25.8	26.33	67.3	2.73	7.0	
	72705-05	35.76	5.33	14.9	7.74	21.6	22.69	63.5	
			5.86	*15.5*	*19.54*	*53.1*		*31.3*	*mean*
West Shore	17 f	37.29	11.39	30.5	23.17	62.1	2.73	7.3	
	18 f	35.12	2.83	8.1	27.53	78.4	4.76	13.6	
	19 f	36.32	5.67	15.6	1.2	3.3	29.45	81.1	
	20 f	37.5	3.22	8.6	18.75	50.0	15.53	41.4	
	21 f	34.72	1.72	5.0	8.75	25.2	24.25	69.8	
	22 f	39.25	5.48	14.0	12.18	31.0	21.59	55.0	
			5.05	*13.6*	*15.26*	*41.7*		*52.2*	*mean*
Cirque Glacier Fan	1 f	33.66	7.27	21.6	17.97	53.4	8.42	25.0	
	2 f	36.44	7.57	20.8	15	41.2	13.87	38.1	
	3 f	32.52	4.48	13.8	15.86	48.8	12.18	37.5	
	4 f	33.47	0.42	1.3	21.74	65.0	11.31	33.8	
			4.94	*14.4*	*17.64*	*52.1*		*33.6*	*mean*
Linneelva Fan	5 f	35.39	0.04	0.1	25.5	72.1	9.85	27.8	
	6 f	37.75	0.04	0.1	18.64	49.4	19.07	50.5	
	7 f	33.13	n/a	n/a	24.52	74.0	8.61	26.0	
			0.04	*0.1*	*22.9*	*65.1*		*34.8*	*mean*
Dolerite Fan	8 f	22.95	5.09	22.2	13.31	58.0	4.55	19.8	
	9 f	34.61	12.44	35.9	19.28	55.7	2.89	8.4	
	10 f	n/a	n/a	n/a	n/a	n/a	n/a	n/a	
			8.77	*29.1*	*16.30*	*56.9*		*14.1*	*mean*
S. Twin Fan	11 f	33.2	1.09	3.3	16.91	50.9	15.2	45.8	
	12 f	32.71	14.94	45.7	13.94	42.6	3.83	11.7	
	13 f	31.5	4.43	14.1	6.04	19.2	21.03	66.8	
			6.8	*21.0*	*12.3*	*37.6*		*41.4*	*mean*
N. Twin Fan	14 f	37.72	10.04	26.6	14.62	38.8	13.06	34.6	
	15 f	31.76	7.65	24.1	16.56	52.1	7.55	23.8	
	16 f	21.4	1.76	8.2	4.79	22.4	14.85	69.4	
			6.5	*19.6*	*12.0*	*37.8*		*42.6*	*mean*
East Central Fan	26 f	36.78	2.11	5.7	28.95	78.7	5.72	15.6	
	27 f	39.48	8.33	21.1	28.7	72.7	2.45	6.2	
	28 f	37.31	10.91	29.2	7.82	21.0	18.58	49.8	
	29 f	36.42	11.94	32.8	8.27	22.7	16.21	44.5	
			8.32	*22.2*	*18.44*	*48.8*		*29.0*	*mean*
Northeast Fan	23 f	20.13	0.83	4.1	16.59	82.4	2.71	13.5	
	24 f	33.66	1.07	3.2	17.28	51.3	15.31	45.5	
	25 f	35.12	2.45	7.0	9.29	26.5	23.38	66.6	
			1.5	*4.8*	*14.4*	*53.4*		*41.8*	*mean*

Table B.1 Grain Size Analysis of Surficial Sediments with Fraction Weights

sample	total wgt. (g)	sand wgt. (g)	sand %	silt wgt. (g)	% silt	clay wgt. (g)	% clay
0	5.9394	0.1599	2.7	5.77	97.1	0.01	0.2
1	1.8145			1.49	82.1	0.32	17.9
3	6.7276	0.1908	2.8	*7*	*104.0*	*-0.46*	*-6.9*
4	2.0071	0.1461	7.3	1.77	88.2	0.09	4.5
5	6.434	0.0702	1.1	6.18	96.1	0.18	2.9
6	1.8213	0.0379	2.1	1.58	86.8	0.20	11.2
7	6.7169	0.0909	1.4	6.15	91.6	0.48	7.1
8	2.0623	0.0367	1.8	1.58	76.6	0.45	21.6
9	6.3218	0.1212	1.9	6.057	95.8	0.14	2.3
10	1.8685	0.108	5.8	1.48	79.2	0.28	15.0
11	2.0297	0.0571	2.8	1.44	70.9	0.53	26.2
12	2.0288	0.08	3.9	1.58	77.9	0.37	18.2

Table B.2 Core 6 Continuous Grain Size Analysis with Fraction Weights

sample	total wgt. (g)	sand wgt. (g)	sand %	silt wgt. (g)	% silt	clay wgt. (g)	% clay
0	2.1422	0.021	1.0	1.8	84.0	0.32	15.0
1	6.2657	0.0512	0.8	5.3	84.6	0.91	14.6
2	2.052	0.0218	1.1	1.36	66.3	0.67	32.7
3	1.9315	0.0202	1.0	1.63	84.4	0.28	14.6
4	2.5104	0.0083	0.3	1.57	62.5	0.93	37.1
5	2.1235	0.0109	0.5	1.55	73.0	0.56	26.5
6	6.1431	0.0279	0.5	5	81.4	1.12	18.2
7	1.3199	0.0105	0.8	1.28	97.0	0.03	2.2
8	1.6306	0.0122	0.7	*1.64*	*100.6*	*-0.02*	*-1.3*
9	1.9708	0.0127	0.6	1.92	97.4	0.04	1.9
10	6.4549	0.0803	1.2	5.84	90.5	0.53	8.3
11	0.844	0.0147	1.7	*1.51*	*178.9*	*-0.68*	*-80.7*
12	1.7877	0.0496	2.8	1.37	76.6	0.37	20.6
13	1.9384	0.0101	0.5	*1.5*	*77.4*	*0.43*	*22.1*
14	2.2835	0.0153	0.7	1.63	71.4	0.64	27.9
15	2.0275	0.0363	1.8	*4.88*	*240.7*	*-2.89*	*142.5*
16	5.2069	0.0091	0.2	1.58	30.3	3.62	69.5
17	2.0704	0.0114	0.6	1.39	67.1	0.67	32.3
18	1.5758	0.0161	1.0	*0.21*	*13.3*	*1.35*	*85.7*
19	1.6885	0.0079	0.5	1.12	66.3	0.56	33.2
20	1.968	0.0099	0.5	1.57	79.8	0.39	19.7
21	4.8474	0.0414	0.9	*17.95*	*370.3*	*-13.14*	*271.2*
22	1.4606	0.0172	1.2	1.25	85.6	0.19	13.2
23	1.8523	0.0342	1.8	*0.32*	*17.3*	*1.50*	*80.9*
24	2.2262	0.0245	1.1	1.7	76.4	0.50	22.5
25	1.882	0.0115	0.6	1.5	79.7	0.37	19.7

Table B.3 Core 8 Continuous Grain Size Analysis with Fraction Weights

sample	total wgt. (g)	sand wgt. (g)	sand %	silt wgt. (g)	% silt	clay wgt. (g)	% clay
0	1.1248	0.0056	0.5	1.04	92.5	0.08	7.0
1	1.2865	0.0052	0.4	1.05	81.6	0.23	18.0
2	1.3916	0.0039	0.3	1.11	79.8	0.28	20.0
3	1.2375	0.0033	0.3	1.13	91.3	0.10	8.4
4	1.2582	0.0067	0.5	1.22	97.0	0.03	2.5
5	4.38	0.087	2.0	2.03	46.3	2.26	51.7
6	2.2645	0.002	0.2	0.96	42.4	1.30	57.5
7	1.2922	0.0013	0.1	1.04	80.5	0.25	19.4
8	1.4045	0.0017	0.1	1.24	88.3	0.16	11.6
9	1.2992	0.0021	0.2	0.95	73.1	0.35	26.7
10	4.72	0.0046	0.1	2.38	50.4	2.34	49.5
11	1.171	0.0022	0.2	0.86	73.4	0.31	26.4
12	1.2928	0.0027	0.2	1.12	86.6	0.17	13.2
13	1.4132	0.0013	0.1	1.36	96.2	0.05	3.7
14	1.3126	0.0064	0.6	0.98	74.7	0.33	24.9
15	2.92	0.0179	*0.6*	*3.62*	*124.0*	*-0.72*	*-24.6*
16	1.8118	0.0057	0.5	1.15	63.5	0.66	36.2
17	1.0935	0.0039	0.4	0.92	84.1	0.17	15.5
18	1.2117	0.0022	0.1	1.03	85.0	0.18	14.8
19	1.1108	0.0046	0.4	0.96	86.4	0.15	13.2
20	0.9543	0.0059	0.5	0.93	97.5	0.02	1.9
21	1.8047	0.0048	0.3	1.42	78.7	0.38	21.1
22	4.09	0.0158	0.4	3.27	80.0	0.80	19.7
23	1.2562	0.0042	0.3	0.92	73.2	0.33	26.4
24	1.274	0.003	0.1	0.89	69.9	0.38	29.9
25	1.4006	0.0022	0.1	1	71.4	0.40	28.4
26	1.2662	0.0028	0.1	1.17	92.4	0.09	7.4
27	1.2262	0.0023	0.1	0.98	79.9	0.24	19.9
28	2.11	0.0034	0.2	0.94	44.5	1.17	55.3
29	2.57	0.0055	0.2	1.15	44.7	1.41	55.0
30	4.63	0.0134	0.3	4.03	87.0	0.59	12.7
31	2.05	0.0043	0.2	1.1	53.7	0.95	46.1
32	1.8	0.0026	0.1	1.07	59.4	0.73	40.4
33	1.68	0.0024	0.1	1.14	67.9	0.54	32.0
34	2.29	0.0014	0.1	1.2	52.4	1.09	47.5
35	2.24	0.0012	0.1	1.1	49.1	1.14	50.8
36	2.02	n/a	n/a	n/a	n/a	n/a	n/a
37	2.06	0.0012	0.1	1.33	65.8	0.69	34.1

Table B.4 Core 12 Continuous Grain Size Analysis with Fraction Weights

sample	total wgt. (g)	sand wgt. (g)	sand %	silt wgt. (g)	% silt	clay wgt. (g)	% clay
0	1.1433	0.0113	1.0	*1.37*	*119.8*	*-0.24*	*-20.8*
1	1.3509	0.0138	1.0	1.05	77.7	0.29	21.3
2	1.2325	0.0061	0.5	0.81	65.7	0.42	33.8
3	4.94	0.0323	0.65	3.54	71.7	1.37	27.7
4	1.3855	0.0067	0.5	1.14	82.3	0.24	17.2
5	1.5929	0.0053	0.3	1.05	65.9	0.54	33.7
6	4.58	0.0185	0.40	3.11	67.9	1.45	31.7
7	1.457	0.0034	0.2	1.01	69.3	0.44	30.4
8	1.3526	0.0053	0.4	0.65	48.1	0.70	51.6
9	1.8933	0.0216	1.1	1.42	75.0	0.45	23.9
10	5.6	0.3331	5.95	4.62	82.5	0.65	11.6
11	1.4148	0.011	0.8	1.07	75.6	0.33	23.6
12	1.4168	0.0105	0.7	1.08	76.2	0.33	23.0
13	1.463	0.0167	1.1	1.25	85.4	0.20	13.4
14	1.3394	0.0078	0.6	1.16	86.6	0.17	12.8
15	4.39	0.0472	1.08	3.2	72.9	1.14	26.0
16	1.4343	0.006	0.4	1.12	78.1	0.31	21.5
17	1.4433	0.0132	0.9	1.26	87.3	0.17	11.8
18	1.7995	0.0108	0.6	1.54	85.6	0.25	13.8
19	5.13	0.0268	0.52	4.22	82.3	0.88	17.2
20	1.6351	0.0054	0.3	1.24	75.8	0.39	23.8
21	1.4382	0.0102	0.7	1.18	82.0	0.25	17.2

Table B.5 Core 11 Continuous Grain Size Analysis with Fraction Weights